Nuclear Science
NEA/WPEC-29
www.oecd-nea.org

International Evaluation Co-operation

Volume 29

Uranium-235 Capture Cross-section in the keV to MeV Energy Region

OECD
BETTER POLICIES FOR BETTER LIVES

NEA
NUCLEAR ENERGY AGENCY

Nuclear Science
NEA/WPEC-29

NEA/NSC/WPEC/DOC(2011)433

International Evaluation Co-operation

Volume 29

Uranium-235 Capture Cross-section in the keV to MeV Energy Region

A report by the Working Party
on International Evaluation Co-operation
of the NEA Nuclear Science Committee

Co-ordinator

O. Iwamoto
Japan Atomic Energy Agency
Japan

Monitor

R. McKnight
Argonne National Laboratory
United States of America

© OECD 2011

NUCLEAR ENERGY AGENCY
Organisation for Economic Co-operation and Development

ORGANISATION FOR ECONOMIC CO-OPERATION AND DEVELOPMENT

The OECD is a unique forum where the governments of 34 democracies work together to address the economic, social and environmental challenges of globalisation. The OECD is also at the forefront of efforts to understand and to help governments respond to new developments and concerns, such as corporate governance, the information economy and the challenges of an ageing population. The Organisation provides a setting where governments can compare policy experiences, seek answers to common problems, identify good practice and work to co-ordinate domestic and international policies.

The OECD member countries are: Australia, Austria, Belgium, Canada, Chile, the Czech Republic, Denmark, Estonia, Finland, France, Germany, Greece, Hungary, Iceland, Ireland, Israel, Italy, Japan, Luxembourg, Mexico, the Netherlands, New Zealand, Norway, Poland, Portugal, the Republic of Korea, the Slovak Republic, Slovenia, Spain, Sweden, Switzerland, Turkey, the United Kingdom and the United States. The European Commission takes part in the work of the OECD.

OECD Publishing disseminates widely the results of the Organisation's statistics gathering and research on economic, social and environmental issues, as well as the conventions, guidelines and standards agreed by its members.

This work is published on the responsibility of the OECD Secretary-General.
The opinions expressed and arguments employed herein do not necessarily reflect the official views of the Organisation or of the governments of its member countries.

NUCLEAR ENERGY AGENCY

The OECD Nuclear Energy Agency (NEA) was established on 1 February 1958. Current NEA membership consists of 30 OECD member countries: Australia, Austria, Belgium, Canada, the Czech Republic, Denmark, Finland, France, Germany, Greece, Hungary, Iceland, Ireland, Italy, Japan, Luxembourg, Mexico, the Netherlands, Norway, Poland, Portugal, the Republic of Korea, the Slovak Republic, Slovenia, Spain, Sweden, Switzerland, Turkey, the United Kingdom and the United States. The European Commission also takes part in the work of the Agency.

The mission of the NEA is:

- to assist its member countries in maintaining and further developing, through international co-operation, the scientific, technological and legal bases required for a safe, environmentally friendly and economical use of nuclear energy for peaceful purposes, as well as
- to provide authoritative assessments and to forge common understandings on key issues, as input to government decisions on nuclear energy policy and to broader OECD policy analyses in areas such as energy and sustainable development.

Specific areas of competence of the NEA include safety and regulation of nuclear activities, radioactive waste management, radiological protection, nuclear science, economic and technical analyses of the nuclear fuel cycle, nuclear law and liability, and public information.

The NEA Data Bank provides nuclear data and computer program services for participating countries. In these and related tasks, the NEA works in close collaboration with the International Atomic Energy Agency in Vienna, with which it has a Co-operation Agreement, as well as with other international organisations in the nuclear field.

Corrigenda to OECD publications may be found on line at: *www.oecd.org/publishing/corrigenda*.
© OECD 2011

You can copy, download or print OECD content for your own use, and you can include excerpts from OECD publications, databases and multimedia products in your own documents, presentations, blogs, websites and teaching materials, provided that suitable acknowledgment of OECD as source and copyright owner is given. All requests for public or commercial use and translation rights should be submitted to *rights@oecd.org*. Requests for permission to photocopy portions of this material for public or commercial use shall be addressed directly to the Copyright Clearance Center (CCC) at *info@copyright.com* or the Centre français d'exploitation du droit de copie (CFC) *contact@cfcopies.com*.

Foreword

The Working Party on International Nuclear Data Evaluation Co-operation (WPEC) was established under the aegis of the OECD/NEA Nuclear Science Committee (NSC) to promote the exchange of information on nuclear data evaluations, validation and related topics. Its aim is also to provide a framework for co-operative activities between the members of the major nuclear data evaluation projects. This includes the possible exchange of scientists in order to encourage co-operation. Requirements for experimental data resulting from this activity are compiled. The WPEC determines common criteria for evaluated nuclear data files with a view to assessing and improving the quality and completeness of evaluated data.

The parties to the project are: ENDF (United States), JEFF/EFF (NEA Data Bank member countries) and JENDL (Japan). Co-operation with evaluation projects of non-OECD countries, specifically the Russian BROND and Chinese CENDL projects, are organised through the Nuclear Data Section of the International Atomic Energy Agency (IAEA).

The following report was issued by WPEC Subgroup 29, whose mission was to investigate C/E discrepancies in uranium-core integral parameters observed with all major evaluated libraries. Members of Subgroup 29 performed sensitivity analyses of integral parameters with respect to differential data and reviewed the capture cross-section of ^{235}U with the objective to determine recommended values in the energy region from 100 eV to 1 MeV

The opinions expressed in this report are those of the authors only and do not necessarily represent the position of any member country or international organisation.

Members of Subgroup 29

G. Chiba, M. Ishikawa, O. Iwamoto, T. Nakagawa, S. Okajima
Japan Atomic Energy Agency
Japan

R. Jacqmin
Commissariat à l'énergie atomique
France

T. Kawano, T.A. Bredeweg
Los Alamos National Laboratory
USA

L.C. Leal
Oak Ridge National Laboratory
USA

C. Lubitz, T.H. Trumbull
Knolls Atomic Power Laboratory
USA

R. McKnight
Argonne National Laboratory
USA

Other Contributors

T. Kugo, M. Fukushima, Y. Kitamura, T. Hazama
Japan Atomic Energy Agency
Japan

T. Iwai, K. Numata
NESI Inc.
Japan

Table of contents

List of figures

List of tables

1. Introduction

The cross-sections of ^{235}U were examined by WPEC Subgroup 18 focusing on the thermal and epithermal energy region. As a result, the ORNL group evaluated resolved resonance parameters of ^{235}U up to 2.25 keV, which are currently used for all major libraries, such as JENDL-3.3, ENDF/B-VII.0 and JEFF-3.1. Using the resolved resonance parameters, prediction accuracy of neutronic characteristics is satisfactory for thermal reactors.

Benchmark analyses with JENDL-3.3 for fast reactor neutronic characteristics, however, revealed a problem regarding the ^{235}U capture cross-section which is based on the ORNL resonance parameters. In the experimental analyses for the fast critical assembly BFS-2, significant underestimation was observed in calculations for the sodium-void reactivity worth measured in a uranium-fuelled zone as shown in Figure 1.1 [1]. The BFS-2 sodium-void reactivity analysis is discussed in more detail in Appendix D.

Figure 1.1: C/E values of accumulative sodium-void reactivity worth measured in the BFS-2 critical assembly [1]

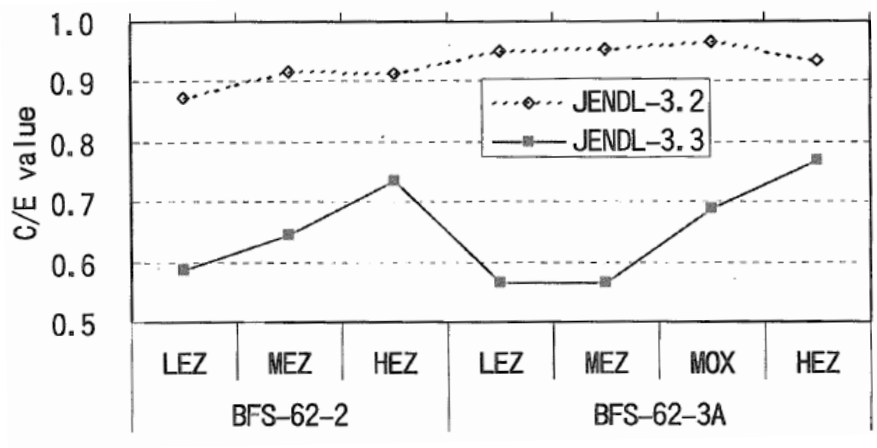

Okajima further pointed out a problem concerning the ^{235}U capture cross-section with the FCA-IX-series benchmark calculations [2]. Figure 1.2 shows C/E values of criticalities of some FCA cores. Here we concentrate on

Figure 1.2: C/E values of criticalities of FCA cores [1]

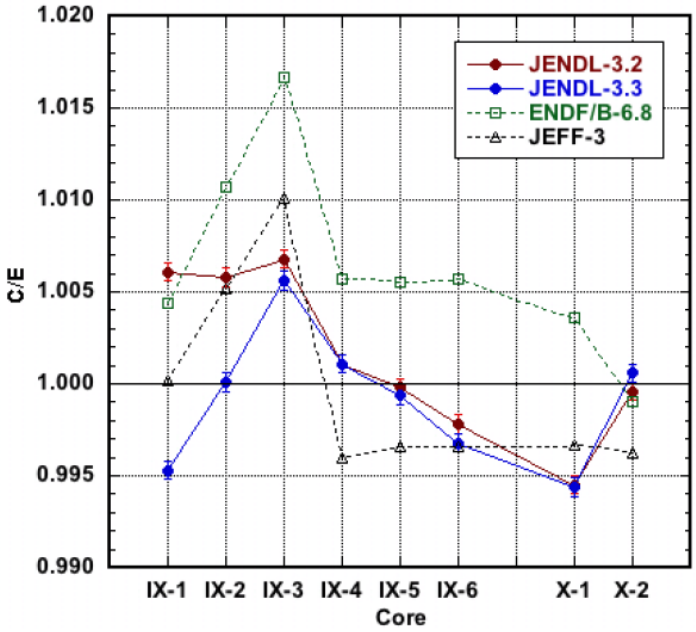

the FCA-IX-1, -2 and -3 cores which were uranium-fuelled and carbon-diluted fast systems, and their neutron energy spectra were adjusted from softer to to harder by changing the amount of loaded carbon. Large C/E dependence on neutron energy spectrum was observed in this figure when JENDL-3.3 was employed.

The same results were obtained for the above benchmark problems when the ENDF/B-VII.0 and JEFF-3.1 libraries were used. Such difficulties have not been observed, however, when the old version of JENDL, JENDL-3.2, was used. Sensitivity analyses suggested that these problems should be attributed to the ^{235}U capture cross-section from 100 eV to 2.25 keV.

Further, there is a large difference in the ^{235}U capture cross-section from 30 keV to 1 MeV among the latest nuclear data libraries, and this difference affects the prediction calculations for some neutronic characteristics for fast reactors. Thus it is desirable to discuss the ^{235}U capture cross-section in both the energy ranges with a consistent manner.

The purpose of the subgroup is to address the problem of the ^{235}U capture cross-section from the viewpoints of differential and integral data analyses and then determine recommended cross-sections in the energy region from 100 eV to 1 MeV.

2. Summary of activities

2.1 FCA-IX benchmark problem

2.1.1 Background

As described in the introduction, the modern nuclear data files, JENDL-3.3, JEFF-3.1 and ENDF/B-VII.0, result in significant dependence of C/E values of criticalities on the neutron energy spectrum in a series of FCA-IX cores. Such dependence, however, is not observed when JENDL-3.2 is employed in the calculation. Sensitivity analyses show that this difference comes from the difference in ^{235}U capture cross-section in the resonance energy range (below 2.25 keV). Figure 2.1 shows sensitivity coefficients of ^{235}U capture cross-section on the criticalities of the FCA-IX cores. Energy spectrum shifting of these sensitivity profiles can be seen in the resonance energy range. This suggests that the criticality data of these cores can be used to discuss the ^{235}U capture cross-section issue. Thus we prepared a benchmark problem of the FCA-IX cores, which is easy to calculate with Monte Carlo or deterministic neutron transport codes.

Figure 2.1: Sensitivity coefficients of ^{235}U capture cross-section on FCA-IX criticality

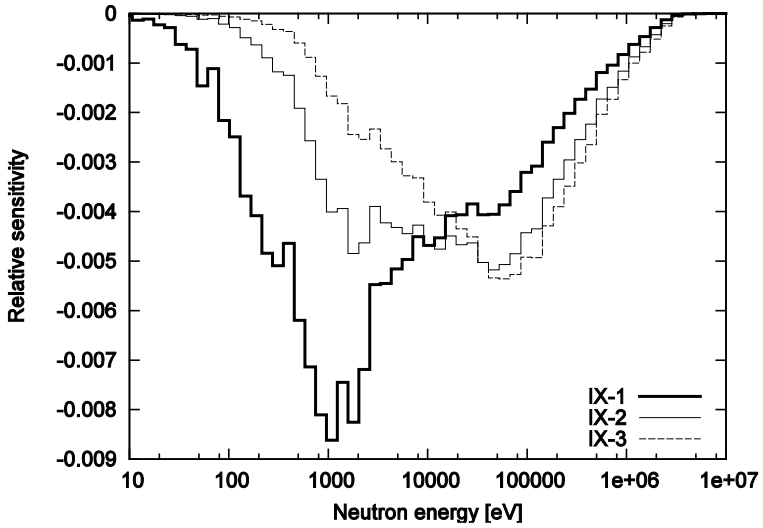

2.1.2 Benchmark problem specification

The geometry of the FCA-IX cores is simplified to a two-dimensional cylindrical model in the benchmark problem. Each core model of the benchmark problem is composed of two material regions, i.e. a fuel region and a blanket region. Cell heterogeneity is neglected in the benchmark model and its effect is considered for the "benchmark" experimental values as described later. Tables 2.1 and 2.2 provide geometrical specifications of the core models and region-wise nuclide number densities, respectively.

Table 2.1: Core specification of FCA-IX benchmark models

Assembly		IX-1	IX-2	IX-3
Fuel region	Outer radius (cm)	30.35	23.10	17.89
	Height (cm)	60.96	40.64	35.56
Blanket region	Outer radius (cm)	61.58	58.18	57.51
	Upper axial thickness (cm)	35.56	35.56	35.56
	Lower axial thickness (cm)	35.56	35.56	35.56

Table 2.2: Region-wise number densities of FCA-IX benchmark models

Unit: 10^{24} atoms/cm^3

Nuclide	Fuel region			Blanket
	IX-1	IX-2	IX-3	
^{235}U	2.260E-3	4.521E-03	6.781E-03	8.442E-05
^{238}U	1.709E-04	3.418E-04	5.127E-04	4.017E-02
^{240}Pu	–	–	–	–
^{241}Pu	–	–	–	–
^{242}Pu	–	–	–	–
^{239}Pu	–	–	–	–
^{241}Am	–	–	–	–
H	5.867E-05	1.173E-04	1.760E-04	–
C	6.524E-02	6.080E-02	5.667E-02	–
O	2.548E-05	5.097E-05	7.645E-05	–
Na	–	–	–	–
Al	–	–	–	–
Si	–	–	–	–
Cr	1.810E-03	1.810E-03	1.810E-03	1.810E-03
Mn	1.203E-04	1.203E-04	1.203E-04	1.203E-04
Fe	6.472E-03	6.472E-03	6.472E-03	6.472E-03
Ni	7.894E-04	7.894E-04	7.894E-04	7.894E-04

Experimental values of the benchmark problem are obtained from the experimental data of the as-built cores and the correction factors for the model simplification. These correction factors are determined as a difference between the continuous-energy Monte Carlo solution for the as-built model

and that for the benchmark model. They are evaluated with several different nuclear data files. The nuclear data-dependent correction factors are shown in Table 2.3. Their averaged values are used to obtain the benchmark experimental values, and their standard deviations are considered as additional uncertainties due to the model simplification.

Table 2.3: Correction factors for model simplification

	JENDL-3.3	JEFF-3.1	ENDF/B-VII.0	JENDL-3.2
FCA-IX-1	-0.0031	-0.0021	-0.0025	-0.0024
FCA-IX-2	-0.0072	-0.0076	-0.0071	-0.0076
FCA-IX-3	-0.0076	-0.0071	-0.0062	-0.0078

The benchmark problem's experimental values and their uncertainties are shown in Table 2.4. C/E values obtained using the continuous-energy Monte Carlo code MVP-II for the benchmark problem are shown in Table 2.5.

Table 2.4: Benchmark experimental values with uncertainties

	Benchmark k	Uncertainty
FCA-IX-1	0.9995	0.0007
FCA-IX-2	0.9958	0.0004
FCA-IX-3	0.9919	0.0012

Table 2.5: C/E values obtained with MVP-II for the benchmark problem

	JENDL-3.3	JEFF-3.1	ENDF/B-VII.0	JENDL-3.2
FCA-IX-1	0.9936	1.0055	1.0051	1.0066
FCA-IX-2	0.9998	1.0109	1.0112	1.0051
FCA-IX-3	1.0049	1.0161	1.0169	1.0064

2.2 Impact of JENDL-3.2 and ENDF/B-VII.0 resonance region

The source of the biases in intermediate-energy benchmark calculations was investigated. The work consists of intermediate benchmark calculations using JENDL-3.2 and ENDF/B-VII.0 and sensitivity calculations. The details are elaborated on in Appendix A.

2.2.1 Comparison of cross-sections

The comparison of capture cross-sections is shown in Figure 2.2. The histograms indicate group cross-sections of JENDL-3.2 and ENDF/B-VII.0. The result of a statistical model calculation is shown by a smooth line. It can be seen that ENDF/B-VII.0 capture cross-section is much larger than JENDL-3.2 and statistical model calculations in the range of about 100 eV to 3 keV.

Figure 2.2: Comparison of capture cross-sections

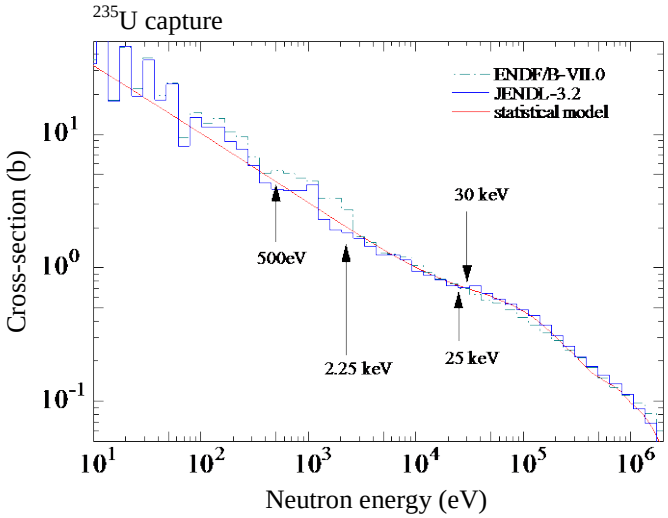

Discrepancies are also found in the elastic scattering cross-sections below 30 keV. The total and fission cross-sections have no such noticeable discrepancies.

Figure 2.3 shows a comparison of α-values (capture/fission ratios) calculated using nuclear data libraries and of experimental data. The ENDF/B-VII.0 α-value is in the upper part of the experimental results. However, JENDL-3.2 agrees well with the experimental results.

Figure 2.3: Comparison of α-values

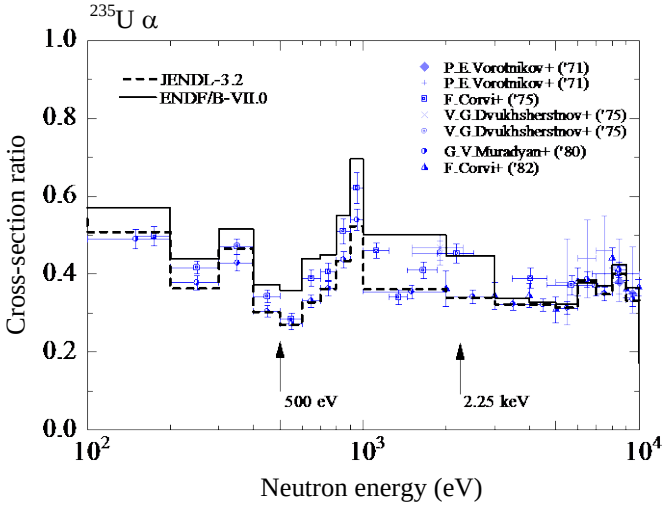

2.2.2 Benchmark results using test libraries

Though sensitivity study, it was found that the difference between ENDF/B-VII.0 and JENDL-3.2 from 500 eV to 2.25 keV has a large impact on both the FCA-IX and ZEUS calculations while the difference below 500 eV has an impact only on the ZEUS calculations.

To understand the reason why the two libraries perform differently, it has been decided to carry out benchmark calculations for test libraries created by merging JENDL resonance parameters in ENDF and *vice versa*. Figure 2.4 shows the results of benchmark calculations for the test libraries. Replacement of the ENDF/B-VII.0 resonance parameters by JENDL-3.2 for ^{235}U makes the C/E dependence on spectrum hardness smaller. However, this also results in unacceptably high C/E values. This can be an indication that there exists another energy region which also contributes to the multiplication factor. These cases require further investigation.

Figure 2.4: Benchmark calculations for several test libraries

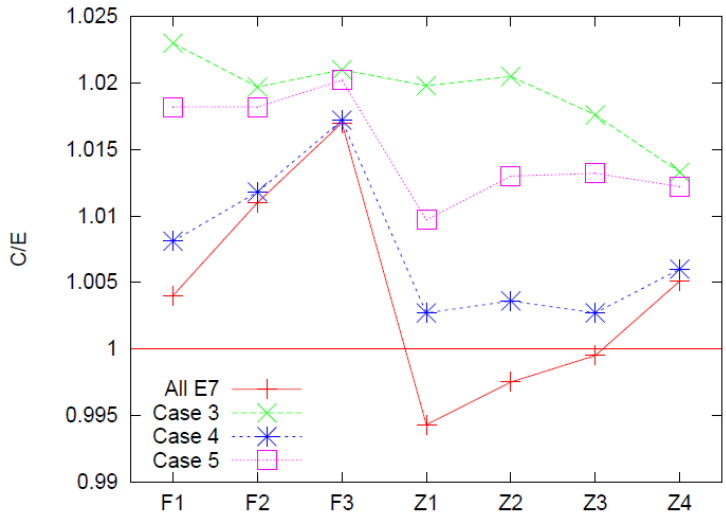

Figure 2.5 shows the results of the benchmark calculations for test libraries whose gamma widths were reduced. A simple decrease in the capture cross-section, i.e. in Γ_γ, reduces the C/E dependence on spectrum hardness. However, it scales the k_{eff} up. These results may indicate that other cross-section or combinations of effects may be causing the biases.

2.2.3 Sensitivity study and adjustment of ^{235}U cross-section using integral data

Detailed neutron balance analyses were performed. The results are shown in Table 2.6. The leakages for the ZEUS benchmark experiments are on the

Figure 2.5: Benchmark calculations for 3% and 10% change in gamma width

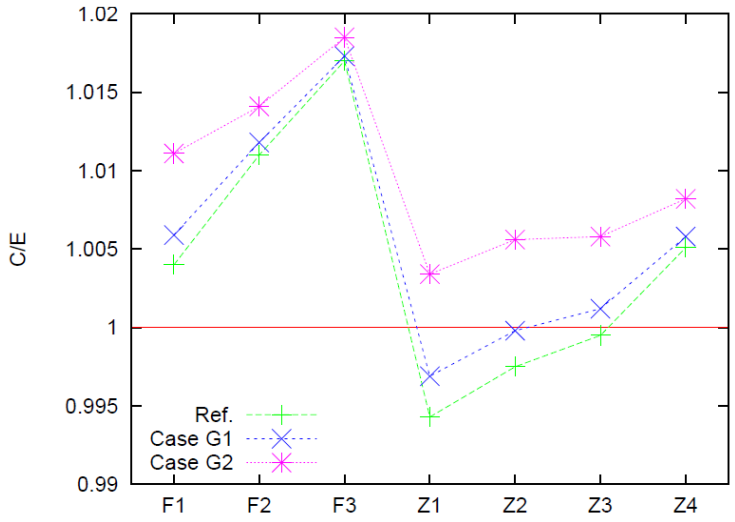

Table 2.6: Contribution to k_{eff} by its components

Core	Production		(n,2n)	Absorption		Leakage
	Fuel	Blanket		Fuel	Blanket	
ZEUS1	1.000		0.000	0.566	0.201	0.247
ZEUS2	1.000		0.000	0.552	0.188	0.276
ZEUS3	1.000		0.000	0.534	0.169	0.306
ZEUS4	1.000		0.001	0.504	0.142	0.358
FCA1	0.872	0.128	0.002	0.481	0.478	0.041
FCA2	0.846	0.154	0.003	0.436	0.524	0.040
FCA3	0.832	0.168	0.003	0.413	0.549	0.034

average of 28% whereas in the FCA it is about 4%. The contribution of each component to k_{eff} for the ZEUS and FCA benchmark experiments are different from each other.

Cross-section adjustment is carried out for ^{235}U of ENDF/B-VII.0 using the integral data of FCA-IX, ZEUS, Godiva and HST001 (HEU-SOL-THERM-001). In this adjustment calculation, C/E values and their uncertainties are set to be 1.0 and 0.0001 for Godiva and HST001 since the C/E values for these data should be unchanged. This indicates that capture cross-section in the resonance range is overestimated (see Figure 2.6).

Figure 2.6: Relative change in ^{235}U capture cross-section through adjustment

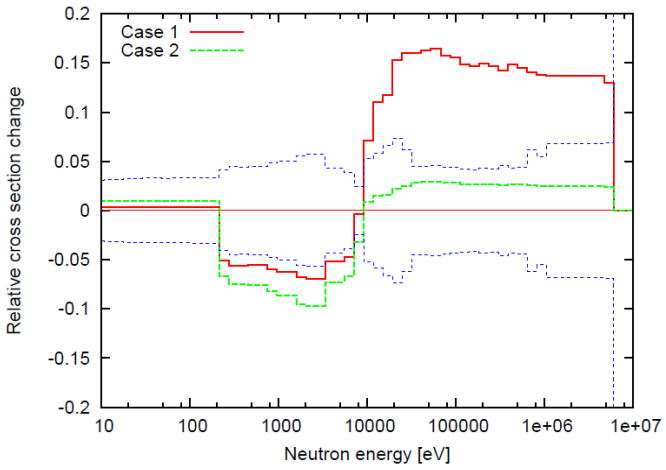

2.3 Benchmark analysis by Trumbull and Lubitz

2.3.1 Introduction

WPEC Subgroup 18 focused on the thermal and epithermal energy region for ^{235}U. Several changes were made to ^{235}U, including a re-evaluation of the resonances by ORNL. The resulting data have become the basis for the current major libraries (ENDF/B-VII.0, JEFF-3.1 and JENDL-3.3). Analysis by JAEA of the FCA-IX and BFS-62 benchmarks shows poor agreement when using the latest nuclear data libraries. The preliminary analysis seems to point to a problem with the ^{235}U fast capture cross-section and the capture-to-fission ratio (α).

SG29 formed in May 2007 to investigate this issue. JAEA has created several new ^{235}U evaluations that substitute ENDF/B-VII.0 and JENDL-3.2 resolved and unresolved resonance parameters in various combinations over various energy ranges. Since better agreement with the FCA-IX and BFS-62 benchmarks was obtained using JENDL-3.2, the new ^{235}U evaluations spliced in the older data into different energy ranges of interest, notably between 500 eV, 2 250 eV and 25 keV. The intent was to identify the set of parameters and energy ranges that produce results closer to expectations for fast and thermal reactor spectra.

2.3.2 Methods approach

2.3.2.1 Codes and data

All analysis at KAPL was performed using the MC21 continuous-energy Monte Carlo code with the NDEX nuclear data system. MC21 cross-section libraries were created for seven of the eight proposed ^{235}U evaluations.

Source data for all other materials in the model come from the ENDF/B-VII.0 data set. A base case library was created using all ENDF/B-VII.0 data. A graphical representation of the sources of nuclear data and resolved/unresolved resonance regions for all cases is provided in Table 2.7.

A library for Case 5 was not created because the ^{235}U evaluation includes two unresolved resonance ranges in File 2. The current version of NDEX creates probability tables for the unresolved resonance range with the expectation that only a single unresolved range is given in File 2. The NDEX team is evaluating an appropriate fix.

Table 2.7: Graphical description of the source nuclear data and energy breakpoints used to define the resolved and unresolved resonance regions for the cases of interest

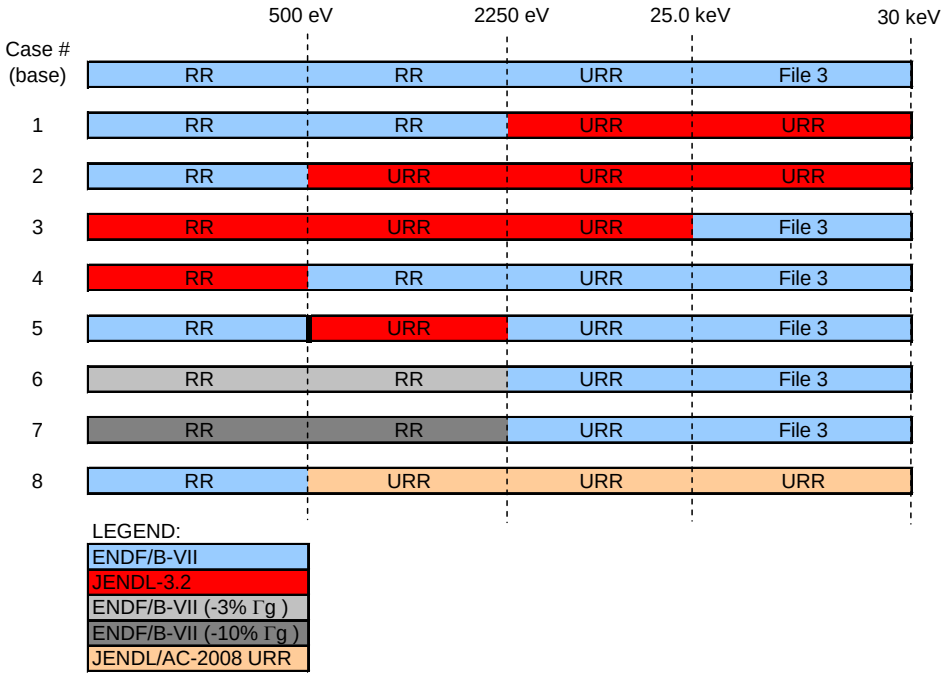

2.3.2.2 Models and analysis

MC21 models were created for the specific models referenced in the previous JAEA analysis: FCA-IX-1, FCA-IX-2, FCA-IX-3, ZEUS1, ZEUS2, ZEUS3 and ZEUS4. The ZEUS models are also listed in ICSBEP as HEU-MET-INTER-006, Cases 1-4. In addition, a set of 128 ICSBEP models were created for MC21 that span a range of neutron energy spectra.

For the larger set of 128 models, the calculated-over-experimental (C/E) values for the effective multiplication factor were calculated and plotted for

each of the eight different ^{235}U evaluations. The ensemble average C/E and standard deviation were calculated for each set of data. If the ensemble average C/E gets closer to 1.0 and the standard deviation decreases, relative to the base case, the candidate ^{235}U evaluation is judged an improvement.

However, another test is performed on the solution tank HEU and LEU critical experiments to ensure that changes to the resonance parameters and ranges do not introduce problems in the thermal energy range that have been solved by SG18, e.g. C/E trends with above thermal leakage (ATL) or above thermal fission (ATF).

For the special cases of the FCA-IX and ZEUS models, more detailed analysis was performed. In addition to calculating the C/E values for each model, the capture, fission, α, slowing down densities, and ATL and ATF, were also calculated and compared for each case.

2.3.3 Results

A detailed discussion of the results and conclusions of this study is provided in Appendix C. A summary is provided in this section.

In the cases analysed, changing the resolved and unresolved resonances by substituting JENDL-3.2 for ENDF/B-VII.0 in the URR, particularly in the range of 500 eV < E < 2 250 eV, seems to improve the trend of increasing C/E with increasing neutron spectra for the FCA and ZEUS benchmarks analysed. This is best demonstrated by Cases 2 and 3, where there is a large reduction in α. However, these cases also have large increases in ensemble average C/E and increases in the spread of the C/E values within the population. In fact, Cases 2 and 3 cause the largest increase in ensemble average C/E (265 pcm and 283 pcm, respectively).

Relative to the FCA and ZEUS models analysed, Cases 2, 3 and 8 produce the "flattest" trend line when C/E is plotted against the average energy of a neutron causing fission. Unfortunately, all the cases containing the JENDL-3.2 data have unacceptably large trends in the HST/LST population, with C/E increasing with increasing ATLF. This would seem to suggest that only Case 8 is a viable candidate.

Case 8 demonstrates a modest increase in ensemble average C/E (14 pcm) and standard deviation, relative to ENDF/B-VII.0. This case also performs well in the LST/HST C/E versus ATLF analysis, and improves the FCA and ZEUS benchmark results.

Since the focus of this study is on the ^{235}U alpha in the intermediate spectrum, additional ICSBEP intermediate spectrum HEU models should be added to the analysis. In addition to HMI-006 (ZEUS), the ICSBEP handbook lists eight other benchmarks in Volume II, HEU, intermediate-energy metal systems that would complement this study.

2.4 Experiment and benchmark calculation for sodium-void reactivity in uranium-fuelled FBR core at FCA

2.4.1 Introduction

Sodium-void reactivity experiments with uranium fuels were carried out in the Fast Critical Assembly (FCA) at the Japan Atomic Energy Agency (JAEA) in 2009, and new integral data were obtained to help to validate the re-evaluated capture cross-section of ^{235}U. The benchmark specification of the sodium-void reactivity experiments has been prepared and the benchmark calculation results are provided in Appendix B. In the benchmark calculations, detailed benchmark calculations have been performed using a continuous-energy Monte Carlo code, MVP, with geometry models made as detailed as possible. The measured data were analysed with the existing libraries JENDL-3.2, -3.3, -4.0, ENDF/B-VII.0 and JEFF-3.1. This section presents an introduction of new integral data obtained at the FCA, the results of the benchmark calculations and the comparison between them including sensitivity analysis results. In this report, the benchmark specification and the results of the benchmark calculations, which contain the results by deterministic methods with various correction factors, are also given in Appendix B.

2.4.2 Experiment

The FCA XXVII-1 cores which are coupled systems comprising a central core zone and surrounding blanket zones, are used for sodium-void reactivity measurement in uranium-fuelled FBR core. In Figure 2.7, an R-Z cross-sectional view of the fixed half assembly of the XXVII core is given. The core zone is composed of low- and high-enriched uranium metals and graphite. The test zone is set up at the centre of the core zone with changing the height of the test zone as listed in Table 2.8. The test zone is composed of low- and high-enriched uranium metals and sodium cans. The sodium cans at the test zone are replaced by voided steel cans to measure the sodium-void reactivity. For Cases 1 and 2, the reactivities are measured using the control rods that have been calibrated beforehand. For Case 3, the reactivity was measured by adopting the source multiplication method. The experimental results are presented in Table 2.9 together with the measurement uncertainties. The effective delayed neutron fraction β_{eff} (= 0.00754±0.00027) was evaluated with JENDL-3.3. The error of β_{eff} was evaluated by its covariance data of ν_d in JENDL-3.3. One sees that the relative errors were about a few per cents. They were small enough to distinguish the differences of the calculated results among the libraries which were observed in the BFS experiments.

Figure 2.7: R-Z cross-sectional view of XXVII core

Height of test zone $2z_t$ and equivalent radius of core zone r_c are given in Table 2.8

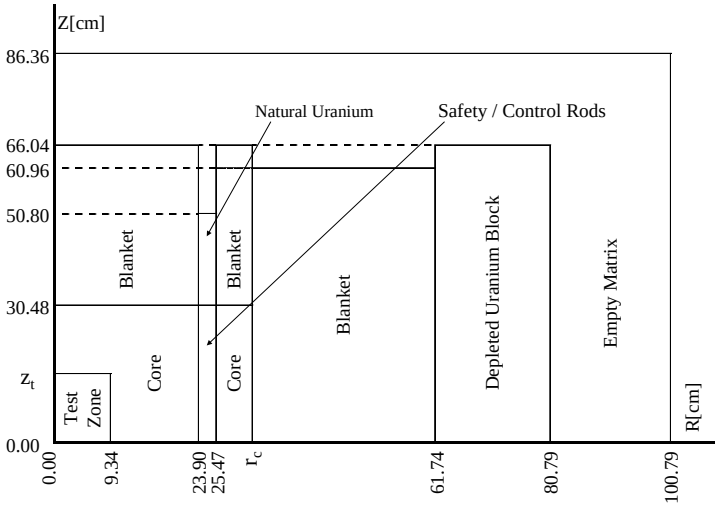

Table 2.8: Core specifications for measurements

Case	Height of test zone ($z_t \times 2$) [cm]	Equivalent radius of test zone [cm]	Equivalent radius of core zone (r_c) [cm]
Case 1	5.08 × 2	9.34	31.30
Case 2	10.16 × 2	9.34	31.45
Case 3	15.24 × 2	9.34	31.45

Table 2.9: Experimental results for sodium-void reactivity

Case	Sodium-void reactivity [× 10^{-3}dk/kk']	
Case 1	-0.40	±0.02*
Case 2	-0.80	±0.03*
Case 3	-1.22	±0.08*

* Experimental errors

2.4.3 Benchmark calculation

The benchmark calculations are performed by deterministic and Monte Carlo methods.

Calculations by a continuous-energy Monte Carlo code, MVP-II, are performed with geometry models made as detailed as possible. The reactivities are obtained from $(k'_{eff} - k_{eff})/k_{eff}k'_{eff}$, where k_{eff} and k'_{eff} are the effective multiplication factors of the reference and perturbed cores in

which the sodium cans and voided steel cans are placed at the test zone, respectively. The MVP calculations are performed with 2 000 000 000 particles. The statistical uncertainties of the MVP calculations are within several per cents of the measured sodium-void reactivities.

The deterministic calculation codes are the following:

Cell calculation	SLAROM-UF
Core calculation	CITATION-FBR (diffusion)
	TRITAC (S_N transport)
Perturbation calculation	PERKY (diffusion)
	SNPERT-3D (S_N transport)

The core calculation by the diffusion theory can be performed by using homogeneous XYZ models with homogenised cell atomic number densities which are obtained by smearing cell heterogeneous plate arrangements. The calculation results can be compared with the experimental results by applying correction factors. The correction factors were prepared for JENDL-3.2, -3.3, -4.0, ENDF/B-VII.0 and JEFF-3.1 and are summarised in Appendix B.

A summary of Monte Carlo calculations together with deterministic calculation results is presented in Figure 2.8. The corrected results by the deterministic calculations agree with the Monte Carlo calculation results within 3σ of statistical uncertainties. One understands from this table that the C/E values of sodium-void reactivities with respect to JENDL-3.3, ENDF/B-VII.0 and JEFF-3.1 are less than those with respect to JENDL-3.2 and -4.0. This tendency of the C/E values is similar to those for the sodium-void reactivity experiments using uranium fuels at the BFS facility. In BFS cores with uranium fuels, the sodium-void reactivities were sensitive to the ^{235}U capture cross-sections at the keV energy region, where a big difference exists among major nuclear data libraries.

A sensitivity analysis was carried out to investigate the differences among the libraries. The sensitivity coefficients were calculated based on the diffusion theory using a generalised perturbation code, SAGEP, and the JENDL-4.0 library. Here, a homogeneous model was adopted. Figure 2.9 shows sensitivity coefficients of the sodium-void reactivities to ^{235}U capture cross-section. For all cases, the reactivities are sensitive in the keV energy region of ^{235}U capture cross-section.

Figure 2.10 shows energy-wise contribution of ^{235}U capture cross-section to the sodium-void reactivity change from JENDL-4.0 to other libraries for Case 2. We find that the differences with respect to JEFF-3.1, JENDL-3.3 and ENDF/B-VII.0 are much larger than that with respect to JENDL-3.2. Figure 2.11 shows nuclide-wise contributions to the sodium-void reactivity change from JENDL-4.0 to other libraries. We further find that the difference of ^{235}U capture cross-sections contributes mainly to the sodium-void

reactivity change. The total differences from JENDL-4.0 to JENDL-3.3, ENDF/B-VII.0 and JEFF-3.1 are up to about 28%, 33% and 24%, respectively. The tendency is consistent with the results by the benchmark calculations. It was clarified that the main cause explaining the difference among libraries was the capture cross-section of ^{235}U.

Figure 2.8: Summary of calculated sodium-void reactivities

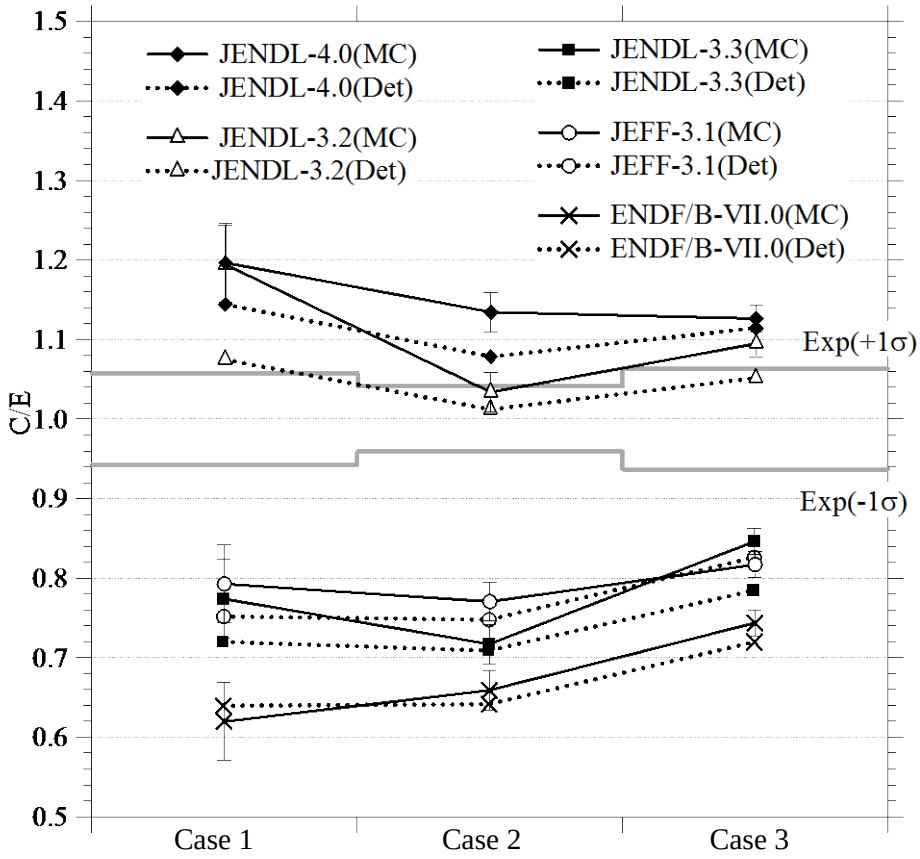

Figure 2.9: Sensitivity of sodium-void reactivity to ^{235}U capture cross-section

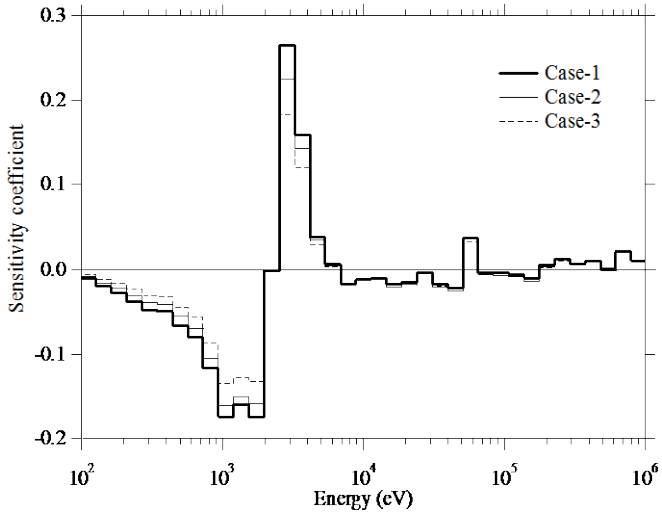

Figure 2.10: Energy-wise contribution of ^{235}U capture cross-section to sodium-void reactivity change for Case 2

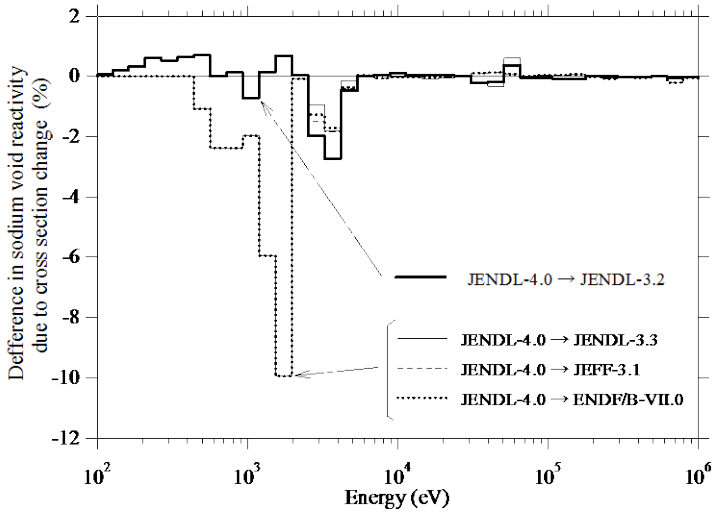

Figure 2.11: Nuclide-wise contribution to sodium-void reactivity change for Case 2

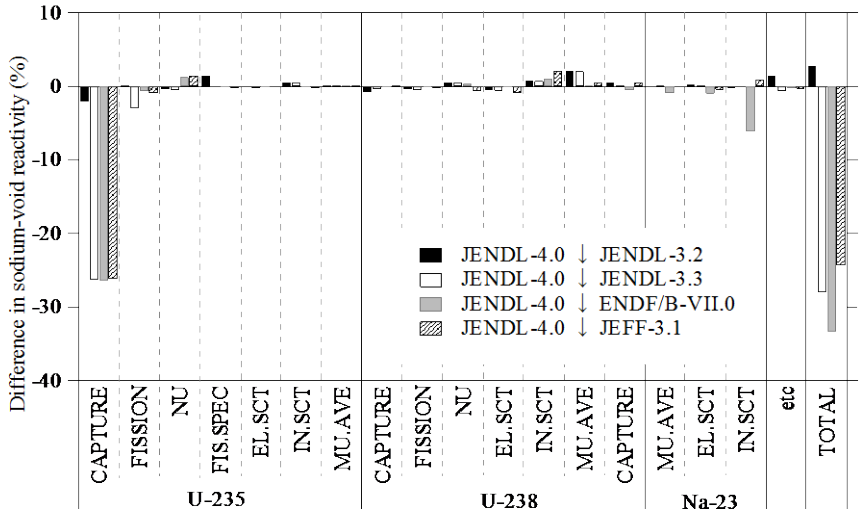

3. Conclusion

The possible overestimation of ^{235}U capture cross-section in the 0.1 to 2.5 keV range is consistent with the alpha measurement and the integral experiments of Na-void reactivity of BFS and FCA, and the criticality trends of FCA and ZEUS. The new FCA experiments were described better with JENDL-3.2 and JENDL-4.0, which have lower ^{235}U capture cross-sections around 1 keV than other libraries. The magnitude of the overestimation could be ~10% or more. However, the problem of overestimating FCA criticalities remains. It may be needed to consider the other contributions.

It is recommended: *i)* to measure accurate alpha measurement in the keV region; *ii)* to perform new resonance analysis in the 0.1 to 2.5 keV region; *iii)* to investigate the reason for the overestimation of criticalities for some benchmarks.

References

[1] Chiba, G., *et al.*, *Integral Test of JENDL-3.3 for Fast Reactors*, JAERI-Conf 2003-006, p. 22 (2003).

[2] Okajima, S., *et al.*, "Benchmark Test for JENDL-3.3 Library by Analyses of a Series of Experiments at the Fast Critical Assembly (FCA) of JAERI", *Proc. of ND2004*.

[3] Fukushima, M., *et al.*, "Benchmark Calculations of Sodium-void Experiments with Uranium Fuels at the Fast Critical Assembly FCA", *Proc. Joint Int. Conf. on Supercomputing in Nuclear Applications and Monte Carlo 2010 (SNA + MC2010)*, Hitotsubashi Memorial Hall, Tokyo, Japan, 17-21 October 2010, *Progress in Nuclear Science and Technology*, Vol. 2 (2011).

Appendix A. Impact of JENDL-3.2 and ENDF/B-VII.0 resonance region (resolved and unresolved) in intermediate-energy benchmark calculations

O. Iwamoto, G. Chiba, T. Nakagawa, L. Leal

Introduction

The ^{235}U ENDF/B-VII.0 evaluation performs very well for thermal and fast reactor benchmark systems. However, for benchmark systems with neutron spectrum in the intermediate-energy region (few electron volts to few million electron volts range) there are still some trends not yet understood. The aim of this note is to investigate the source of the biases in the calculations. The work will consist of intermediate benchmark calculations using JENDL-3.2 and ENDF/B-VII.0 and sensitivity calculations.

Comparisons of cross-sections in JENDL-3.2 and ENDF/B-VII.0

Results of calculations of intermediate-energy benchmark experiments indicate that JENDL-3.2 performs better than ENDF/B-VII.0. It appears that the observed biases in the system multiplication factor (k_{eff}) are related to the capture cross-sections in the resolved resonance (RRR) and unresolved resonance (URR) regions. Figures A.1(a) through A.1(d) show, respectively, comparisons of the cross-sections for JENDL-3.2, ENDF/B-VII.0 and statistical model calculations.

It can be seen that the ENDF/B-VII.0 capture cross-section is much larger than JENDL-3.2 and statistical model calculations in the range of about 100 eV to 3 keV. Discrepancies are also found in the elastic scattering cross-sections below 30 keV. The total and fission cross-sections have no such noticeable discrepancies. Figure A.2 displays a comparison of capture/fission ratio for ENDF/B-VII.0 and JENDL-3.2.

Figure A.1(a): Comparison of capture cross-sections

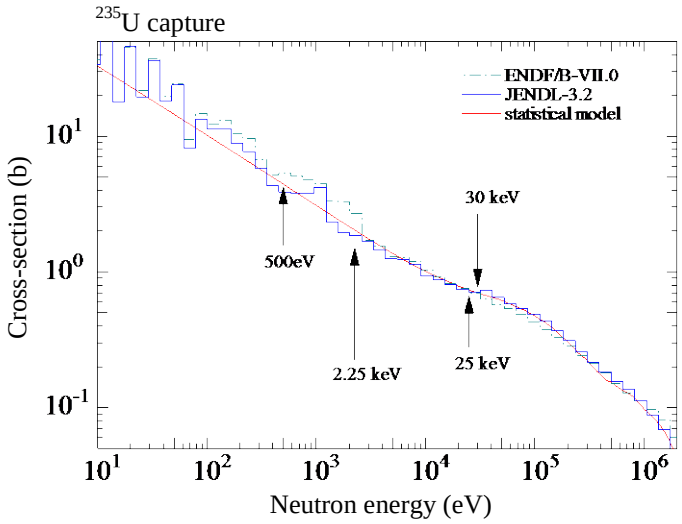

Figure A.1(b): Comparison of fission cross-sections

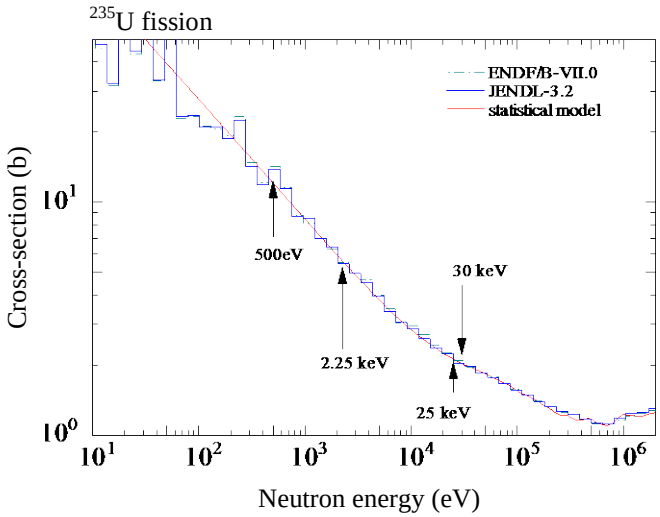

Figure A.1(c): Comparison of elastic scattering cross-sections

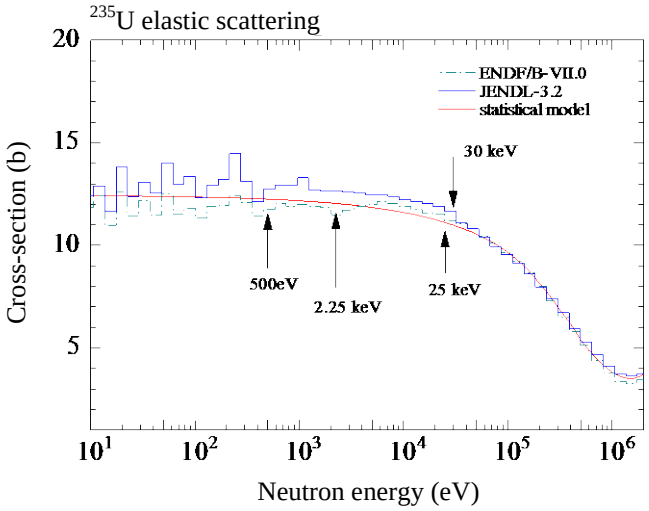

Figure A.1(d): Comparison of total cross-sections

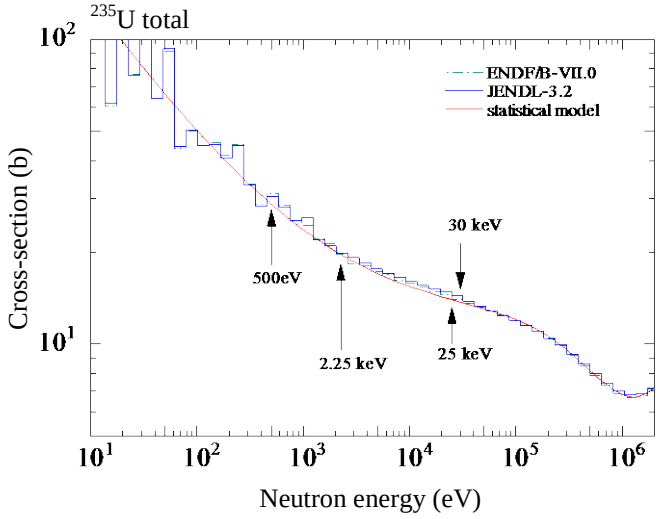

Figure A.2: Comparison of α values

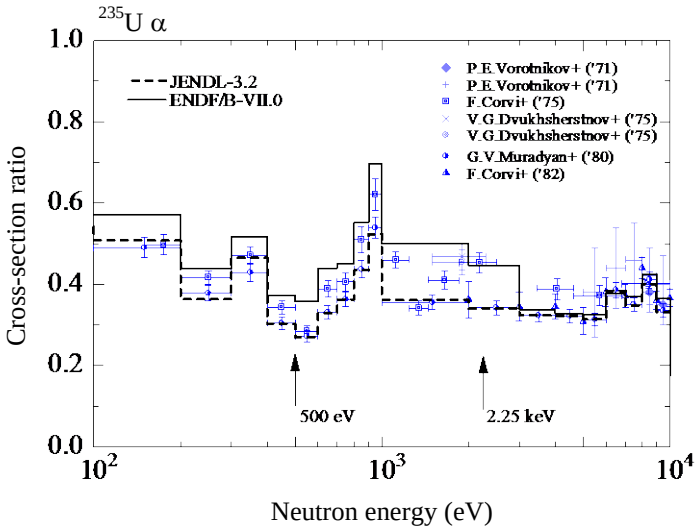

The capture/fission ratio of ^{235}U is sensitive to its derivation method. It can be calculated with the following two methods:

Method 1	$\langle\alpha\rangle_i = \frac{1}{(E_{i+1} - E_i)} \int_{E_i}^{E_{i+1}} \frac{\sigma_c(E)}{\sigma_f(E)} dE$
Method 2	$\langle\alpha\rangle_i = \frac{\langle\sigma_c\rangle_i}{\langle\sigma_f\rangle_{ii}}$

Figure A.2 shows the data calculated with Method 2, and only experimental data which seem to have been measured with Method 2. Method 1 gives cross-sections larger than Method 2.

The ENDF/B-VII.0 α results are in the upper part of the experimental results. However, JENDL-3.2 agrees well with the experimental results.

JENDL-3.2 and ENDF/B-VII.0 resonance parameters combinations

Preliminary sensitivity calculations have indicated that a reduction in the capture cross-section of ^{235}U is needed. However, in addition to the difference in the resonance representation in the two libraries there may be other quantities that may also have an effect on the benchmark results. Therefore, to better understand the reason why the two libraries perform differently, it has been decided to carry out benchmark calculations by merging JENDL resonance parameters in ENDF and *vice versa*. There are

quite a few possible combinations. Table A.1 displays the resolved and unresolved energy regions for JENDL and ENDF.

Table A.1: Resonance energy range for JENDL-3.2 and ENDF/B-VII.0

Resonance region	JENDL-3.2	ENDF/B-VII.0
RRR	10^{-5} eV-500 eV	10^{-5} eV-2.25 keV
URR	500 eV-30 keV	2.25 keV-25 keV

The benchmark systems used to study the different ENDF and JENDL combinations were four intermediate benchmark experiments taken at the Los Alamos National Laboratory (LANL) and three benchmark experiments done at the Japan Atomic Energy Agency (JAEA). The energies of the average lethargy causing fission for these benchmarks are shown in Table A.2. Also shown in Table A.2 are the specifications of these benchmarks as given in the International Handbook of Evaluated Criticality Benchmark Experiments (ICSBEP).

Table A.2: Energy of the average lethargy causing fission (AVG)

Name	Spectrum	Handbook ID	AVG (keV)
ZEUS1	Intermediate	HEU-MET-INTER-006, case1	5.05
ZEUS2	Intermediate	HEU-MET-INTER-006, case2	10.33
ZEUS3	Intermediate	HEU-MET-INTER-006, case3	24.02
ZEUS4	Intermediate	HEU-MET-INTER-006, case4	
FCA-IX-1	Intermediate		29.90
FCA-IX-2	Intermediate		116.52
FCA-IX-3	Intermediate		211.30

The following are possible JENDL-ENDF resonance parameter combinations that are expected to provide a better understanding in the bias in k_{eff} due to the ^{235}U capture cross-sections. The study consisted of keeping one cross-section library as reference and replacing its resonance parameter representation. They are done as follows:

Keeping JENDL-3.2 for ^{235}U as the reference library

Case 1: JENDL-3.2 resolved resonance parameters replaced with the ENDF/B-VII.0 parameters up to 2.25 keV

The calculation was done with everything else taken from JENDL-3.2. This calculation will be referred to as Case 1.

Note that the JENDL unresolved representation from 500 eV to 2.25 keV will also be replaced with ENDF resolved resonance parameters. This can be seen from Table A.3. From 2.25 keV to 30 keV the JENDL unresolved representation is used.

Table A.3: Resonance energies for the merged library (Case 1)

500 eV	2.25 keV	25 keV	30 keV
RR (ENDF)	RR (ENDF)	UR (JENDL)	UR (JENDL)

Thermal values and integral quantities integrated over the microscopic cross-section for the JENDL and the modified library is shown in Table A.4. These quantities are total nu (ν_t), thermal (0.0253 eV) capture cross-section (σ_γ), resonance integral (I_x), Wescott g-factors (g_x, where x can be gamma, fission or absorption), capture-to-fission resonance integral ratio (α), and K_1. The resonance integrals were calculated in the energy range from 0.5 eV to 25 keV. The cross-sections and resonance integral units are in barns. The JENDL resonance capture integral is about 5% smaller than that of the modified library. JENDL-3.2 calculates a smaller capture-to-fission ratio.

Table A.4: Thermal and integral quantities for JENDL-3.2 and modified library

Integral quantity	JENDL-3.2	Modified library
ν_t	2.4359	2.4359
σ_γ	98.818	98.706
I_γ	131.5	138.9
g_γ	0.9897	0.9912
σ_f	584.321	585.076
I_f	268.3	266.1
g_f	0.9789	0.9767
σ_a	683.14	683.781
I_a	399.8	405.0
g_a	0.9805	0.9788
α	0.4901	0.5277
K_1	723.50	722.69

The merged library was used in the calculation of the three FCA benchmarks. The C/E results are shown in Figure A.3, as are the results of calculations using ^{235}U and everything else from the JENDL-3.2 library. The figure indicates that the biases in the FCA remain.

Case 2: JENDL-3.2 resolved resonance parameters replaced with the ENDF/B-VII.0 parameters only up to 500 eV

The calculation was done with everything else taken from JENDL-3.2. This calculation will be referred to as Case 2.

Only the contribution of the ENDF/B-VII.0 resolved resonance parameters up to 500 eV will be taken into account in the benchmark calculations. The unresolved representation is from JENDL. From 500 eV to 30 keV the JENDL unresolved representation is used. This can be seen from Table A.5.

Figure A.3: C/E results for Case 1

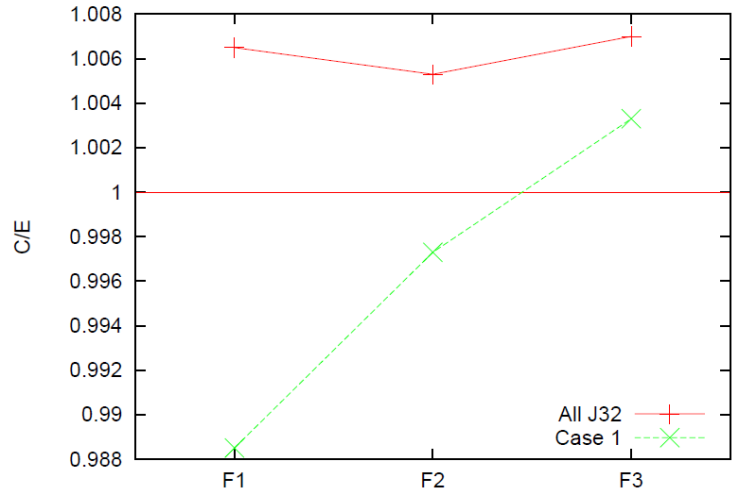

Table A.5: Resonance energies for the merged library (Case 2)

500 eV	2.25 keV	25 keV	30 keV
RR (ENDF)	UR (JENDL)	UR (JENDL)	UR (JENDL)

Thermal values and integral quantities integrated over the microscopic cross-section for the JENDL and the modified library is shown in Table A.6. The JENDL resonance capture integral is about 4% smaller than that of the modified library.

Table A.6: Thermal and integral quantities for JENDL-3.2 and modified library

Integral quantity	JENDL-3.2	Modified library
ν_t	2.4359	2.4359
σ_γ	98.818	98.706
I_γ	131.5	137.2
g_γ	0.9897	0.9912
σ_f	584.321	585.076
I_f	268.3	266.1
g_f	0.9789	0.9767
σ_a	683.14	683.781
I_a	399.8	403.3
g_a	0.9805	0.9788
α	0.4901	0.5156
K_1	723.50	722.69

The merged library was used in the calculation of the three FCA benchmarks. The C/E results are shown in Figure A.4, as are the results of calculations using only the JENDL-3.2 library and the Case 1 results. The figure indicates some improvement for the FCA-IX-2 and FCA-IX-3 benchmarks. However, the trend in the biases still remains.

Figure A.4: C/E results for Case 2

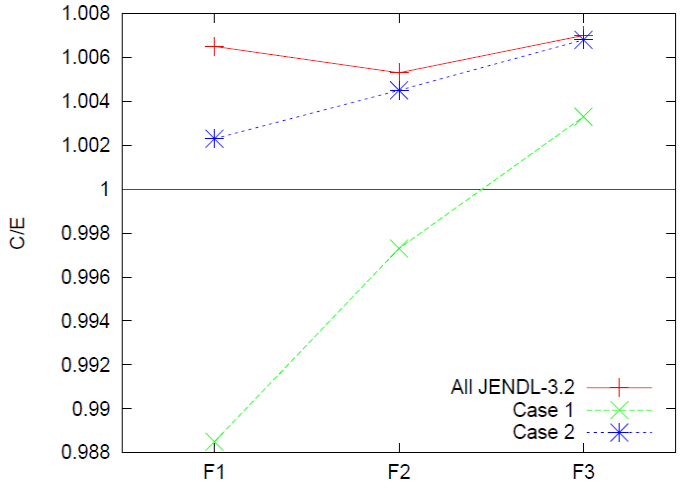

Keeping ENDF/B-VII.0 as the reference library

Case 3: ENDF/B-VII.0 resolved and unresolved parameters are replaced with JENDL-3.2 parameters

The calculation was done with everything else taken from the ENDF/B-VII.0. This calculation will be referred to as Case 3.

Although the unresolved resonance for JENDL-3.2 goes up to 30 keV it was used only up to 25 keV. This can be seen from Table A.7.

Table A.7: Resonance energies for the merged library (Case 3)

	500 eV	2.25 keV	25 keV	30 keV
RR (JENDL)	UR (JENDL)	UR (JENDL)	ENDF FILE 3	

Thermal values and integral quantities integrated over the microscopic cross-section for ENDF/B-VII.0 and the modified library is shown in Table A.8. The modified resonance capture integral is about 5% smaller than that of ENDF/B-VII.0.

The merged library was used in the calculation of the three FCA and the ZEUS benchmarks. The C/E results are shown in Figure A.5, as is the result of calculations using only the ENDF/B-VII.0 library.

Table A.8: Thermal and integral quantities for ENDF/B-VII.0 and modified library

Integral quantity	ENDF/B-VII.0	Modified library
ν_t	2.4367	2.4367
σ_γ	98.706	98.818
I_γ	139.0	131.5
g_γ	0.9912	0.9897
σ_f	585.076	584.321
I_f	266.2	268.3
g_f	0.9767	0.9789
σ_a	683.781	683.14
I_a	405.2	399.8
g_a	0.9788	0.9805
α	0.5222	0.4901
K_1	723.15	723.95

Figure A.5: C/E results for Case 3

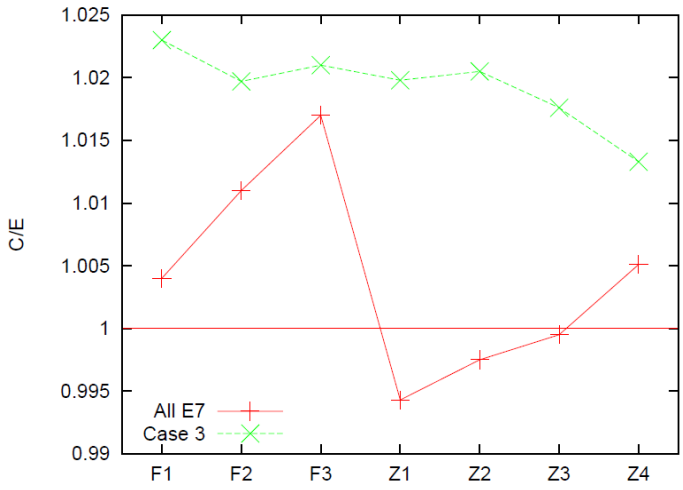

The results shown in Figure A.5 suggest an improvement on the biases for the FCA and ZEUS benchmarks when the JENDL-3.2 resonance representations (resolved and unresolved) are used in ENDF/B-VII.0. However, Figure A.5 also shows an increase in the calculated multiplication factor. This can be an indication that there exists another energy region which also contributes to the multiplication factor. These cases require further investigation.

Case 4: ENDF/B-VII.0 resolved resonance parameters up to 500 eV are replaced with JENDL-3.2

The calculation was done with everything else taken from ENDF/B-VII.0. This calculation will be referred to as Case 4. Note that the ENDF/B-VII.0 resolved resonance parameters from 500 eV to 2.25 keV will be used. This can be seen from Table A.9.

Table A.9: Resonance energies for the merged library (Case 4)

	500 eV	2.25 keV	25 keV	30 keV
RR (JENDL)	RR (ENDF)	UR (ENDF)	ENDF FILE 3	

Thermal values and integral quantities integrated over the microscopic cross-section for ENDF/B-VII.0 and the modified library are shown in Table A.10. The modified resonance capture integral is about 4% smaller than that of ENDF/B-VII.0.

Table A.10: Thermal and integral quantities for ENDF/B-VII.0 and modified library

Integral quantity	ENDF/B-VII.0	Modified library
ν_t	2.4367	2.4367
σ_γ	98.706	98.818
I_γ	139.0	133.3
g_γ	0.9912	0.9897
σ_f	585.076	584.321
I_f	266.2	268.5
g_f	0.9767	0.9789
σ_a	683.781	683.14
I_a	405.2	401.8
g_a	0.9788	0.9805
α	0.5222	0.4965
K_1	723.15	723.95

The merged library was used in the calculation of the three FCA and the ZEUS benchmarks. The C/E results are shown in Figure A.6, as are the results of calculations using only the ENDF/B-VII.0 library and Case 3.

It appears that including the resonance parameters of JENDL-3.2 in ENDF/B-VII.0 leads to an improvement in the biases, mainly for ZEUS.

Figure A.6: C/E results for Case 4

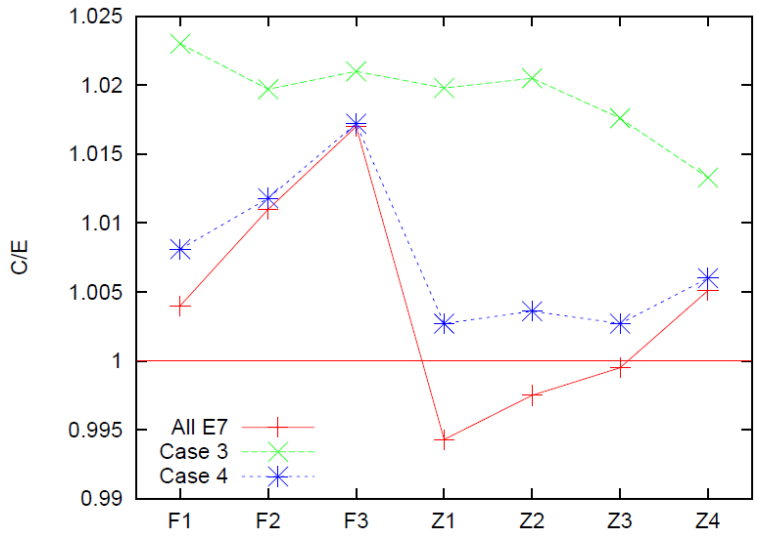

Case 5: ENDF/B-VII.0 resolved resonance parameter from 500 eV to 2.25 keV replaced with the JENDL-3.2 unresolved parameters

The calculation was done with everything else taken from ENDF/B-VII.0. This calculation will be referred to as Case 5. Table A.11 displays the resonance region representation in the modified library.

Table A.11: Resonance energies for the merged library (Case 5)

	500 eV	2.25 keV	25 keV	30 keV
RR (ENDF)	UR (JENDL)	UR (ENDF)	ENDF FILE 3	

Thermal values and integral quantities integrated over the microscopic cross-section for ENDF/B-VII.0 and the modified library are shown in Table A.12. The modified resonance capture integral is about 1.2% smaller than that of ENDF/B-VII.0.

The merged library was used in the calculation of the three FCA and ZEUS benchmarks. The C/E results are shown in Figure A.7, as are the results of calculations using only the ENDF/B-VII.0 library, Cases 3 and 4.

Table A.12: Thermal and integral quantities for ENDF/B-VII.0 and modified library

Integral quantity	ENDF/B-VII.0	Modified library
ν_t	2.4367	2.4367
σ_γ	98.706	98.706
I_γ	139.0	137.3
g_γ	0.9912	0.9912
σ_f	585.076	585.076
I_f	266.2	266.2
g_f	0.9767	0.9767
σ_a	683.781	683.781
I_a	405.2	403.5
g_a	0.9788	0.9788
α	0.5222	0.5158
K_1	723.15	723.15

Figure A.7: C/E results for Case 5

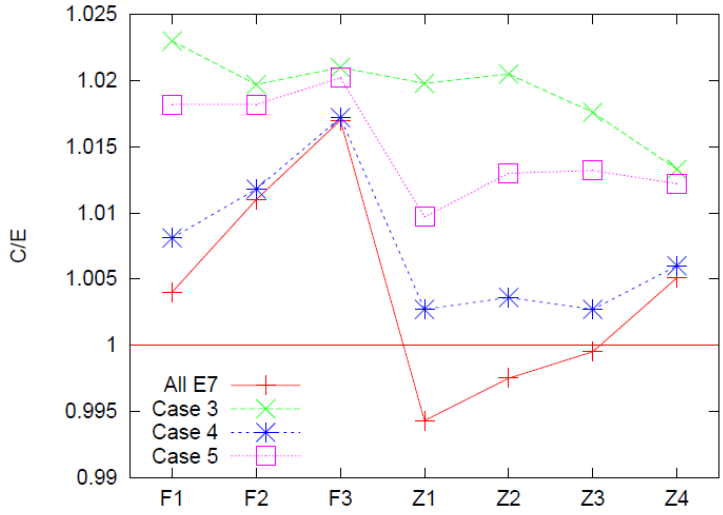

From the above studies, it has been found that a difference between ENDF/B-VII.0 and JENDL-3.2 from 500 eV to 2.25 keV has a large impact on both the FCA-IX and ZEUS calculations, while a difference below 500 eV has an impact only on the ZEUS calculations.

Replacement of the ENDF/B-VII.0 resonance parameters by JENDL-3.2 for ^{235}U makes the C/E dependence on spectrum hardness smaller. However, this also results in unacceptably high C/E values. This can be an indication that there exists another energy region which also contributes to the multiplication factor. These cases need further investigation.

Effects on the reduction of the ^{235}U gamma width above 200 eV

Comparison of the JENDL-3.2 capture cross-section with the ENDF/B-VII.0 capture cross-section indicates a smaller value of the capture cross-section for JENDL mainly above 200 eV. A study has been conducted which consists of decreasing the gamma (Γ_γ) width in the ^{235}U resolved resonance parameters of the ENDF/B-VII.0 by 3% and 10% and performing benchmark calculations. The results of calculations performed with two modified libraries are shown in Figure A.8. The case labelled "G1" corresponds to a change of 3% in Γ_γ (decrease of 2% in σ_γ and increase of 1% in σ_f), whereas the 10% change in Γ_γ (decrease of 7% in σ_γ and increase of 3% in σ_f) is labelled "G2". The reference case, labelled "Ref" in the figure, corresponds to calculations using ENDF/B-VII.0. The calculations were done for the FCA and ZEUS benchmark experiments. Clearly, a simple decrease in the capture cross-section, i.e. in Γ_γ, reduces the C/E dependence on spectrum hardness. However, it scales the k_{eff} up. These results may indicate that other cross-sections or combinations of effects may be causing the biases.

Figure A.8: Benchmark calculations for 3% and 10% change in gamma width

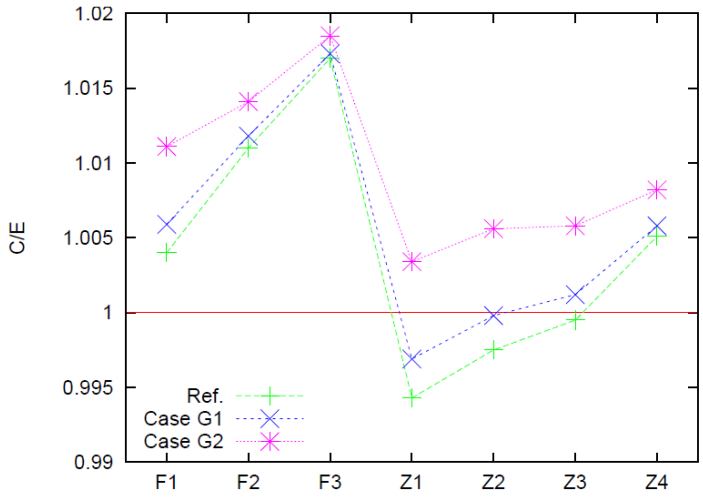

Sensitivity study of the benchmarks experiments FCA and ZEUS

Detailed neutron balance analyses of FCA and ZEUS were done to identify and understand the k_{eff} bias for these systems. The calculations were done with a two-dimensional discrete ordinates code using a 70-group cross-section library based on ENDF/B-VII.0. Without loss of generality, the k_{eff} can be written as the neutron production divided by absorption and leakage which in the diffusion approximation is given as:

$$k_{eff} = \frac{< \nu\Sigma_f\phi > + < \Sigma_{n2n}\phi >}{< \Sigma_a\phi > + < DB^2\phi >} \quad (1)$$

In this equation D is the diffusion coefficient and B is the buckling which relates to reactor size. The detailed study consisted of calculating each component of Eq. (1) for each energy group.

Both the ZEUS and the FCA benchmarks utilise highly-enriched uranium with enrichment of 93%. In the ZEUS cores the fuel region is surrounded by copper which is used as a reflector. In the FCA benchmark the core is surrounded by depleted uranium with 0.3% enrichment. The results of calculation of each component in Eq. (1) are given in Table A.13. The total fission production has been normalised to one.

Table A.13 indicates that the leakages for the ZEUS benchmark experiments are on the average of 28% whereas in the FCA it is about 4%. The contribution of each component to k_{eff} for the ZEUS and FCA benchmark experiments are different from each other.

Table A.13: Contribution to k_{eff} by its components

Core	Production		(n,2n)	Absorption		Leakage
	Fuel	Blanket		Fuel	Blanket	
ZEUS1	1.000		0.000	0.566	0.201	0.247
ZEUS2	1.000		0.000	0.552	0.188	0.276
ZEUS3	1.000		0.000	0.534	0.169	0.306
ZEUS4	1.000		0.001	0.504	0.142	0.358
FCA1	0.872	0.128	0.002	0.481	0.478	0.041
FCA2	0.846	0.154	0.003	0.436	0.524	0.040
FCA3	0.832	0.168	0.003	0.413	0.549	0.034

The contribution of each component to k_{eff} for the ZEUS and FCA benchmark experiments are displayed in Figures A.9 to A.15, respectively. The vertical lines indicate the boundary of the resolved resonance region (2.25 keV) and unresolved resonance region (25 keV) for ENDF/B-VII.0.

We carry out the same calculations with an ENDF/B-VII.0-based library in which ^{235}U and ^{238}U are replaced by JENDL-3.2. From Figures A.16 to A.18, component-wise contribution to k_{eff} for FCA-IX-3, in which a large difference is observed between JENDL3-2 and ENDF/B-VII.0, is shown. We can see a significant difference in the leakage contribution, which is caused by a difference in P1 elastic scattering cross-sections of ^{238}U.

Figure A.9: Production, absorption and leakage contribution to k_{eff} for ZEUS1

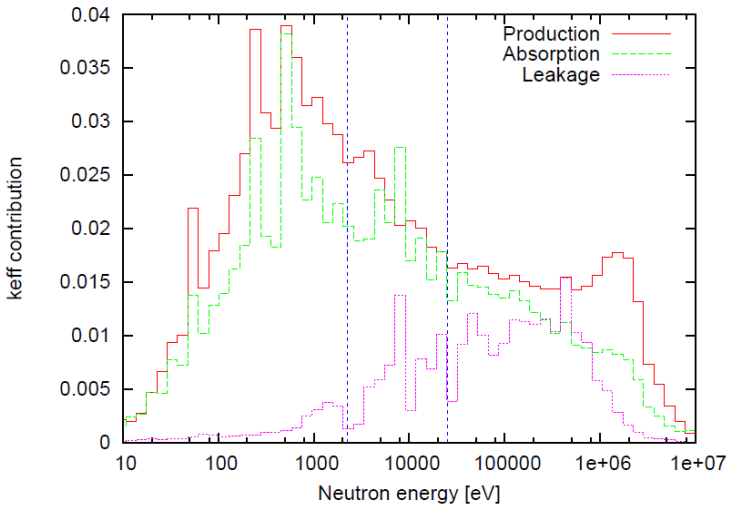

Figure A.10: Production, absorption and leakage contribution to k_{eff} for ZEUS2

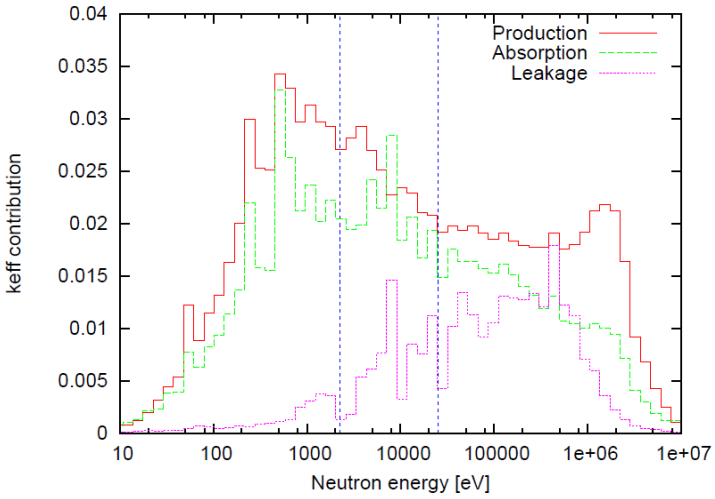

Figure A.11: Production, absorption and leakage contribution to k_{eff} for ZEUS3

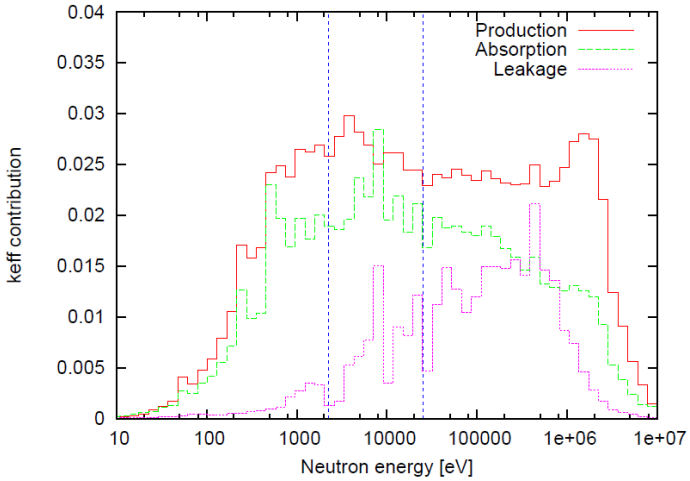

Figure A.12: Production, absorption and leakage contribution to k_{eff} for ZEUS4

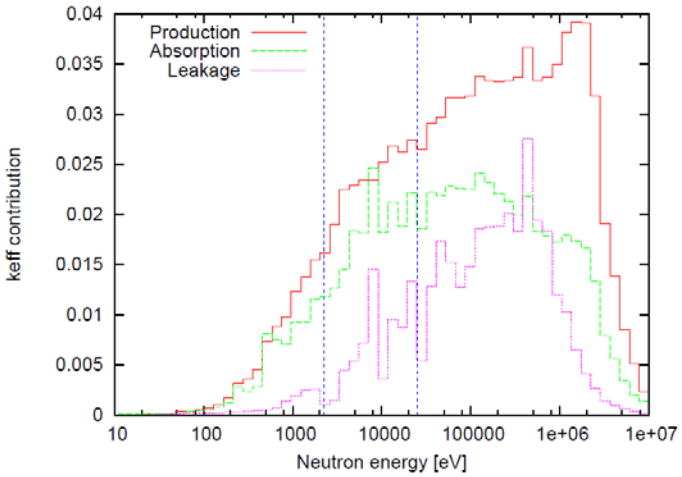

Figure A.13: Production, absorption and leakage contribution to k_{eff} for FCA-IX-1

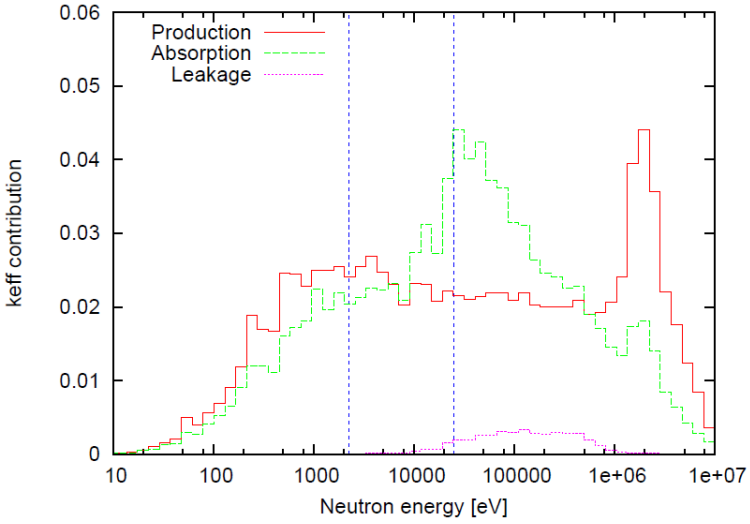

Figure A.14: Production, absorption and leakage contribution to k_{eff} for FCA-IX-2

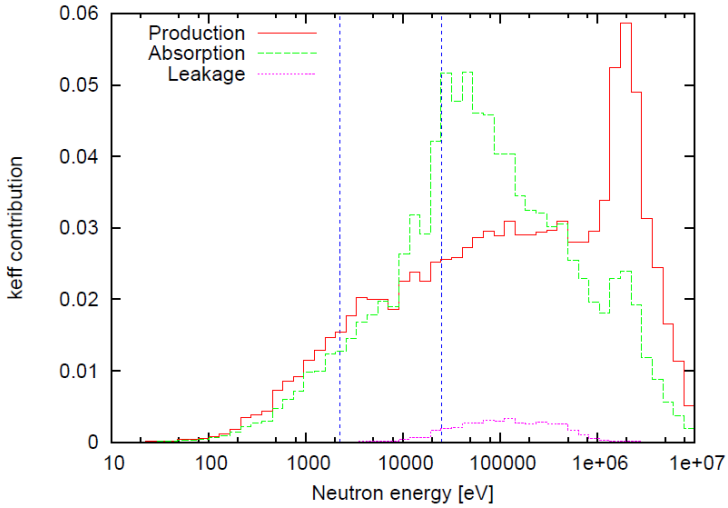

Figure A.15: Production, absorption and leakage contribution to k_{eff} for FCA-IX-3

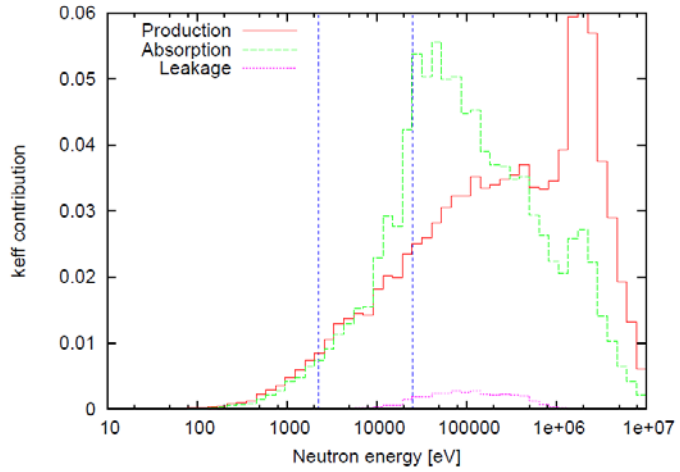

Figure A.16: Production contribution to k_{eff} for FCA-IX-3

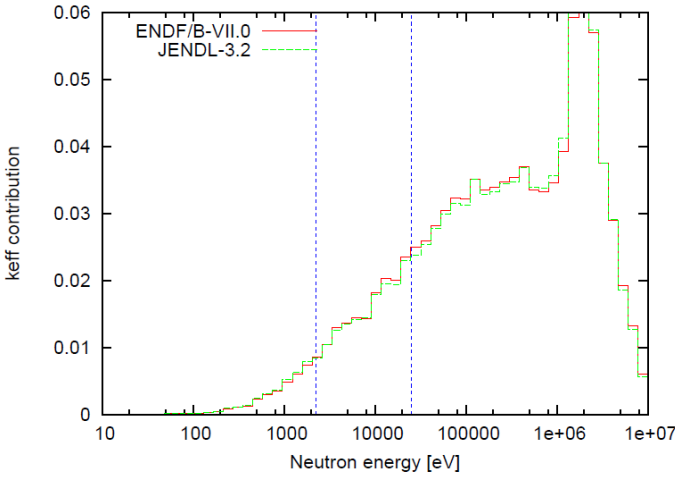

Figure A.17: Absorption contribution to k_{eff} for FCA-IX-3

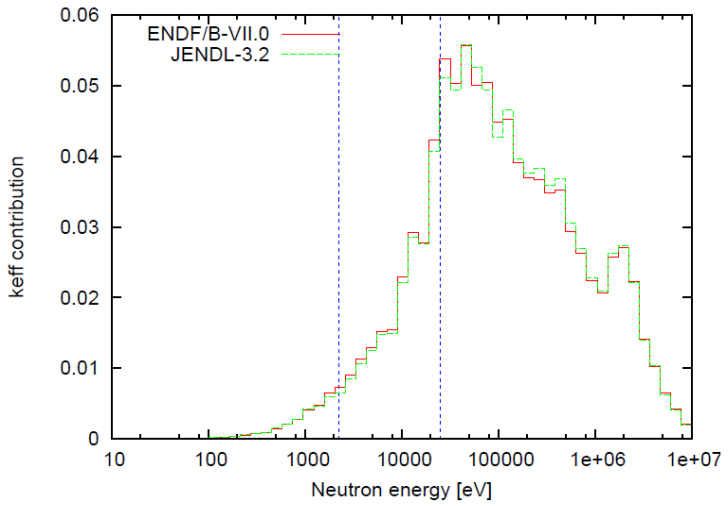

Figure A.18: Leakage contribution to k_{eff} for FCA-IX-3

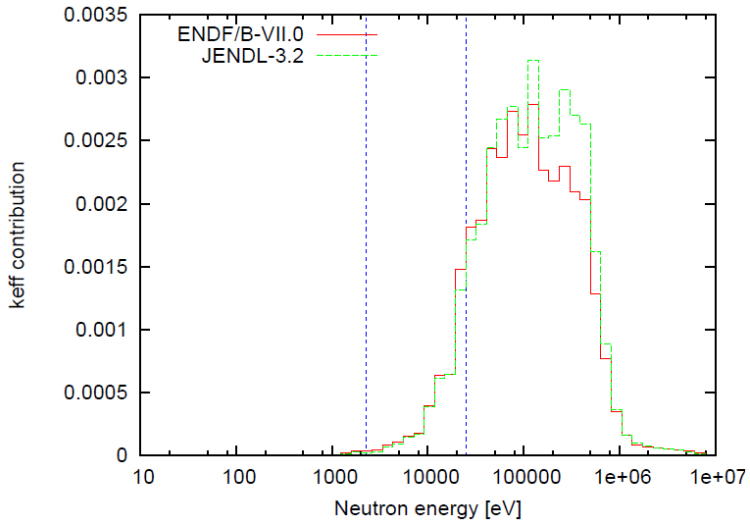

Adjustment of ^{235}U cross-section using several integral data

Nuclear data adjustment for ^{235}U of ENDF/B-VII.0 is carried out using a set of integral data: a series of FCA-IX (3 data), a series of ZEUS (4 data), Godiva and HEU-SOL-THERM-001 (HST001) in the ICSBEP handbook. Figure A.19 shows sensitivity profiles of ^{235}U capture cross-sections to criticalities of

these integral data. It is found that these integral data are sensitive to the ^{235}U nuclear data and have different energy spectra with each other. Using these integral data, the ^{235}U cross-section is optimised with the cross-section adjustment technique.

Figure A.19: Sensitivity profiles of ^{235}U capture cross-section to criticalities

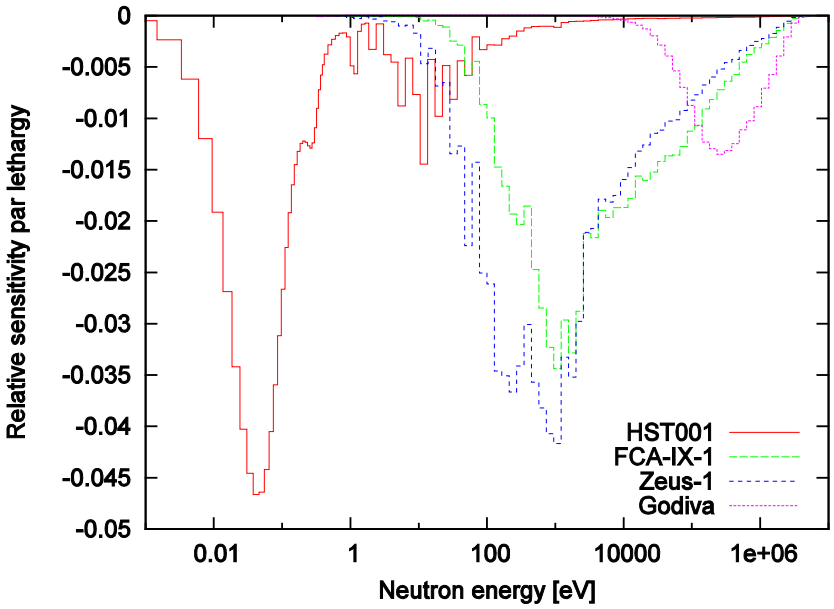

C/E values and experimental uncertainties are assumed to be 1.0 and 0.0001 for Godiva and HST001 since we do not want to change the nuclear data in the high energy range and the thermal energy range through the adjustment. C/E values of FCA-IX and ZEUS are obtained from calculations with the continuous-energy Monte Carlo code and the ENDF/B-VII.0 library. Uncertainties of experimental values of FCA-IX and ZEUS are assumed as follows:

- *Case 1*: The uncertainties are 0.1% dk/kk′ and the correlations among the data of the same critical assembly (FCA-IX or ZEUS) are 0.8.
- *Case 2*: The uncertainties are 1.0% dk/kk′ and the correlations among the data of the same critical assembly are 0.95.

The assumption of Case 1 is realistic while some unknown systematic uncertainties are assumed in Case 2.

We use the covariance data for the ^{235}U nuclear data evaluated by Shibata [1]. Please note that correlation between the thermal range and the resonance range is not given in this covariance data. Since the covariance data is provided only for ^{235}U, only the ^{235}U nuclear data is adjusted.

Figure A.20 shows C/E values before and after the adjustment. C/E values for Godiva and HST001 are not shown since these are unchanged through the adjustment. Changes in nuclear data through the adjustment are also shown in Figures A.21 to A.25, as are standard deviations.

In both cases, the ^{235}U capture cross-section from 200 eV to 7 keV is reduced by 5% to 10%. This suggests the overestimation of the ^{235}U capture cross-section of ENDF/B-VII.0 in this energy range.

Case 1 gives good agreement between C- and E-values. As shown in Figure A.21, however, the ^{235}U capture cross-section above 10 keV is increased about 15% through the adjustment. This cross-section change is larger than two times the standard deviation and is unrealistic. In addition, other nuclear data, such as the inelastic scattering cross-section and fission spectrum, are also significantly changed through the adjustment.

In the Case 2 result, core dependence of C/E values almost disappears, while C/E values are not close to unity. The nuclear data change through the adjustment is considered reasonable as shown in the figures.

The above calculations have allowed determining that something causes systematic overestimation of the C/E values of FCA-IX. The absolute C/E values should be discarded and only the core dependence of C/E values should be concentrated on in the discussions on the ^{235}U capture cross-section issue.

Figure A.20: C/E values before and after adjustment

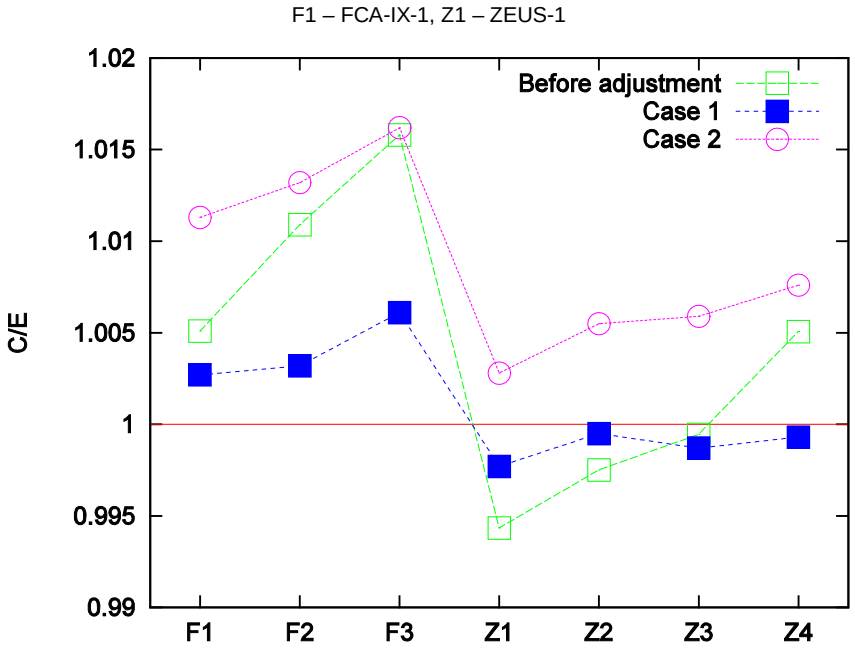

Figure A.21: Change in ^{235}U capture cross-sections

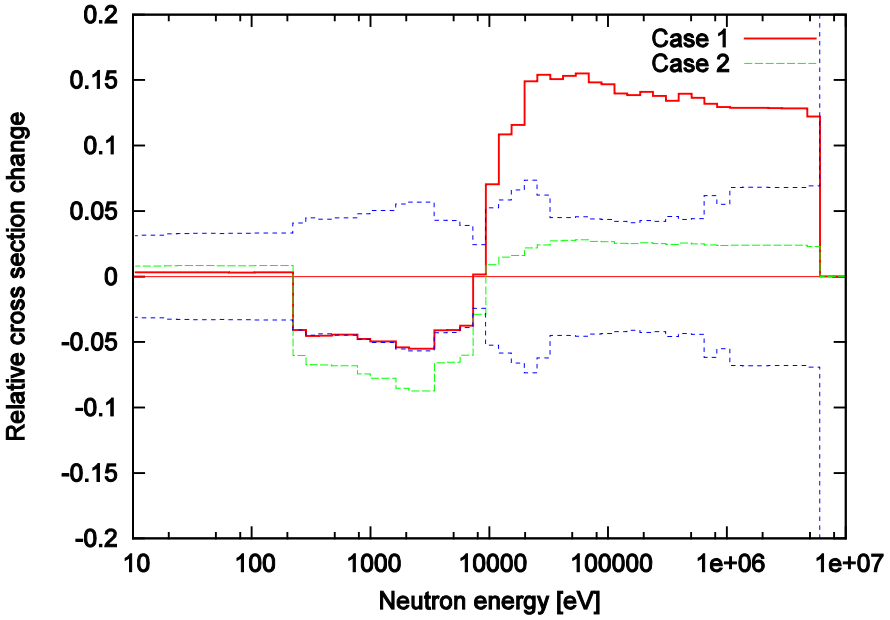

Figure A.22: Change in ^{235}U fission cross-section

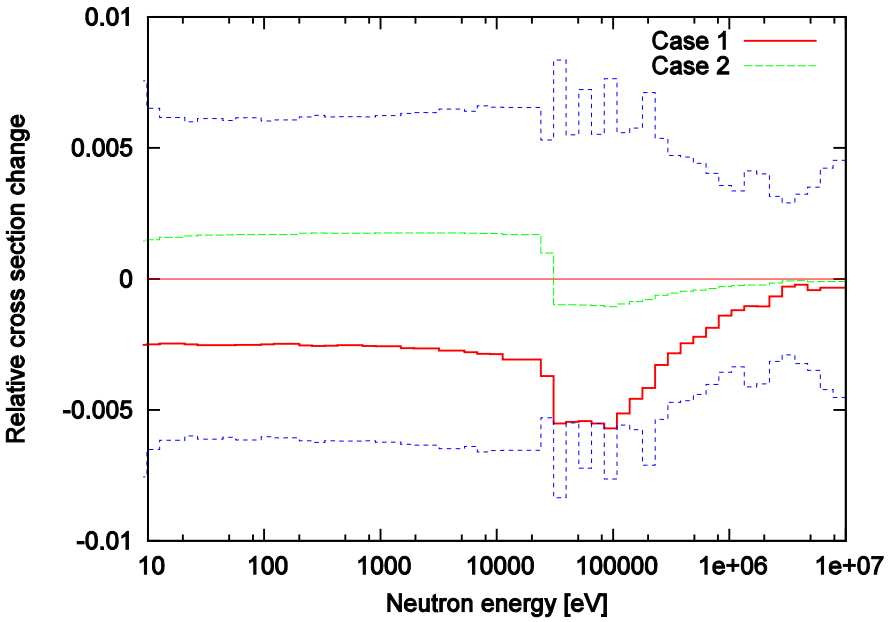

Figure A.23: Change in ^{235}U inelastic scattering cross-section

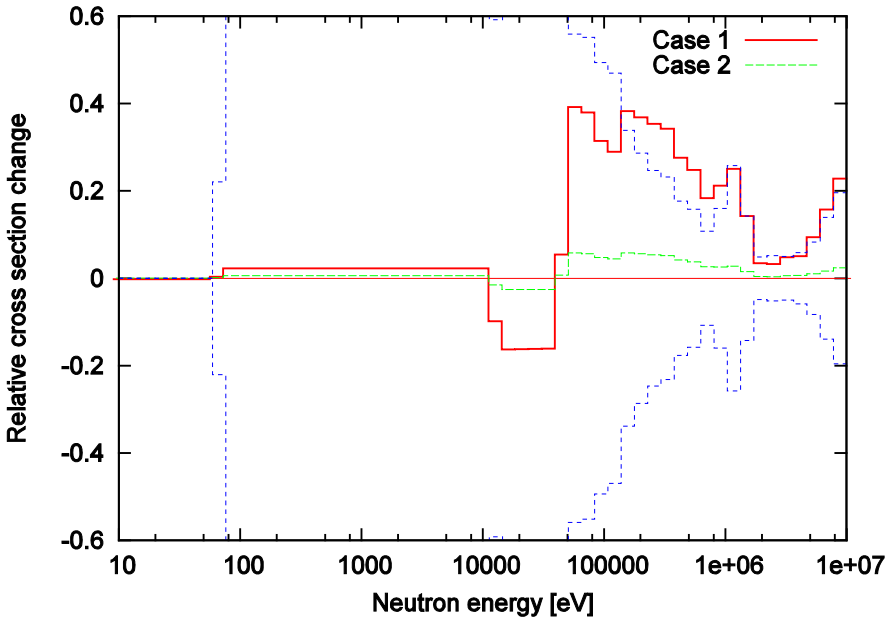

Figure A.24: Change in ^{235}U fission spectrum

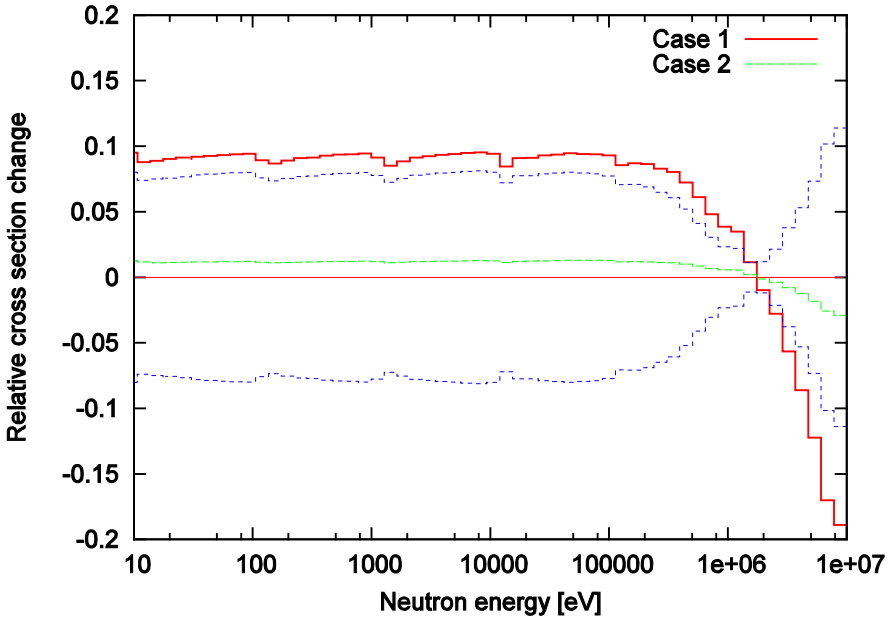

Figure A.25: Change in ^{235}U fission yield

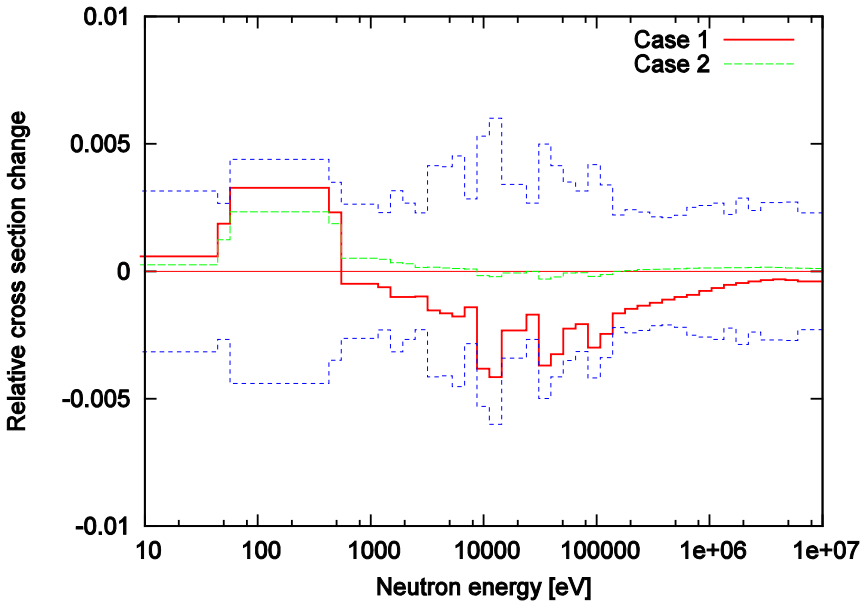

Conclusions

In order to investigate some trends observed in benchmark calculations for intermediate neutron systems, several sensitivity studies have been carried out. The present study can be concluded as follows:

- It can be seen that ENDF/B-VII.0 capture cross-section is much larger than JENDL-3.2 and statistical model calculations in the range of about 100 eV to 3 keV. Discrepancies are also found in the elastic scattering cross-sections below 30 keV. The total and fission cross-sections have no such noticeable discrepancies.
- The ENDF/B-VII.0 α results are in the upper part of the experimental results. JENDL-3.2, however, agrees well with experimental results.
- The difference between ENDF/B-VII.0 and JENDL-3.2 from 500 eV to 2.25 keV has a large impact on both the FCA-IX and ZEUS calculations while the difference below 500 eV has an impact only on the ZEUS calculations.
- Replacement of the ENDF/B-VII.0 resonance parameters by JENDL-3.2 for ^{235}U makes the C/E dependence on spectrum hardness smaller. However, this also results in unacceptably high C/E values. This can be an indication that there exists another energy region which also contributes to the multiplication factor. These cases need further investigation.

- A simple decrease in the capture cross-section, i.e. in Γ_γ, reduces the C/E dependence on spectrum hardness. However, it scales the k_{eff} up. These results may indicate that other cross-section or combinations of effects may be causing the biases.
- Detailed neutron balance analyses indicate that the leakages for the ZEUS benchmark experiments are on the average of 28% whereas in the FCA benchmark it is about 4%. The contribution of each component to k_{eff} for the ZEUS and FCA benchmark experiments are different from each other.
- Through cross-section adjustment with the integral data and the covariance information for ^{235}U cross-sections, it is indicated that capture cross-section in the resonance range is overestimated.

Reference – Appendix A

[1] Shibata, K., "Uncertainty Analyses of Neutron Cross Sections for ^{235}U in the Resonance Region", *J. Nucl. Sci. Technol.*, Vol. 42, p. 130 (2005).

Appendix B. Experiment and benchmark calculation for sodium-void reactivity in uranium-fuelled FBR core at FCA

T. Kugo, M. Fukushima, Y. Kitamura

Introduction

The OECD/NEA/NSC/WPEC Subgroup 29 has re-evaluated the capture cross-section of ^{235}U by focusing on the energy region from 100 eV to 1 MeV from the viewpoints of differential and integral data analyses since 2007. Sodium-void reactivity experiments with uranium fuels were carried out in the Fast Critical Assembly (FCA) at the Japan Atomic Energy Agency (JAEA) in 2009 and new integral data were obtained to help to validate the re-evaluated capture cross-section of ^{235}U [1]. This report presents an introduction of new integral data obtained at the FCA, the results of the benchmark calculations and the comparison between them.

Experiment

The FCA XXVII-1 cores, which are coupled systems comprising a central core zone and surrounding blanket zones, are used for sodium-void reactivity measurement in a uranium-fuelled FBR core. The core zone is composed of low- and high-enriched uranium metals and graphite. The average enrichment of the core zone is approximately 30%. The height of the core zone is approximately 61 cm. In the radial direction, the core zone is surrounded by two radial blanket zones; an inner blanket zone contains a significant amount of depleted uranium dioxide and sodium, and an outer blanket zone contains only a depleted uranium block. The test zone is set up at the centre of the core zone, varying the height of the test zone by the following lengths: 10.16 cm (Case 1), 20.32 cm (Case 2) and 30.48 cm (Case 3). X-Z cross-sectional views of the XXVII-1 cores are given for Cases 1, 2 and 3 in Figure B.1. X-Y cross-sectional views for Case 1 are given in Figure B.2. Those for Cases 2 and 3 are given in Figure B.3. The core zone for Cases 2 and 3 is increased by one fuel drawer to attain criticality. The test zone is composed of low- and high-enriched uranium metals and sodium cans. The sodium cans at the test zone are replaced by voided steel cans to measure the sodium-void reactivity. For Cases 1 and 2, the reactivities are

measured using the control rods that have been calibrated beforehand. For Case 3, the reactivity was measured by adopting the source multiplication method. The experimental results are presented in Table B.1 together with the measurement uncertainties. The effective delayed neutron fraction β_{eff} (= 0.00754±0.00027) is evaluated with JENDL-3.3.

Benchmark calculation

The benchmark calculations are performed employing deterministic and Monte Carlo methods.

Deterministic calculation

The deterministic calculation codes are the following:

Cell calculation	SLAROM-UF[2]
Core calculation	CITATION-FBR [3] (diffusion)
	TRITAC [4] (S_N transport)
Perturbation calculation	PERKY [5] (diffusion)
	SNPERT-3D [6] (S_N transport)

The core calculation by the diffusion theory can be performed using the XYZ models shown in Figures B.1, B.2 and B.3. The homogenised atomic number densities presented in Tables B.2 and B.3 are used for the calculations with JENDL-3.2 and for the calculations with JENDL-3.3, JENDL-4.0, ENDF/B-VII.0 and JEFF-3.1, respectively. Calculation results can be compared with the experimental results by applying correction factors.

The correction factors are prepared for JENDL-3.2, JENDL-3.3, JENDL-4.0, ENDF/B-VII.0 and JEFF-3.1. The correction factors are evaluated by the exact perturbation theory, since the sodium-void reactivity consists of various components. The components are generally classified into two terms, the non-leakage term and the leakage term. The correction factors are prepared for the two terms. The calculation methods to evaluate the correction factors and definitions of them are summarised in Table B.4.

In Method 1, the base calculation method, the effective macroscopic cross-sections for each region are prepared to take into account the resonance self-shielding effect in infinite homogeneous media. Region names in Table B.2 correspond to those in Figures B.1, B.2 and B.3. The cell calculation and the core calculation in the base method are performed using 70 energy groups (lethargy width: 0.25 in the energy range from 0.3 eV to 10 MeV) and are used for all calculation methods except for Method 2. The core calculation is performed using the XYZ models, also used for all calculation methods. The mesh intervals in the core calculation are 2.76 cm in the X and Y directions, and 2.54 cm in the Z direction. These values are used for all calculation methods.

In Method 2, used for the evaluation of the "Hetero + Ultrafine/Homo" correction factor, the cell calculation is performed with one-dimensional slab heterogeneous geometry. The resonance self-shielding is evaluated by the collision probability method with an ultrafine energy group structure (lethargy width: 0.00003125 for 5247.52 eV-9118.82 eV, 0.0000625 for 9118.82 eV-4307.43 eV, 0.000125 for 4307.43 eV-961.117 eV, 0.00025 for 961.117 eV-130.073 eV and 0.0005 for 130.073 eV-0.118611 eV). The correction factor is evaluated by a ratio of the result of Method 2 to that of Method 1.

In Methods 3 and 4, used for the evaluation of the "Transport" correction factor, the cell calculation is performed with one-dimensional slab heterogeneous geometry. The correction factor is evaluated by a ratio of the result of the S_N transport calculation to that of the diffusion calculation. The S_N transport calculation is performed with the S_8 quadrature set and with the transport cross-section defined by the extended transport approximation. The diffusion coefficient is defined by one-third of the inverse of the transport cross-section used in the transport calculation.

The "Aniso/Iso" correction factor, which is caused by the discrepancy of the neutron leakage parallel or perpendicular to the plate-type fuel arrangement in the cells, is negligibly small.

The correction factors for the non-leakage term and the leakage term are applied independently for the non-leakage term and the leakage term of the base calculation. The final sodium-void reactivity is evaluated by summing up the corrected non-leakage term and the corrected leakage term. The obtained correction factors are summarised in Table B.6. The JENDL-3.3, ENDF/B-VII.0 and JEFF-3.1 correction factors have different tendencies than those of JENDL-3.2 and JENDL-4.0. The difference could be due to the discrepancies of the capture cross-sections of ^{235}U among those libraries. It is recommended to use the correction factors of the corresponding library.

Monte Carlo calculation

Calculations by a continuous-energy Monte Carlo code [7], MVP-II, are performed with geometry models made as detailed as possible. The reactivities are obtained from $(k'_{eff} - k_{eff})/k_{eff}k'_{eff}$, where k_{eff} and k'_{eff} are the effective multiplication factors of the reference and perturbed cores in which the sodium cans and voided steel cans are placed at the test zone, respectively. The MVP calculations are performed with 2 000 000 000 particles. The statistical uncertainties of the MVP calculations are within several per cents of the measured sodium-void reactivities.

The calculated sodium-void reactivities using the MVP calculations together with the statistical uncertainties are shown in Table B.7. In this table, the ratios of calculation to experimental (C/E) values together with the uncertainties of the calculations are also summarised. A summary of

Monte Carlo calculations together with deterministic calculation results is presented in Figure B.4. The corrected results by the deterministic calculations agree with the Monte Carlo calculation results within 3σ of statistical uncertainties.

References – Appendix B

[1] Fukushima, M., *et al.*, "Benchmark Calculations of Sodium-void Experiments with Uranium Fuels at the Fast Critical Assembly FCA", *Proc. Joint Int. Conf. on Supercomputing in Nuclear Applications and Monte Carlo 2010 (SNA + MC2010)*, Hitotsubashi Memorial Hall, Tokyo, Japan, 17-21 October 2010, *Progress in Nuclear Science and Technology*, Vol. 2 (2011).

[2] Hazama, T., G. Chiba, K. Sugino, "Development of a Fine and Ultra-fine Group Cell Calculation Code SLAROM-UF for Fast Reactor Analysis", *J. Nucl. Sci. Technol.*, 43, 908 (2006).

[3] Fowler, T.B., *et al.*, *Nuclear Reactor Analysis Code: CITATION*, ORNL-TM-2496 Rev.2 (1971).

[4] Yamamoto, T., *et al.*, "Three-dimensional Transport Correction in Fast Reactor Core Analysis", *J. Nucl. Sci. Technol.*, 23, 849 (1986).

[5] Iijima, S., H. Yoshida, H. Sakuragi, *Calculation Program for Fast Reactor Design (Multi-dimensional Perturbation Theory Code Based on Diffusion Approximation: PERKY)*, JAERI-M 6993 (1977).

[6] Nakano, K., *et al.*, *User's Manual of SNPERT-3D Code*, JNC Report, Japan Atomic Energy Agency, PNC ZJ9270 94-003 (1994) [in Japanese].

[7] Nagaya, Y., *et al.*, *MVP/GMVP II: General Purpose Monte Carlo Codes for Neutron and Photon Transport Calculations Based on Continuous Energy and Multigroup Methods*, JAERI 1348, Japan Atomic Energy Research Institute (2005).

Table B.1: Experimental results for sodium-void reactivity

	Unit: ¢		Unit: 10^{-3} dk/kk′	
Case 1	-5.3	±0.2	-0.40	±0.02
Case 2	-10.6	±0.2	-0.80	±0.03
Case 3	-16.2	±0.8	-1.22	±0.08

Table B.2: Atomic number densities of homogeneous media for FCA XXVII-1 used for calculations with JENDL-3.2

Unit: 10^{24} atoms/cm^3

Region name	DUB2	DUB4	EU-C	EU-CLR	EU-NA	EU-VD	MTX	NUB	SB	SCR
^{1}H	6.3057E-05	5.0421E-05	1.0432E-04	1.1521E-04	8.8638E-05	8.8638E-05		3.1237E-05		1.0204E-04
^{10}B			3.0540E-09	3.0540E-09	1.0505E-08	1.0519E-08				2.5450E-09
^{11}B			1.2298E-08	1.2298E-08	3.8216E-08	3.8267E-08				1.0248E-08
^{nat}C	5.2914E-05	42311E-05	5.2548E-02	5.2557E-02	9.6274E-05	9.6303E-05		2.6213E-05		5.0624E-02
^{14}N	2.8359E-07	2.2676E-07	3.9864E-07	4.4764E-07	3.9864E-07	3.9864E-07		1.4027E-07		3.9864E-07
^{16}O	2.7310E-05	2.1837E-05	4.6224E-05	5.0942E-05	3.8389E-05	3.8389E-05		1.3529E-05	1.8430E-02	4.5083E-05
^{19}F	2.0908E-05	1.6718E-05	2.9390E-05	3.3003E-05	2.9390E-05	2.9390E-05		1.0358E-05		2.9390E-05
^{23}Na					1.1799E-02				7.6559E-03	
^{nat}Si			1.3381E-07	1.3381E-07	9.3628E-05	9.3753E-05				1.1151E-07
^{31}P					5.6032E-06	5.6107E-06				
^{nat}S					4.9197E-07	4.9263E-07				
^{nat}Cr	1.8102E-03	1.8102E-03	1.8102E-03	1.8102E-03	3.6703E-03	3.6728E-03	1.2287E-03	1.8102E-03	3.1174E-03	2.5176E-03
^{55}Mn	1.2033E-04	1.2033E-04	1.2033E-04	1.2033E-04	1.9978E-04	1.9989E-04	8.1671E-05	1.2033E-04	2.2969E-04	1.6735E-04
^{nat}Fe	6.4720E-03	6.4720E-03	6.4720E-03	6.4720E-03	1.3214E-02	1.3223E-02	4.3928E-03	6.4720E-03	1.1216E-02	9.0012E-03
^{nat}Ni	7.8931E-04	7.8931E-04	7.8931E-04	7.8931E-04	1.5393E-03	1.5403E-03	5.3574E-04	7.8931E-04	1.4132E-03	1.0978E-03
^{93}Nb					5.6607E-07	5.6683E-07				
^{nat}Mo					1.2060E-05	1.2076E-05				
^{235}U	8.4132E-05	8.4339E-05	2.8360E-03	3.7180E-03	2.8360E-03	2.8360E-03		2.8911E-04	1.8689E-05	2.8360E-03
^{238}U	4.0047E-02	4.0146E-02	6.8723E-03	5.9886E-03	6.8723E-03	6.8723E-03		3.9875E-02	9.1988E-03	6.8723E-03

Table B.3: Atomic number densities of homogeneous media for FCA XXVII-1 used for calculations with JENDL-3.3, JENDL-4.0, ENDF/BVII.0 and JEFF-3.1

Unit: 10^{24} atoms/cm^3

Region name	DUB2	DUB4	EU-C	EU-CLR	EU-NA	EU-VD	MTX	NUB	SB	SCR
^{1}H	6.3057E-05	5.0421E-05	1.0432E-04	1.1521E-04	8.8638E-05	8.8638E-05		1.2495E-04		1.0204E-04
^{10}B			3.0540E-09	3.0540E-09	1.0505E-08	1.0519E-08				2.5450E-09
^{11}B			1.2298E-08	1.2298E-08	3.8216E-08	3.8267E-08				1.0248E-08
^{12}C	5.2914E-05	4.2311E-05	5.2548E-02	5.2557E-02	9.6274E-05	9.6303E-05		1.0485E-04		5.0624E-02
^{14}N	2.8359E-07	2.2676E-07	3.9864E-07	4.4764E-07	3.9864E-07	3.9864E-07		5.6197E-07		3.9864E-07
^{16}O	2.7310E-05	2.1837E-05	4.6224E-05	5.0942E-05	3.8389E-05	3.8389E-05		5.4117E-05	1.8430E-02	4.5083E-05
^{19}F	2.0908E-05	1.6718E-05	2.9390E-05	3.3003E-05	2.9390E-05	2.9390E-05		4.1431E-05		2.9390E-05
^{23}Na					1.1799E-02				7.6559E-03	
^{28}Si			1.2342E-07	1.2342E-07	8.6353E-05	8.6468E-05				1.0285E-07
^{29}Si			6.2668E-09	6.2668E-09	4.3848E-06	4.3906E-06				5.2223E-09
^{30}Si			4.1310E-09	4.1310E-09	2.8904E-06	2.8942E-06				3.4425E-09
^{31}P					5.6032E-06	5.6107E-06				
^{32}S					4.6703E-07	4.6765E-07				
^{33}S					3.7390E-09	3.7440E-09				
^{34}S					2.1106E-08	2.1134E-08				
^{36}S					9.8394E-11	9.8526E-11				
^{50}Cr	7.8653E-05	7.8653E-05	7.8653E-05	7.8653E-05	1.5947E-04	1.5958E-04	5.3387E-05	7.8653E-05	1.3545E-04	1.0939E-04
^{52}Cr	1.5168E-03	1.5168E-03	1.5168E-03	1.5168E-03	3.0753E-03	3.0774E-03	1.0295E-03	1.5168E-03	2.6121E-03	2.1095E-03
^{53}Cr	1.7199E-04	1.7199E-04	1.7199E-04	1.7199E-04	3.4871E-04	3.4895E-04	1.1674E-04	1.7199E-04	2.9619E-04	2.3920E-04
^{54}Cr	4.2811E-05	4.2811E-05	4.2811E-05	4.2811E-05	8.6802E-05	8.6861E-05	2.9059E-05	4.2811E-05	7.3727E-05	5.9542E-05
^{55}Mn	1.2033E-04	1.2033E-04	1.2033E-04	1.2033E-04	1.9978E-04	1.9989E-04	8.1671E-05	1.2033E-04	2.2969E-04	1.6735E-04
^{54}Fe	3.7829E-04	3.7829E-04	3.7829E-04	3.7829E-04	7.7236E-04	7.7289E-04	2.5676E-04	3.7829E-04	6.5557E-04	5.2612E-04
^{56}Fe	5.9383E-03	5.9383E-03	5.9383E-03	5.9383E-03	1.2125E-02	1.2133E-0	4.0306E-03	5.9383E-03	1.0291E-02	8.2589E-03
^{57}Fe	1.3714E-04	1.3714E-04	1.3714E-04	1.3714E-04	2.8001E-04	2.8020E-04	9.3083E-05	1.3714E-04	2.3767E-04	1.9074E-04
^{58}Fe	1.8251E-05	1.8251E-05	1.8251E-05	1.8251E-05	3.7264E-05	3.7289E-05	1.2388E-05	1.8251E-05	3.1629E-05	2.5383E-05

Table B.3: Atomic number densities of homogeneous media for FCA XXVII-1 used for calculations with JENDL-3.3, JENDL-4.0, ENDF/BVII.0 and JEFF-3.1 (*cont.*)

Unit: 10^{24} atoms/cm^3

Region name	DUB2	DUB4	EU-C	EU-CLR	EU-NA	EU-VD	MTX	NUB	SB	SCR
^{58}Ni	5.3733E-04	5.3733E-04	5.3733E-04	5.3733E-04	1.0479E-03	1.0486E-03	3.6472E-04	5.3733E-04	9.6204E-04	7.4732E-04
^{60}Ni	2.0698E-04	2.0698E-04	2.0698E-04	2.0698E-04	4.0366E-04	4.0393E-04	1.4049E-04	2.0698E-04	3.7057E-04	2.8787E-04
^{61}Ni	8.9973E-06	8.9973E-06	8.9973E-06	8.9973E-06	1.7547E-05	1.7558E-05	6.1069E-06	8.9973E-06	1.6109E-05	1.2513E-05
^{62}Ni	2.8687E-05	2.8687E-05	2.8687E-05	2.8687E-05	5.5947E-05	5.5984E-05	1.9472E-05	2.8687E-05	5.1361E-05	3.9898E-05
^{64}Ni	7.3058E-06	7.3058E-06	7.3058E-06	7.3058E-06	1.4248E-05	1.4257E-05	4.9588E-06	7.3058E-06	1.3080E-05	1.0161E-05
^{93}Nb					5.6607E-07	5.6683E-07				
^{92}Mo					1.7897E-06	1.7921E-06				
^{94}Mo					1.1155E-06	1.1170E-06				
^{95}Mo					1.9199E-06	1.9225E-06				
^{96}Mo					2.0116E-06	2.0143E-06				
^{97}Mo					1.1517E-06	1.1533E-06				
^{98}Mo					2.9100E-06	2.9139E-06				
^{100}Mo					1.1614E-06	1.1629E-06				
^{235}U	8.4132E-05	8.4339E-05	2.8360E-03	3.7180E-03	2.8360E-03	2.8360E-03		2.8911E-04	1.8689E-05	2.8360E-03
^{238}U	4.0047E-02	4.0146E-02	6.8723E-03	5.9886E-03	6.8723E-03	6.8723E-03		3.9875E-02	9.1988E-03	6.8723E-03

Table B.4: Calculation methods and definition of correction factors

	Cell model	Energy groups for cell calc.	Energy groups for core calc.	Theory
Method 1	Homogeneous	70	70	Diffusion
Method 2	Heterogeneous	Ultrafine	175	Diffusion
Method 3	Heterogeneous	70	70	Diffusion
Method 4	Heterogeneous	70	70	Transport

Correction factors	
"Hetero + Ultrafine/Homo"	= method-2/method-1
"Transport"	= method-4/method-3

Table B.5: Correction factors for sodium-void reactivity

		Hetero+Ultrafine group/homo		Transport	
		Non-leakage	Leakage	Non-leakage	Leakage
Case 1	JENDL-3.2	1.0331	1.0435	0.9415	0.7466
	JENDL-3.3	1.0587	1.0466	0.9047	0.7483
	JENDL-4.0	1.0508	1.0536	0.9450	0.7501
	ENDF/B-7.0	1.0195	1.0569	0.9085	0.7454
	JEFF-3.1	1.0196	1.0517	0.9281	0.7506
Case 2	JENDL-3.2	1.0291	1.0419	0.9387	0.7837
	JENDL-3.3	1.0520	1.0447	0.9042	0.7857
	JENDL-4.0	1.0451	1.0523	0.9429	0.7863
	ENDF/B-7.0	1.0216	1.0541	0.9090	0.7822
	JEFF-3.1	1.0144	1.0487	0.9287	0.7872
Case 3	JENDL-3.2	1.0262	1.0297	0.9371	0.7866
	JENDL-3.3	1.0470	1.0311	0.9034	0.7880
	JENDL-4.0	1.0415	1.0371	0.9416	0.7892
	ENDF/B-7.0	1.0204	1.0370	0.9088	0.7854
	JEFF-3.1	1.0102	1.0337	0.9285	0.7892

Table B.6: Summary of deterministic calculations

		Base calculations ($\times 10^{-3}$ dk/kk')			Corrected results ($\times 10^{-3}$ dk/kk')			C/E
		Non-leakage	Leakage	Total	Non-leakage	Leakage	Total	
Case 1	JENDL-3.2	-0.388	-0.070	-0.457	-0.377	-0.054	-0.431	1.08
	JENDL-3.3	-0.239	-0.077	-0.316	-0.229	-0.060	-0.289	0.72
	JENDL-4.0	-0.407	-0.069	-0.476	-0.404	-0.054	-0.459	1.15
	ENDF/B-VII.0	-0.220	-0.068	-0.287	-0.204	-0.053	-0.256	0.64
	JEFF-3.1	-0.255	-0.077	-0.331	-0.241	-0.060	-0.301	0.75
Case 2	JENDL-3.2	-0.701	-0.162	-0.863	-0.678	-0.132	-0.810	1.01
	JENDL-3.3	-0.442	-0.179	-0.621	-0.420	-0.147	-0.567	0.71
	JENDL-4.0	-0.740	-0.161	-0.901	-0.729	-0.133	-0.863	1.08
	ENDF/B-VII.0	-0.415	-0.155	-0.570	-0.385	-0.128	-0.513	0.64
	JEFF-3.1	-0.480	-0.177	-0.657	-0.452	-0.146	-0.598	0.75
Case 3	JENDL-3.2	-0.977	-0.423	-1.400	-0.939	-0.344	-1.280	1.05
	JENDL-3.3	-0.625	-0.450	-1.070	-0.591	-0.367	-0.957	0.78
	JENDL-4.0	-1.030	-0.422	-1.460	-1.010	-0.347	-1.360	1.11
	ENDF/B-VII.0	-0.594	-0.401	-0.995	-0.550	-0.328	-0.878	0.72
	JEFF-3.1	-0.684	-0.447	-1.130	-0.641	-0.366	-1.010	0.83

Table B.7: Summary of Monte Carlo calculations

Case	Library	MC calculations [× 10^{-3} Δk/kk′]		C/E	
Case 1	JENDL-3.2	-0.479	±0.020*	1.20	±0.09**
	JENDL-3.3	-0.310	±0.020*	0.78	±0.07**
	JENDL-4.0	-0.480	±0.020*	1.20	±0.09**
	ENDF/B-VII.0	-0.248	±0.020*	0.62	±0.06**
	JEFF-3.1	-0.318	±0.020*	0.79	±0.07**
Case 2	JENDL-3.2	-0.827	±0.020*	1.03	±0.05**
	JENDL-3.3	-0.574	±0.020*	0.72	±0.04**
	JENDL-4.0	-0.908	±0.020*	1.13	±0.05**
	ENDF/B-VII.0	-0.528	±0.020*	0.66	±0.04**
	JEFF-3.1	-0.617	±0.020*	0.77	±0.04**
Case 3	JENDL-3.2	-1.336	±0.020*	1.09	±0.07**
	JENDL-3.3	-1.032	±0.020*	0.85	±0.06**
	JENDL-4.0	-1.374	±0.020*	1.13	±0.07**
	ENDF/B-VII.0	-0.907	±0.020*	0.74	±0.05**
	JEFF-3.1	-0.997	±0.020*	0.82	±0.05**

* Statistical uncertainties of Monte Carlo calculations.

** Statistical uncertainties of MC calculations and the experimental errors.

Figure B.1(a): X-Z cross-sectional views of the FCA XVVII-1 cores – Case 1

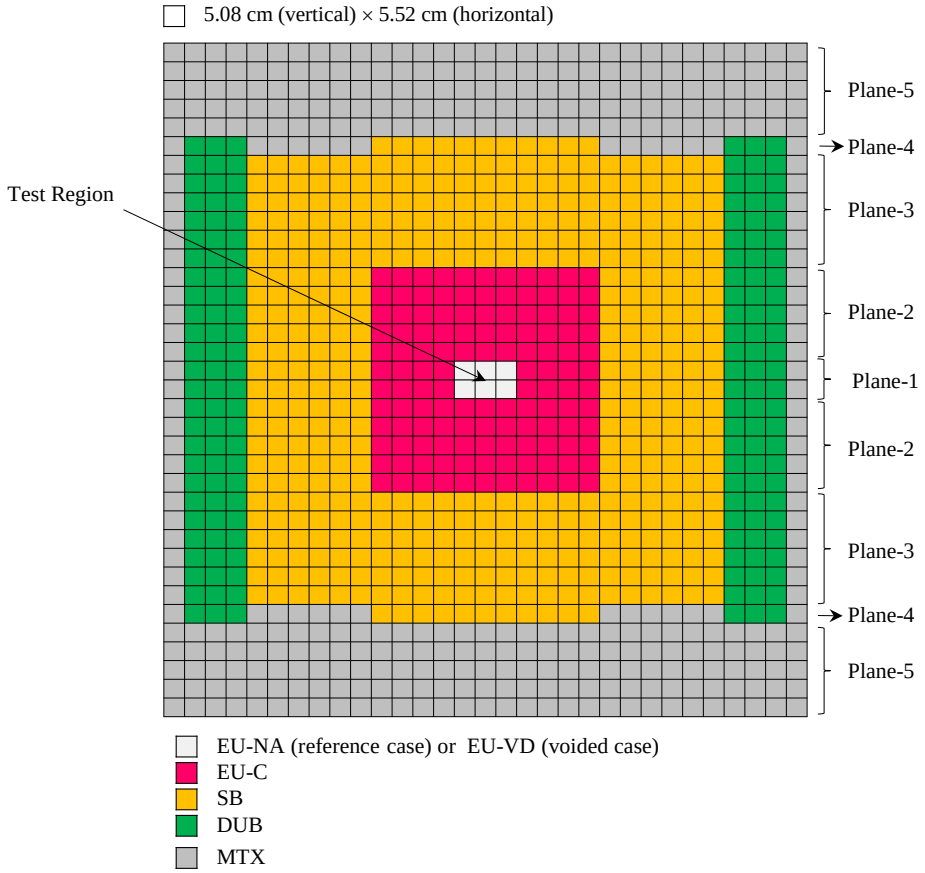

Figure B.1(b): X-Z cross-sectional views of the FCA XVVII-1 cores – Case 2

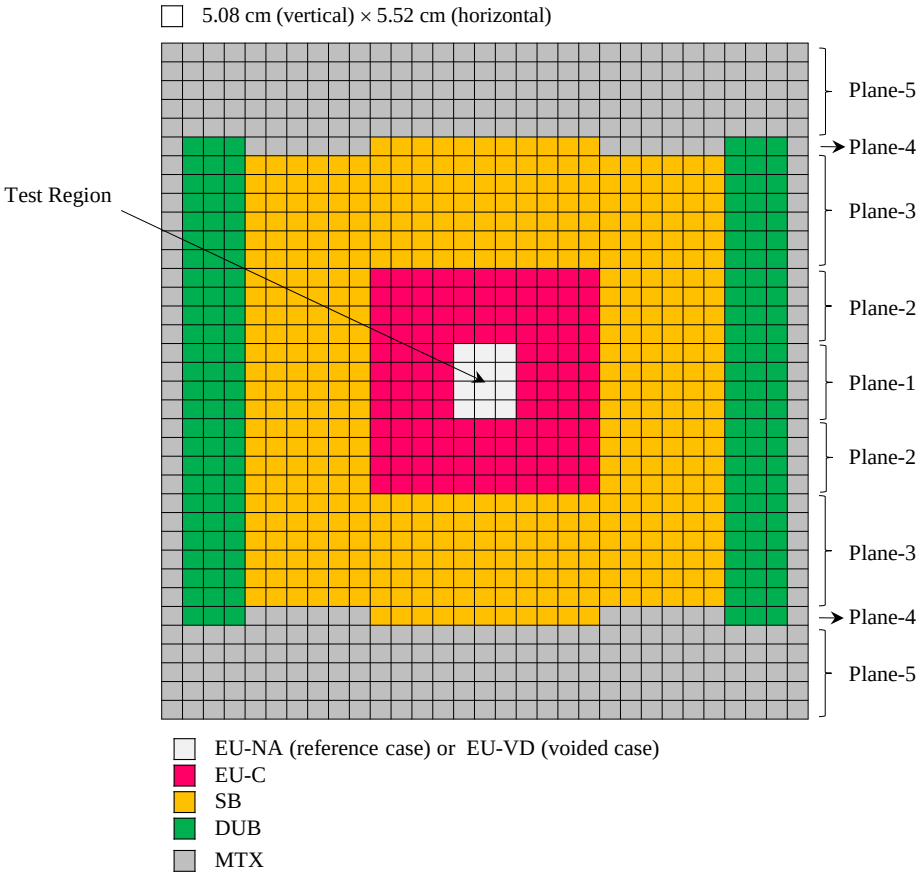

Figure B.1(c): X-Z cross-sectional views of the FCA XVVII-1 cores – Case 3

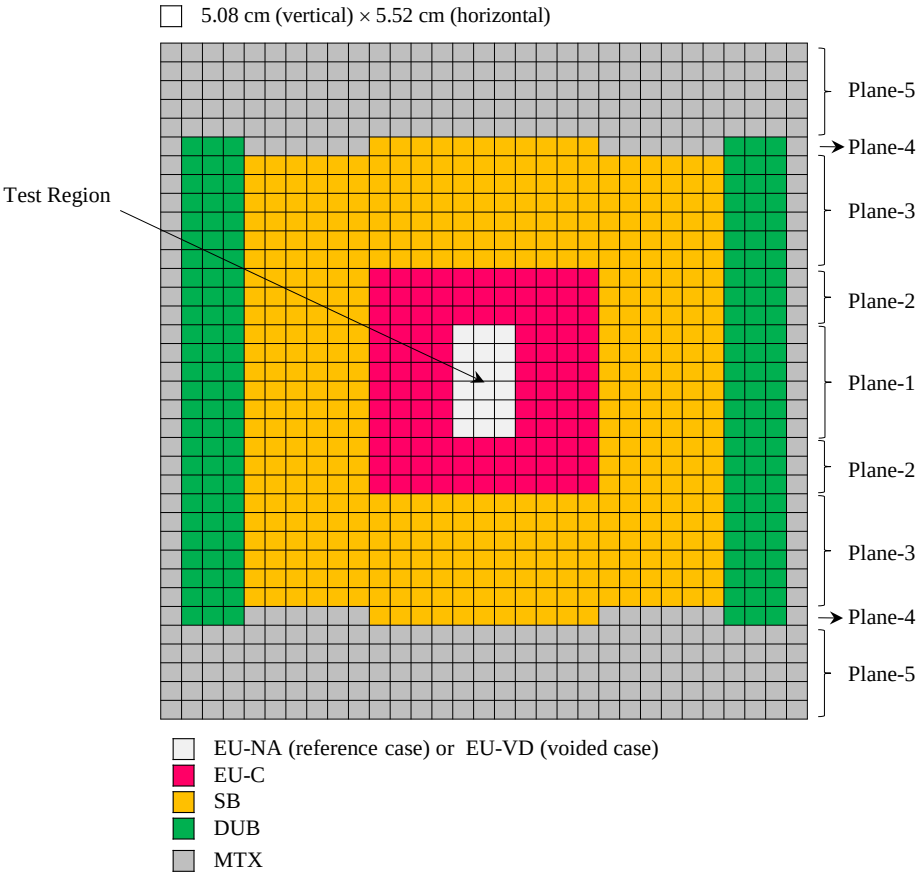

Figure B.2(a): X-Y cross-sectional views of the FCA XVVII-1 core for Case 1 – Plane 1

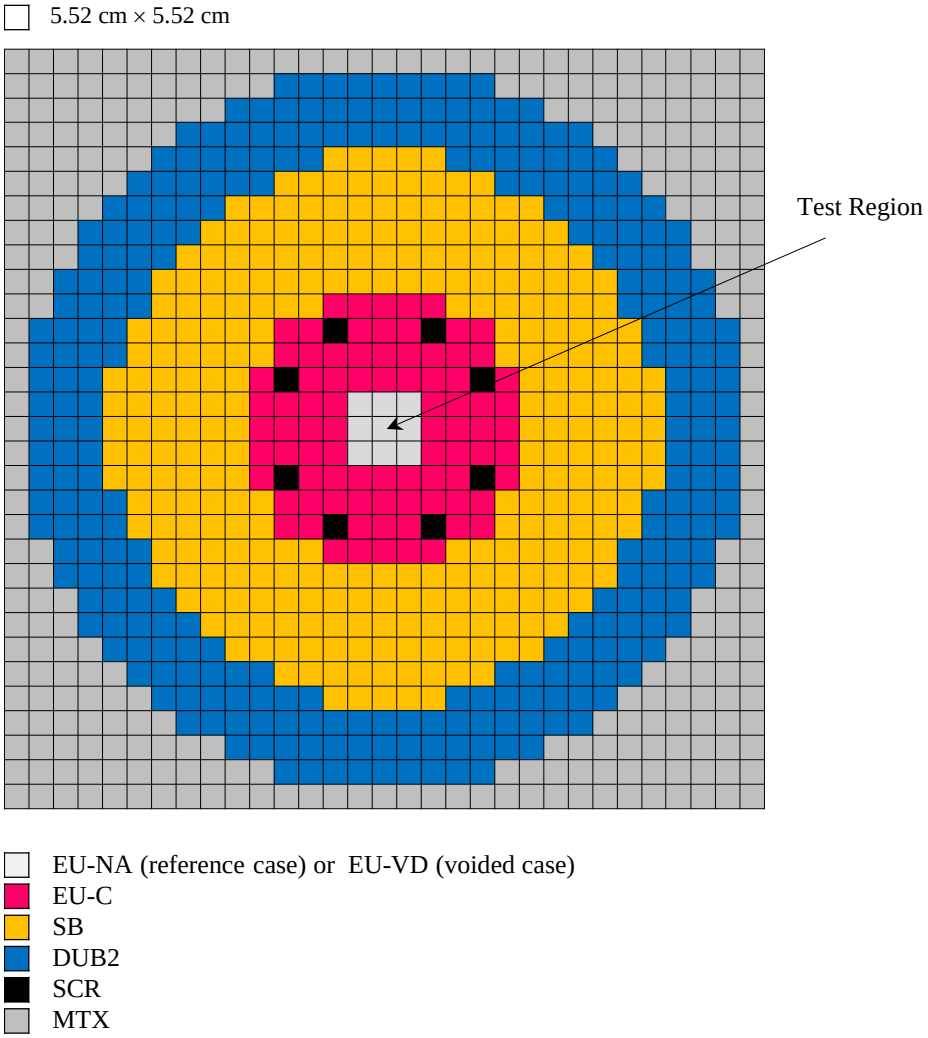

Figure B.2(b): X-Y cross-sectional views of the FCA XVVII-1 core for Case 1 – Plane 2

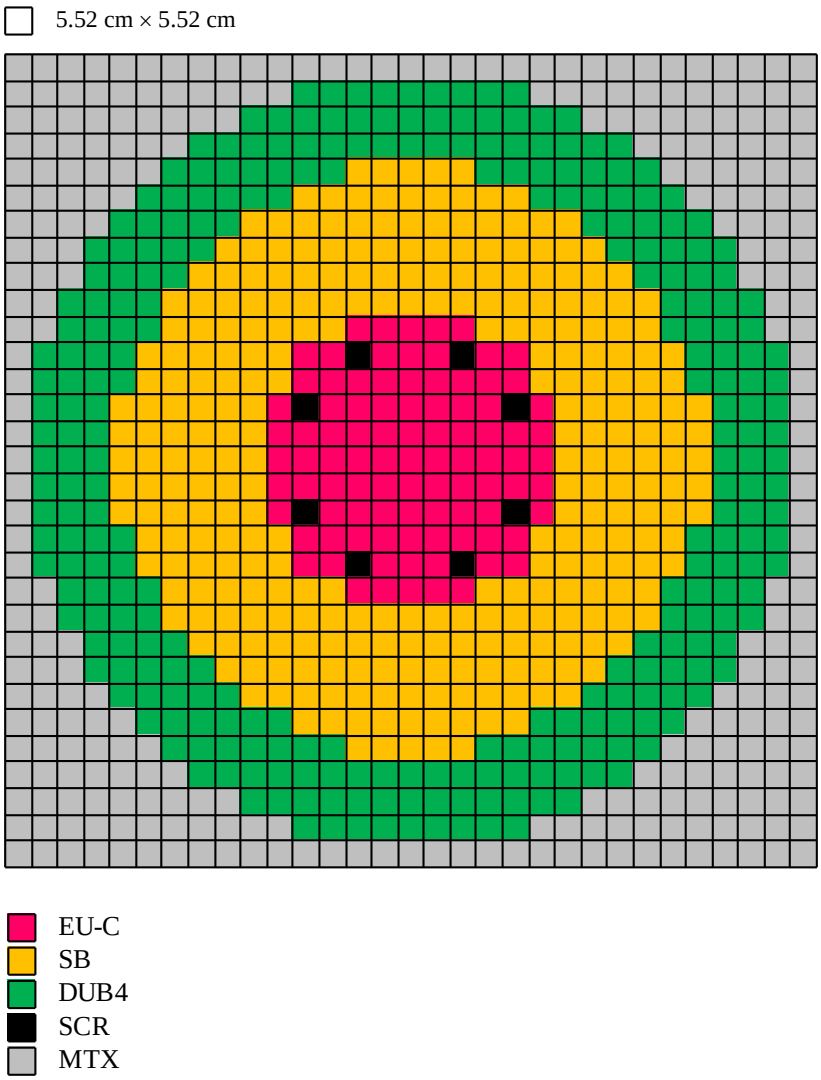

Figure B.2(c): X-Y cross-sectional views of the FCA XVVII-1 core for Case 1 – Plane 3

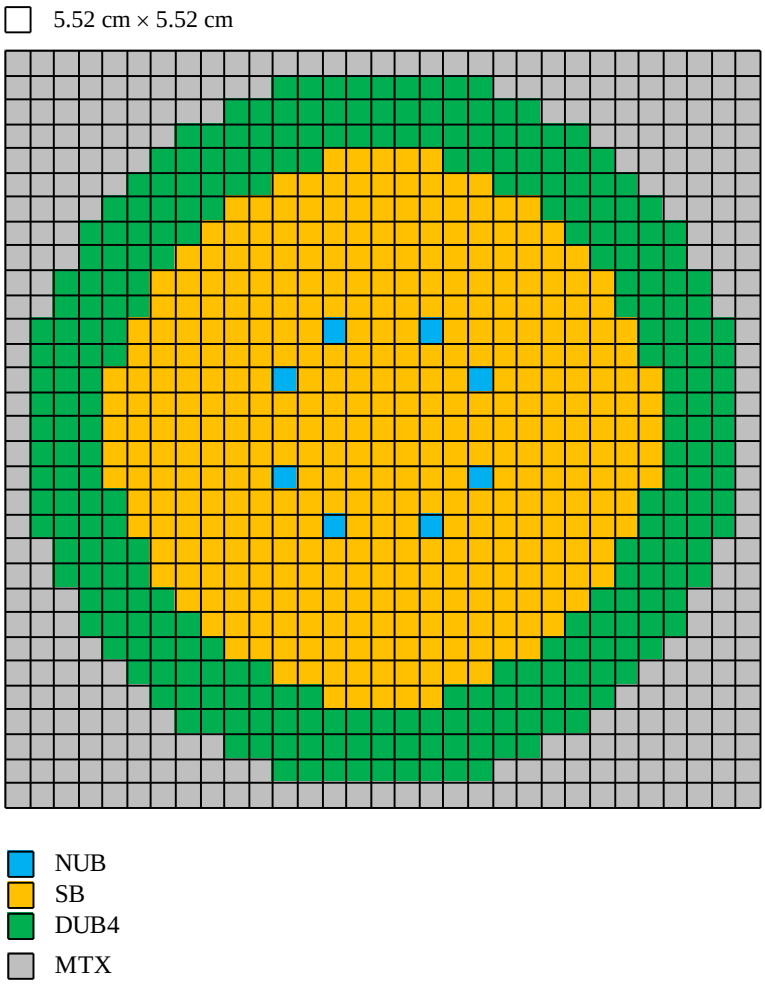

Figure B.2(d): X-Y cross-sectional views of the FCA XVVII-1 core for Case 1 – Plane 4

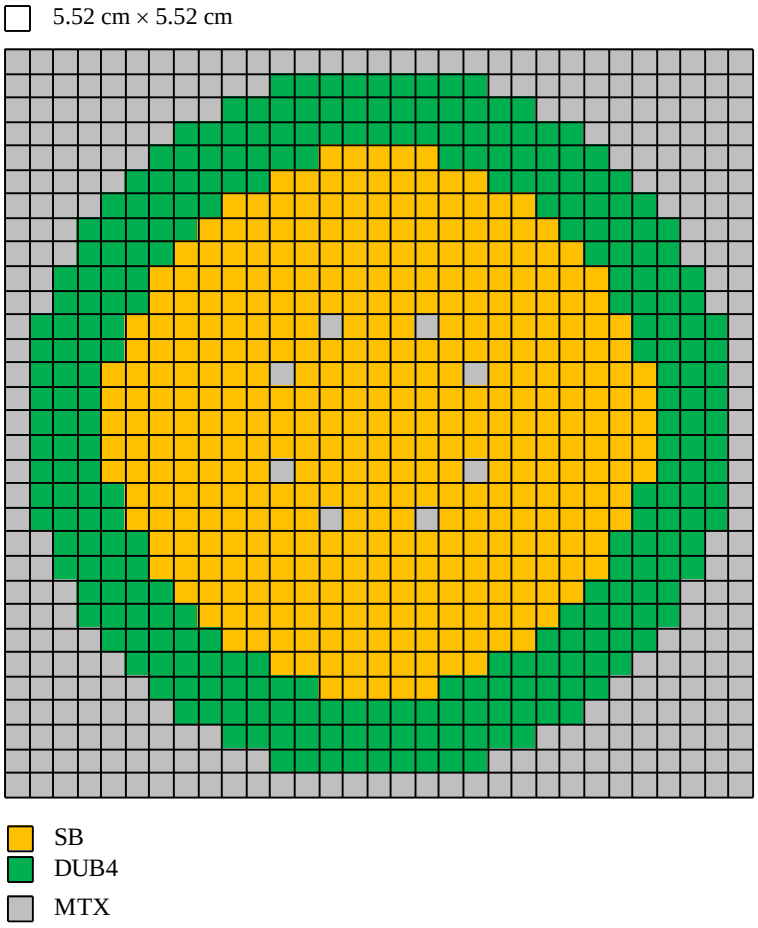

Figure B.2(e): X-Y cross-sectional views of the FCA XVVII-1 core for Case 1 – Plane 5

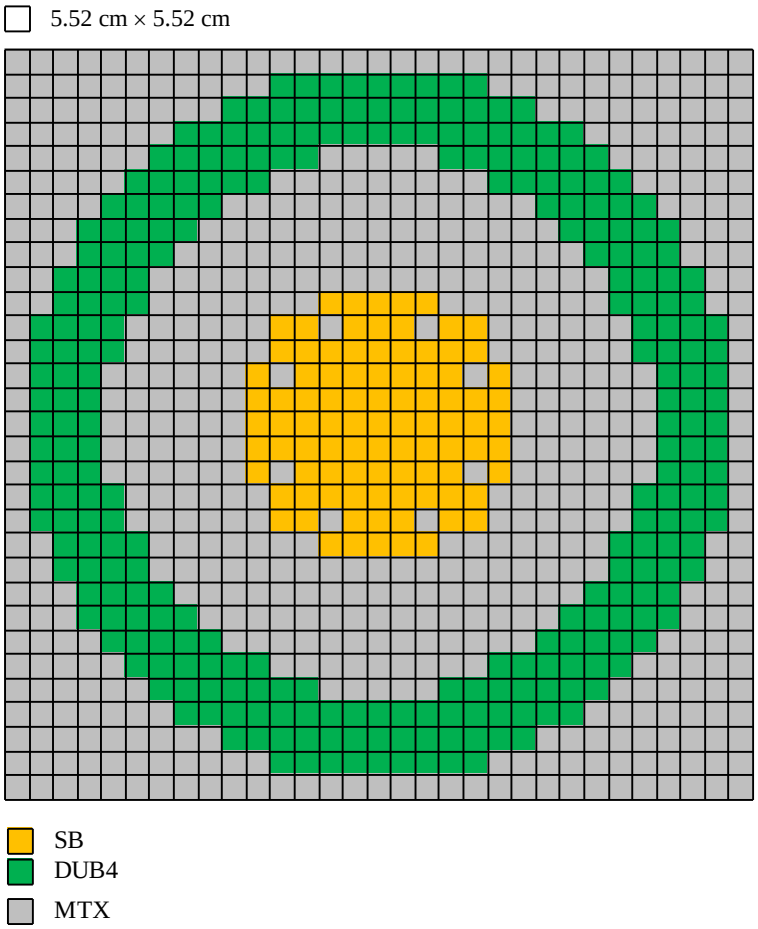

Figure B.2(f): X-Y cross-sectional views of the FCA XVVII-1 core for Case 1 – Plane 6

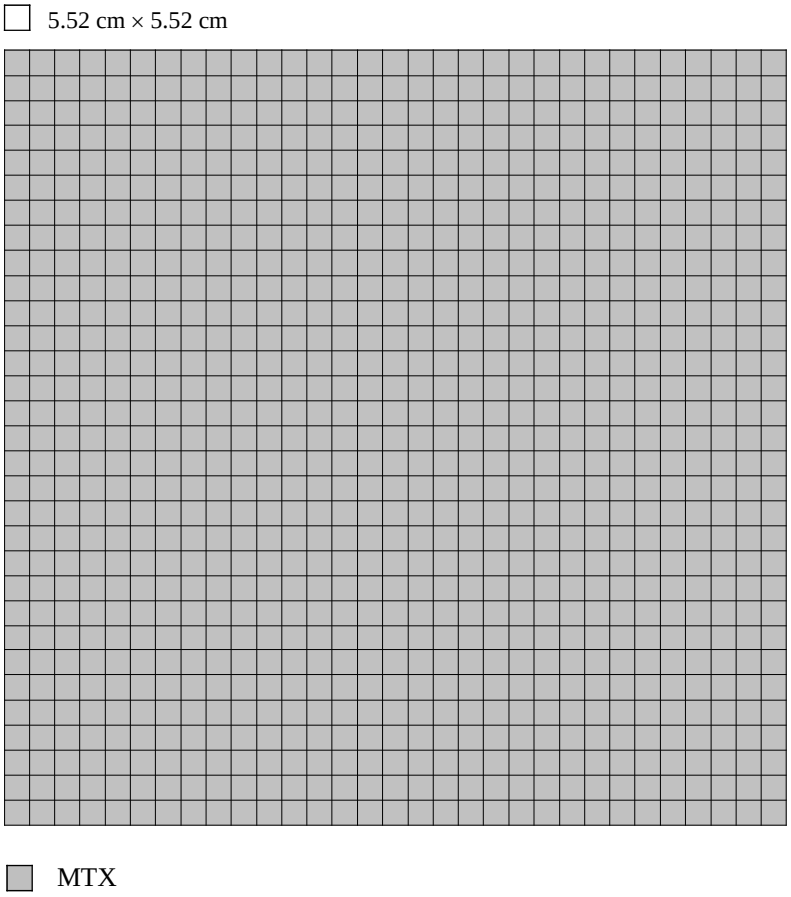

Figure B.3(a): X-Y cross-sectional views of the FCA XVVII-1 core for Cases-2 and -3 – Plane-1

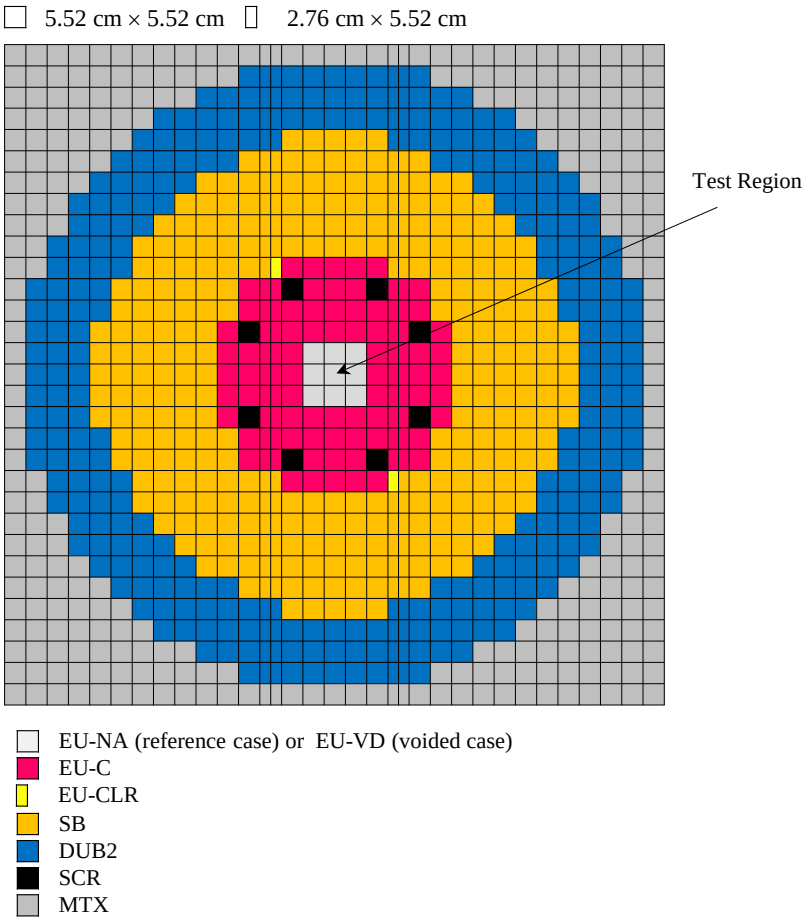

Figure B.3(b): X-Y cross-sectional views of the FCA XVVII-1 core for Cases 2 and 3 – Plane 2

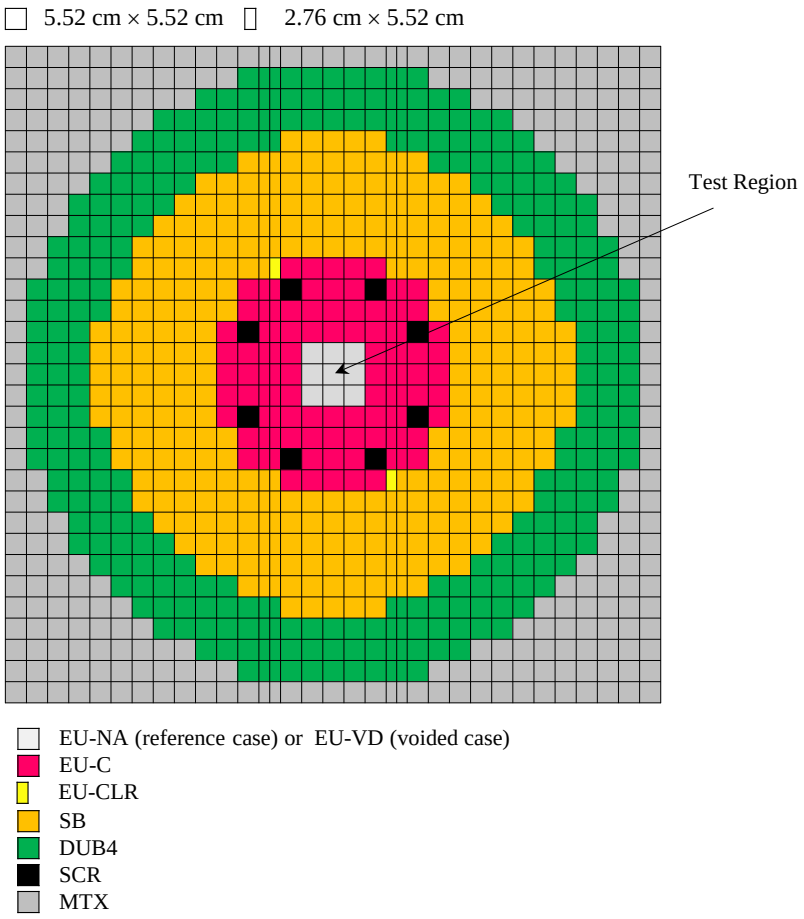

Figure B.3(c): X-Y cross-sectional views of the FCA XVVII-1 core for Cases 2 and 3 – Plane 3

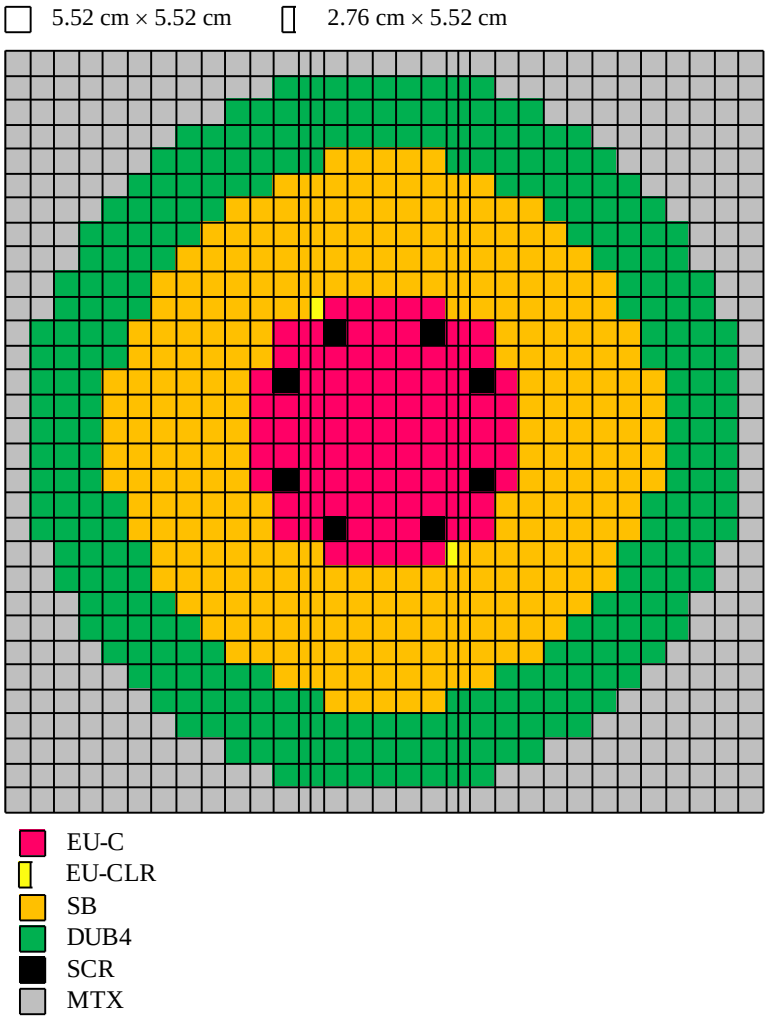

Figure B.3(d): X-Y cross-sectional views of the FCA XVVII-1 core for Cases 2 and 3 – Plane 4

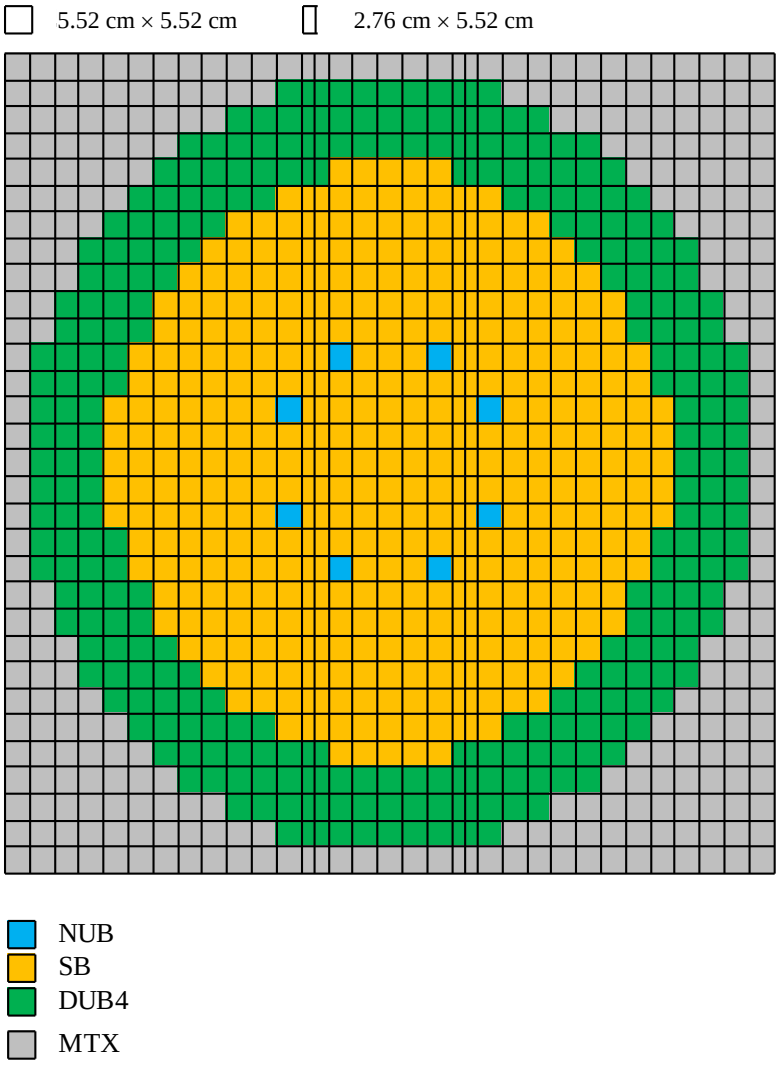

Figure B.3(e): X-Y cross-sectional views of the FCA XVVII-1 core for Cases 2 and 3 – Plane 5

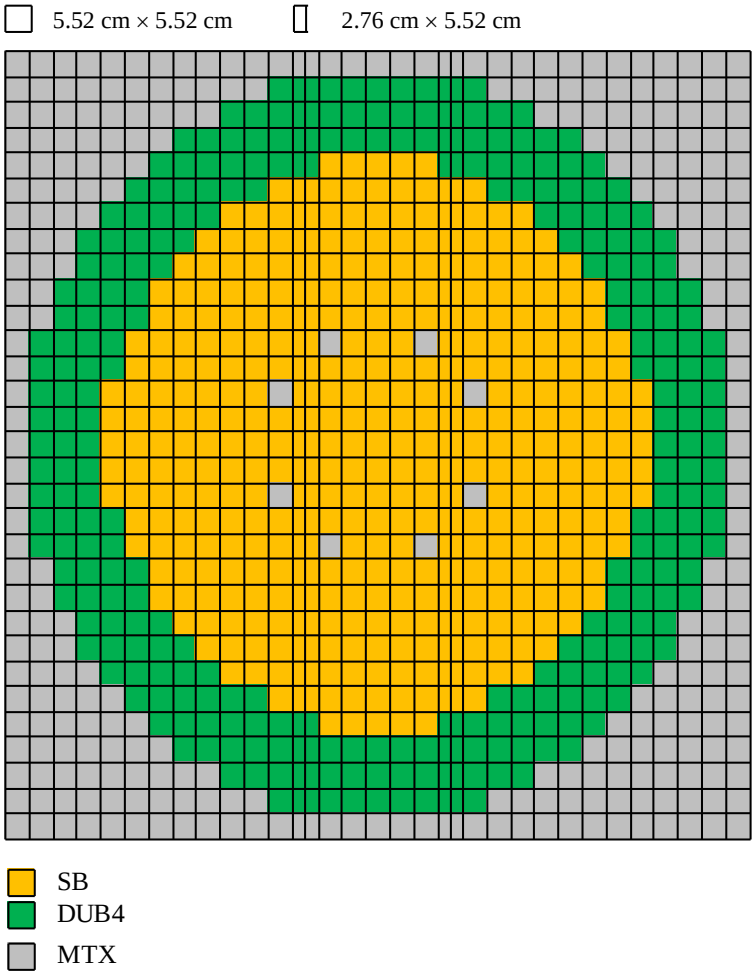

Figure B.3(f): X-Y cross-sectional views of the FCA XVVII-1 core for Cases 2 and 3 – Plane 6

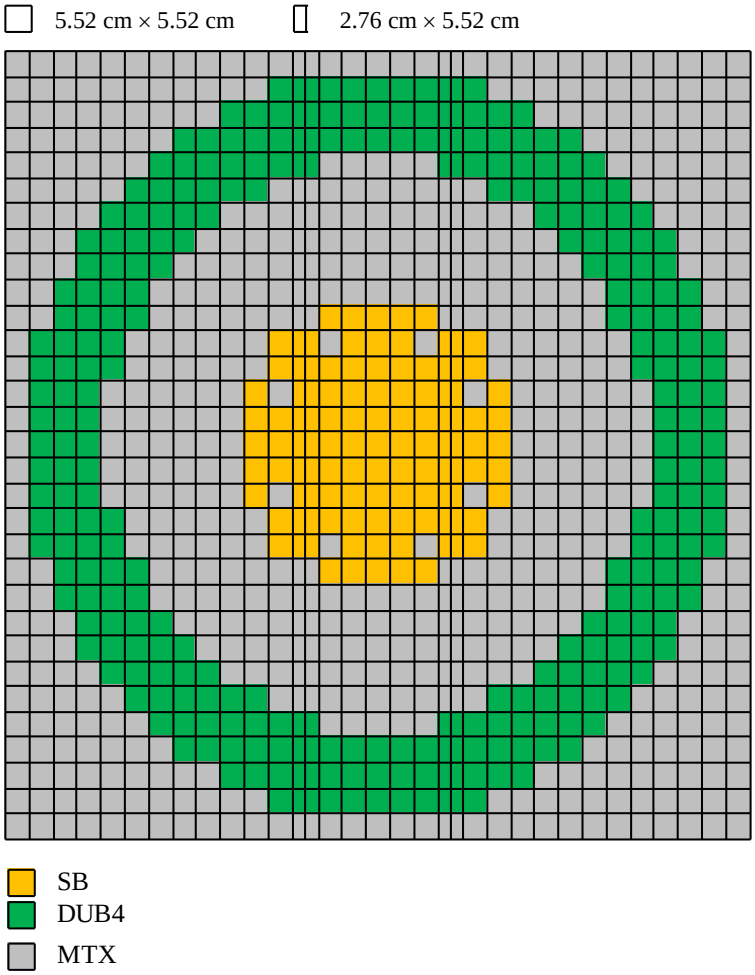

Figure B.3(g): X-Y cross-sectional views of the FCA XVVII-1 core for Cases 2 and 3 – Plane 7

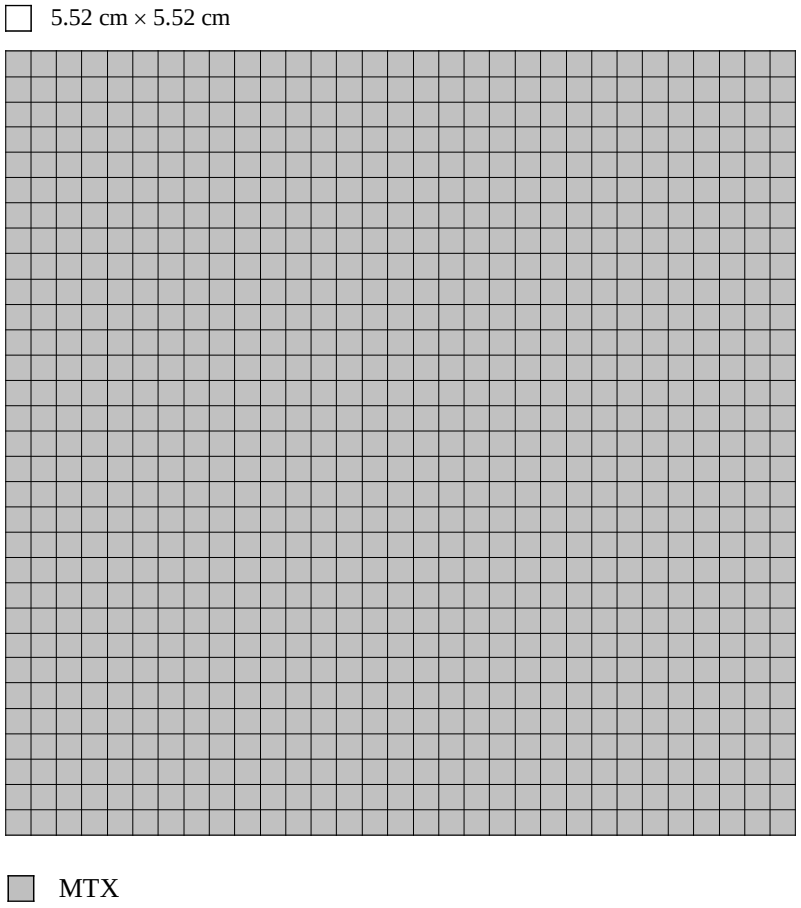

Figure B.4: Summary of calculation results

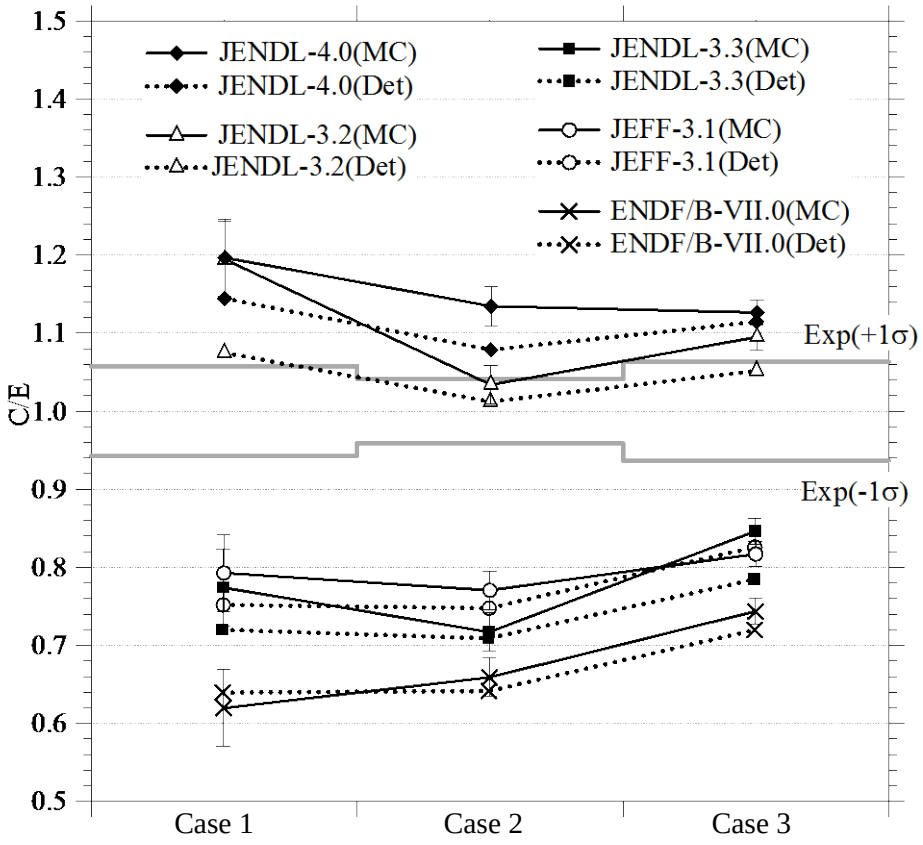

Appendix C: Initial benchmark analysis of ^{235}U capture cross-section in the energy region from 100 eV to 1 MeV

T.H. Trumbull, C.R. Lubitz

Introduction

WPEC Subgroup 18 focused on the thermal and epithermal energy region for ^{235}U. Several changes were made to ^{235}U, including a re-evaluation of the resonances by ORNL. The resulting data have become the basis for the current major libraries (ENDF/B-VII.0, JEFF-3.1 and JENDL-3.3).

Analysis by JAEA of the FCA-IX and BFS-62 benchmarks shows poor agreement when using the latest nuclear data libraries. The preliminary analysis seems to point to a problem with the ^{235}U fast capture cross-section and the capture-to-fission ratio (α).

SG29 formed in May 2007 to investigate this issue. JAEA has created several new ^{235}U evaluations that substitute ENDF/B-VII.0 and JENDL-3.2 resolved and unresolved resonance parameters in various combinations over various energy ranges. Since better agreement with the FCA-IX and BFS-62 benchmarks was obtained using JENDL-3.2, the new ^{235}U evaluations spliced in the older data into different energy ranges of interest, notably between 500 eV, 2 250 eV and 25 keV. The intent was to identify the set of parameters and energy ranges that produce results closer to expectations for fast and thermal reactor spectra.

Methods approach

Codes and data

All analysis at KAPL has been performed using the MC21 continuous energy Monte Carlo code with the NDEX nuclear data system [1]. MC21 cross-section libraries were created for seven of the eight proposed ^{235}U evaluations. Source data for all other materials in the model come from the ENDF/B-VII.0 data set. A base case library was created using all ENDF/B-VII.0 data. Table C.1 lists the case numbers and the associated ^{235}U evaluation. A graphical representation of the sources of nuclear data and resolved/unresolved resonance regions for all cases is provided in Table C.2.

A library for Case 5 was not created because the ^{235}U evaluation includes two unresolved resonance ranges in File 2. The current version of NDEX creates probability tables for the unresolved resonance range with the expectation that only a single unresolved range is given in File 2. The NDEX team is evaluating an appropriate fix.

Models and analysis

MC21 models were created for the specific models referenced in the previous JAEA analysis [2]: FCA-IX-1, FCA-IX-2, FCA-IX-3, ZEUS1, ZEUS2, ZEUS3 and ZEUS4. The ZEUS models are also listed in ICSBEP as HEU-MET-INTER-006, Cases 1-4. In addition, a set of 128 ICSBEP [3] models were created for MC21 that span a range of neutron energy spectra.

For the larger set of 128 models, the calculated-over-experimental (C/E) values for the effective multiplication factor were calculated and plotted for each of the eight different ^{235}U evaluations. The ensemble average *C/E* and standard deviation were calculated for each set of data. If the ensemble average *C/E* gets closer to 1.0 and the standard deviation decreases, relative to the base case, the candidate ^{235}U evaluation is judged an improvement. Table C.3 shows the listing of the ICSBEP models used in the study.

However, another test is performed on the solution tank HEU and LEU critical experiments to ensure that changes to the resonance parameters and ranges do not introduce problems in the thermal energy range that have been solved by SG18, e.g. *C/E* trends with above thermal leakage (ATL) or above thermal fission (ATF).

For the special cases of the FCA-IX and ZEUS models, more detailed analysis was performed. In addition to calculating the *C/E* values for each model, the capture, fission, α, slowing down densities, and ATL and ATF, were also calculated and compared for each case.

Results to date

Effect on FCA-IX and ZEUS critical benchmarks

Each case of ^{235}U source data was run in the FCA-IX and ZEUS (HMI-006) models and the resulting *C/E* are plotted in Figures C.1, C.2 and C.3. The plots are "line" plots in the sense that the abscissa is not an independent parameter. As such, the observed trends are only useful in a very general way, since the models are in order from left to right, based on increasing average energy of the neutrons causing fission.

The per source neutron capture and fission reaction rates for each model and each candidate ^{235}U were tallied over several energy ranges of interest. The tally group breakpoints were chosen to isolate effects over the various regions of interest, i.e. $E < 500$ eV, 500 eV $< E <$ 2 250 eV, 2 250 eV $< E <$ 25 keV and 25 keV $< E <$ 30 keV. Results are shown in Figure C.4.

Cases 2, 3 and 8 all have notably lower α values in the bins 500 eV < *E* < 2 250 eV. This appears to have a favourable effect on the C/E trends, based on the values plotted in Figures C.2 and C.3. However, to judge the trends definitively, the C/E values should be plotted against an independent variable that is a measure of the neutron energy spectrum in the models. Since the FCA and HMI have fast spectra, the traditional ATLF tally would be of little value. Instead, the average energy of a neutron causing fission was used as the spectral index for these models. The C/E versus average energy of a neutron causing fission plot is shown in Figure C.5.

In general, trends in *C/E* for critical system eigenvalues when plotted against a spectral index should be flat. A pronounced trend (slope) suggests that some energy-dependent cross-section parameter is affecting the results, e.g. capture-to-fission ratio. The "strength" of the trend is indicated by increasing value of r^2.

From the plots in Figure C.5 and the linear regression results shown in Table C.4, definite trends exist with all the cases analysed. Case 3 has a considerably lower slope and r^2 value (less trend) than the other cases. Cases 2 and 8 also show less of a trend when compared to the other cases.

Effect on C/E for selected ICSBEP critical benchmarks

This analysis was performed using the new data sets to assess the effect on the eigenvalue and the spread of the calculated eigenvalues on the population of ICSBEP benchmarks. The baseline was taken to be the results using ENDF/B-VII.0. For each data set, the ensemble average of the C/E, the sample standard deviation, and a "goodness-of-fit" parameter were calculated. The goodness-of-fit parameter, χ^2, was calculated using:

$$\chi^2 = \frac{1}{N-1}\sum_{i=1}^{N}\frac{\left(1-C_i/E_i\right)^2}{\left(\sigma_{C,i}^2+\sigma_{E,i}^2\right)^{1/2}} \qquad \text{(C.1)}$$

where: C_i is the calculated eigenvalue for the i^{th} benchmark;

E_i is the experimental *k*-effective for the i^{th} benchmark;

$\sigma_{C,i}^2$ and $\sigma_{E,i}^2$ are the squared uncertainties on the calculated and experimental *k* values;

N is the number of benchmark jobs analysed.

However, in considering that the ENDF/B-VII data (base case) has had ample "tuning", e.g. adjusting ^{235}U *K1* to improve comparisons to benchmarks, and the other cases have not, the data were "normalised" such that the ensemble average C/E is identically 1.0. The goodness-of-fit metric was then re-calculated. The overall effect of this normalisation is to isolate the variability of the data from systematic increases (or decreases) in reactivity inherent in the modified ^{235}U cases. The ensemble average,

standard deviation, "goodness-of-fit" metric, χ^2, and goodness-of-fit following normalisation, $\hat{\chi}^2$, for each case are listed in Table C.5. Smaller values of χ^2 represent better fits of the C/E values to the benchmark values.

Figure C.6 shows the results of the C/E for all 128 ICSBEP models using the ENDF/B-VII.0 data. The ensemble average and standard deviation were calculated to be 1.00036 and 0.00372, respectively. Approximately 72% of the *C/E* values fall inside one standard deviation of the mean and 100% of the data fall inside two standard deviations of the mean for this case. The $\hat{\chi}^2$ metric for this case is 4.77E-03.

The effect of Case 1 is to raise the ensemble average eigenvalue by 187 pcm. The standard deviation of the population also increased slightly to 407 pcm. The $\hat{\chi}^2$ metric for this case increased to 6.25E-03. Approximately 70% of the *C/E* values fall inside one standard deviation of the mean and approximately 96% of the data fall inside two standard deviations of the mean for this case. The Case 1 results are shown in Figure C.7.

Case 2 increases the ensemble average difference relative to the base case to 265 pcm. There is also some increase in the standard deviation (431 pcm) and several of the HCI models now fall outside of one standard deviation, as shown in Figure C.8. The $\hat{\chi}^2$ metric for this case is 6.37E-03, which is an improvement relative to Case 1, but remains higher than the base case. In all, approximately 73% of the *C/E* values fall inside one standard deviation of the mean and approximately 95% of the data fall inside two standard deviations of the mean.

Case 3 results in another increase in ensemble average with a difference relative to the base case of 283 pcm. However, there is considerably more scatter, as evidenced by the standard deviation increasing to 585 pcm. This is also apparent in the "goodness of fit," where the $\hat{\chi}^2$ metric has increased to 9.53E-03. Approximately 80% of the C/E values fall inside one standard deviation of the mean and approximately 95% of the data fall inside two standard deviations of the mean. Of particular note, the entire HCI set has been pushed outside of one standard deviation of the mean, as shown in Figure C.9.

The results of Case 4 are less reactive than Cases 2 and 3 and very similar to Case 1. The ensemble average C/E is 202 pcm higher than the base case and the standard deviation is 78 pcm greater. Approximately 76% of the data fall inside one standard deviation of the mean and approximately 95% fall inside two standard deviations of the mean. The $\hat{\chi}^2$ metric for this case is 6.44E-03. Again, the HCI set of models appear to be more sensitive to the changes. The Case 4 results are shown in Figure C.10.

Results for Case 6 are shown in Figure C.11. This case approaches the base case with only a 10 pcm difference in ensemble average and a nearly identical standard deviation of 377 pcm. The $\hat{\chi}^2$ metric is 4.80E-03 and is also very similar to the base case. This is not a surprising result given that

the difference between the base case and Case 6 source data was limited to an approximate 3% reduction in the Γ_γ for the resolved resonances. Approximately 70% of the data fall within one standard deviation of the mean and approximately 94% fall within two standard deviations of the mean.

Case 7 results are shown in Figure C.12. The ensemble average is increased relative to the base case by 42 pcm and the standard deviation is similar in magnitude to Cases 6 and 1. The $\hat{\chi}^2$ metric for this case is 5.18E-03. The results are consistent given that the difference in source data is limited to a 10% reduction in the Γ_γ for the resolved resonances. Approximately 73% of the data fall within one standard deviation of the mean and approximately 95% fall within two standard deviations of the mean.

Case 8 takes the resolved resonance parameters from the ENDF/B-VII.0 evaluation up to 500 eV and uses unresolved resonance parameters from a new analysis, independent of JENDL-3.2 or ENDF/B-VII.0. The results are shown in Figure C.13. The ensemble average increased by 14 pcm and the standard deviation increased to 425 pcm. The calculated $\hat{\chi}^2$ for this case is 5.61E-03. Approximately 75% of the data fall within one standard deviation of the mean and approximately 95% fall within two standard deviations of the mean.

The behaviour of the HCI set of benchmarks follows expectations. The reduction in α over the energy range of 500 eV to 2.25 keV is likely to affect intermediate spectrum reactors, such as HMI and HCI benchmarks. The result is to raise the reactivity of the HCI models, as seen in Figures C.8 and C.9. This is consistent with the response of the HMI models shown in Figure C.3.

Changes in the ^{235}U source data to better match results in the fast energy range could potentially introduce unintended effects in the thermal energy range. To judge these effects, the calculated C/E values for the HST and LST series of benchmarks were plotted against the ATLF for each model using each of the cases of ^{235}U source data. The ATLF is defined to be the net neutron leakage from the region in each model that encompasses the fuel. Figure C.14 shows the data and the linear trend lines associated with each data set. Linear regression results are provided in Table C.6. Cases 1, 2, 3 and 4 have non-zero slopes and coefficient of determination factors that indicate a definite trend.

Conclusions

In the cases analysed, changing the resolved and unresolved resonances by substituting JENDL-3.2 for ENDF/B-VII.0 in the URR, particularly in the range of 500 eV < E < 2 250 eV, seems to improve the trend of increasing C/E with increasing neutron spectra for the FCA and ZEUS benchmarks analysed. This is best demonstrated by Cases 2 and 3, where there is a large reduction

in α. However, these cases also have large increases in ensemble average C/E and increases in the spread of the C/E values within the population. In fact, Cases 2 and 3 cause the largest increase in ensemble average C/E (265 pcm and 283 pcm, respectively).

Relative to the FCA and ZEUS models analysed, Cases 2, 3 and 8 produce the "flattest" trend line when C/E is plotted against the average energy of a neutron causing fission. Unfortunately, all the cases containing the JENDL-3.2 data have unacceptably large trends in the HST/LST population, with C/E increasing with increasing ATLF. This would seem to suggest that only Case 8 is a viable candidate.

Case 8 demonstrates a modest increase in ensemble average C/E (14 pcm) and standard deviation, relative to ENDF/B-VII.0. This case also performs well in the LST/HST C/E versus ATLF analysis, and improves the FCA and ZEUS benchmark results. Since the focus of this study is on the ^{235}U alpha in the intermediate spectrum, additional ICSBEP intermediate spectrum HEU models should be added to the analysis. In addition to HMI-006 (ZEUS), the ICSBEP handbook lists eight other benchmarks in Volume II, HEU, intermediate-energy metal systems that would complement this study.

References – Appendix C

[1] Sutton, T.M., *et al.*, "The MC21 Monte Carlo Transport Code", *Proc. Joint Int. Topical Meeting on Mathematics and Computation and Supercomputing in Nuclear Applications*, Monterey, California, USA, 15-19 April (2007).

[2] Iwamoto, O., *et al.*, "Impact of JENDL-3.2 and ENDF/B-VII.0 Resonance Region (Resolved and Unresolved) in Intermediate Energy Benchmark Calculations", accessed 19 January 2009, *wwwndc.jaea.go.jp/iwamoto/sg29/Impact%20of%20JENDL3.2Final.pdf* (see Appendix A).

[3] Nuclear Energy Agency, *International Handbook of Evaluated Criticality Safety Benchmark Experiments*, NEA/NSC/DOC(95)03, OECD/NEA, Paris, CD-ROM (2008).

Table C.1: Description of candidate ^{235}U evaluations and corresponding case and NDEX version numbers

Case number	NDEX version	Notes	RR	URR
(Base)	V250	Base case with all ENDF/B-VII.0 data	≤ 2 250 eV	2 250 eV < *E* ≤ 25 keV
1	V260	Case 1 JENDL-3.2, RR (<2.25 keV) from ENDF/B-VII.0	≤ 2 250 eV	2 250 eV < *E* ≤ 30 keV
2	V261	Case 2 JENDL-3.2 + RR (<500 eV) from ENDF/V-VII	≤ 500 eV	500 eV < *E* ≤ 30 keV
3	V262	ENDF/B-VII.0 + JENDL-3.2 (<25 keV)	≤ 4 eV 4 eV < *E* ≤ 110 eV 110 eV < *E* ≤ 300 eV 300 eV < *E* ≤ 500 eV	500 eV < *E* ≤ 25 keV
4	V263	ENDF/B-VII.0 + JENDL-3.2 (<500 eV)	≤ 4 eV 4 eV < *E* ≤ 110 eV 110 eV < *E* ≤ 300 eV 300 eV < *E* ≤ 500 eV 500 eV < *E* ≤ 2 250 eV	2 250 eV < *E* ≤ 25 keV
5	V264	ENDF/B-VII.0(<500eV) + JENDL-3.2 (<2.5 keV) + ENDF/B-VII.0 (<25 keV)	≤ 500 eV	500 eV < *E* ≤ 2 250 eV 2 250 eV < *E* ≤ 25 keV
6 (g1)	V265	Has different RR parameters than ENDF/B-VII.0, otherwise identical. Γ_γ reduced approx. 3% from ENDF/B-VII.0 values for *Er* > 200.2028 eV.	≤ 2 250 eV	2 250 eV < *E* ≤ 25 keV
7 (g2)	V266	Has different RR parameters than ENDF/B-VII.0 and V265, otherwise identical. Γ_γ reduced approx. 10% from ENDF/B-VII.0 values for *Er* > 200.2028 eV.	≤ 2 250 eV	2 250 eV < *E* ≤ 25 keV
8	V267	JENDL/AC-2008 ^{235}U has RR parameters from ENDF/B-VII.0 evaluation. URR parameters from new analysis.	≤ 500 eV	500 eV < *E* ≤ 30 keV

Table C.2: Graphical description of the source nuclear data and energy breakpoints used to define the resolved and unresolved resonance regions for the cases of interest

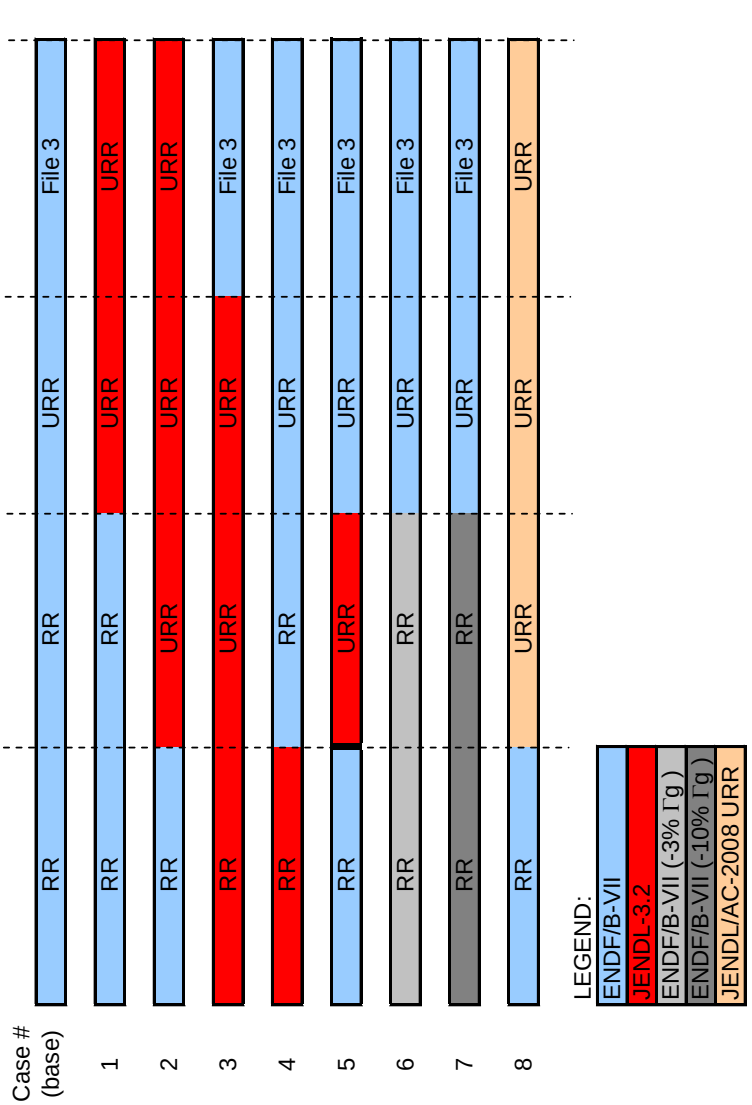

Table C.3: Listing of ICSBEP models used in this analysis

ICSBEP ID	Job ID	Exp. k_{eff}	Exp. unc.
HMT_001_01#	1	1.00100	0.00600
HMT_001_01D#	2	1.00100	0.00600
HMT_014_01	3	0.99390	0.00150
HMF_001_01A*	4	1.00000	0.00100
HMF_001_01B*	5	1.00000	0.00100
HMF_002_01	6	1.00000	0.00300
HMF_002_02	7	1.00000	0.00300
HMF_002_03	8	1.00000	0.00300
HMF_002_04	9	1.00000	0.00300
HMF_002_05	10	1.00000	0.00300
HMF_002_06	11	1.00000	0.00300
HMF_003_01	12	1.00000	0.00500
HMF_003_02	13	1.00000	0.00500
HMF_003_03	14	1.00000	0.00500
HMF_003_04	15	1.00000	0.00300
HMF_003_05	16	1.00000	0.00300
HMF_003_06	17	1.00000	0.00300
HMF_003_07	18	1.00000	0.00300
HMF_004_01	19	1.00200	0.00010
HMF_009_01	20	0.99920	0.00150
HMF_015_01	21	0.99960	0.00170
HMF_018_01	22	1.00000	0.00140
HMF_019_01	23	1.00000	0.00280
HMF_019_02	24	1.00000	0.00280
HMF_020_01	25	1.00000	0.00280
HMF_021_01	26	1.00000	0.00240
HMF_022_01	27	1.00000	0.00190
HMF_027_01	28	1.00000	0.00250
HMF_028_01	29	1.00000	0.00300
HMF_029_01	30	1.00000	0.00200
HMF_032_01	31	1.00000	0.00160
HMF_032_02	32	1.00000	0.00270
HMF_032_03	33	1.00000	0.00170
HMF_032_04	34	1.00000	0.00170
HMF_034_01	35	0.99900	0.00120
HMF_034_02	36	0.99900	0.00120
HMF_034_03	37	0.99900	0.00120
HCI_003_01	38	1.00000	0.00570
HCI_003_02	39	1.00000	0.00610
HCI_003_03	40	1.00000	0.00560
HCI_003_04	41	1.00000	0.00550
HCI_003_05	42	1.00000	0.00470
HCI_003_06	43	1.00000	0.00470
HCI_003_07	44	1.00000	0.00500
IMF_003	45	1.00000	0.00170
IMF_005	46	1.00000	0.00210
IMF_006	47	1.00000	0.00230
IMF_009	48	1.00000	0.00530
LCT_002_01	49	0.99970	0.00200
LCT_002_02	50	0.99970	0.00200
LCT_002_03	51	0.99970	0.00200
LCT_002_04	52	0.99970	0.00200
LCT_002_05	53	0.99970	0.00200
LCT_010_01	54	1.00000	0.00210
LCT_010_08	55	1.00000	0.02100
LCT_010_12	56	1.00000	0.00210
LCT_010_17	57	1.00000	0.00280
LCT_010_21	58	1.00000	0.00280
LCT_010_30	59	1.00000	0.00280
HST_001_01	60	1.00040	0.00600
HST_001_02	61	1.00210	0.00720
HST_001_03	62	1.00030	0.00350
HST_001_04	63	1.00080	0.00530
HST_001_05	64	1.00010	0.00490
HST_001_06	65	1.00020	0.00460
HST_001_07	66	1.00080	0.00400
HST_001_08	67	0.99980	0.00380
HST_001_09	68	1.00080	0.00540
HST_001_10	69	0.99930	0.00540
HST_009_01	70	0.99900	0.00430
HST_009_02	71	1.00000	0.00390
HST_009_03	72	1.00000	0.00360
HST_009_04	73	0.99860	0.00350
HST_010_01	74	1.00000	0.00290
HST_010_02	75	1.00000	0.00290
HST_010_03	76	1.00000	0.00290
HST_010_04	77	0.99920	0.00290
HST_011_01	78	1.00000	0.00230

* The “A” and “B” designate the shell model and solid sphere models, respectively.

\# The “D” designates the detailed geometry model for this benchmark.

Table C.3: Listing of ICSBEP models used in this analysis (*cont.*)

ICSBEP ID	Job ID	Exp. k_{eff}	Exp. unc.
HST_011_02	79	1.00000	0.00230
HST_012_01	80	0.99990	0.00580
HST_013_01	81	1.00120	0.00260
HST_013_02	82	1.00070	0.00360
HST_013_03	83	1.00090	0.00360
HST_013_04	84	1.00030	0.00360
HST_032_01	85	1.00150	0.00260
HST_042_01	86	0.99570	0.00390
HST_042_02	87	0.99650	0.00360
HST_042_03	88	0.99940	0.00280
HST_042_04	89	1.00000	0.00340
HST_042_05	90	1.00000	0.00340
HST_042_06	91	1.00000	0.00370
HST_042_07	92	1.00000	0.00360
HST_042_08	93	1.00000	0.00350
HST_043_01	94	0.99860	0.00310
HST_043_02	95	0.99950	0.00260
HST_043_03	96	0.99900	0.00250
LST_001_01	97	0.99910	0.00290
LST_002_01	98	1.00380	0.00400
LST_002_02	99	1.00240	0.00370
LST_002_03	100	1.00240	0.00440
LST_003_01	101	0.99970	0.00390
LST_003_02	102	0.99930	0.00420
LST_003_03	103	0.99950	0.00420
LST_003_04	104	0.99950	0.00420
LST_003_05	105	0.99970	0.00480
LST_003_06	106	0.99990	0.00490
LST_003_07	107	0.99940	0.00490
LST_003_08	108	0.99930	0.00520
LST_003_09	109	0.99960	0.00520
LST_004_01	110	0.99940	0.00080
LST_004_29	111	0.99990	0.00090
LST_004_33	112	0.99990	0.00090
LST_004_34	113	0.99990	0.00100
LST_004_46	114	0.99990	0.00100
LST_004_51	115	0.99940	0.00110
LST_004_54	116	0.99960	0.00110
LST_007_14	117	0.99610	0.00090
LST_007_30	118	0.99730	0.00090
LST_007_32	119	0.99850	0.00100
LST_007_36	120	0.99880	0.00110
LST_007_49	121	0.99830	0.00110
LST_016_105	122	0.99960	0.00130
LST_016_113	123	0.99990	0.00130
LST_016_125	124	0.99940	0.00140
LST_016_129	125	0.99960	0.00140
LST_016_131	126	0.99950	0.00140
LST_016_140	127	0.99920	0.00150
LST_016_196	128	0.99940	0.00150

Table C.4: Linear regression results of C/E plotted using the average energy of a neutron causing fission as the independent variable

Coefficient of determination (r^2) values indicate definite trends for all cases; Cases 2, 3 and 8 have the smallest slopes of the cases tested

Case #	Slope	Intercept	r^2
(Base)	3.31933×10^{-8}	0.98463	0.99
1	3.02917×10^{-8}	0.98196	0.99
2	1.31073×10^{-8}	1.00235	0.68
3	6.10880×10^{-9}	1.01405	0.17
4	2.05846×10^{-8}	0.99566	0.93
6	3.02542×10^{-8}	0.98765	0.99
7	2.37662×10^{-8}	0.99474	0.94
8	1.36315×10^{-8}	0.99912	0.69

Table C.5: Statistical analysis of the benchmark results for various cases of ^{235}U

Case	$\bar{x}$	σ	χ^2	$\hat{\chi}^2$
Base	1.00036	0.00372	4.93E-03	4.77E-03
Case 1	1.00223	0.00407	8.85E-03	6.25E-03
Case 2	1.00301	0.00431	1.05E-02	6.37E-03
Case 3	1.00319	0.00585	1.33E-02	9.53E-03
Case 4	1.00238	0.00450	8.85E-03	6.44E-03
Case 6	1.00046	0.00377	5.01E-03	4.80E-03
Case 7	1.00078	0.00399	5.58E-03	5.18E-03
Case 8	1.00050	0.00425	5.82E-03	5.61E-03

Table C.6: Linear regression results of C/E plotted using the above thermal leakage fraction as the independent variable

Coefficient of determination (r^2) values indicate definite trends for Cases 1, 2, 3 and 4

Case #	Slope	Intercept	r^2
(Base)	4.66075×10^{-5}	0.99963	0.00
1	1.01086×10^{-2}	1.00034	0.18
2	1.12537×10^{-2}	1.00025	0.22
3	7.94428×10^{-3}	0.99999	0.11
4	6.24822×10^{-3}	1.00010	0.07
6	4.34652×10^{-4}	0.99948	0.00
7	8.85455×10^{-4}	0.99950	0.00
8	8.39705×10^{-4}	0.99942	0.00

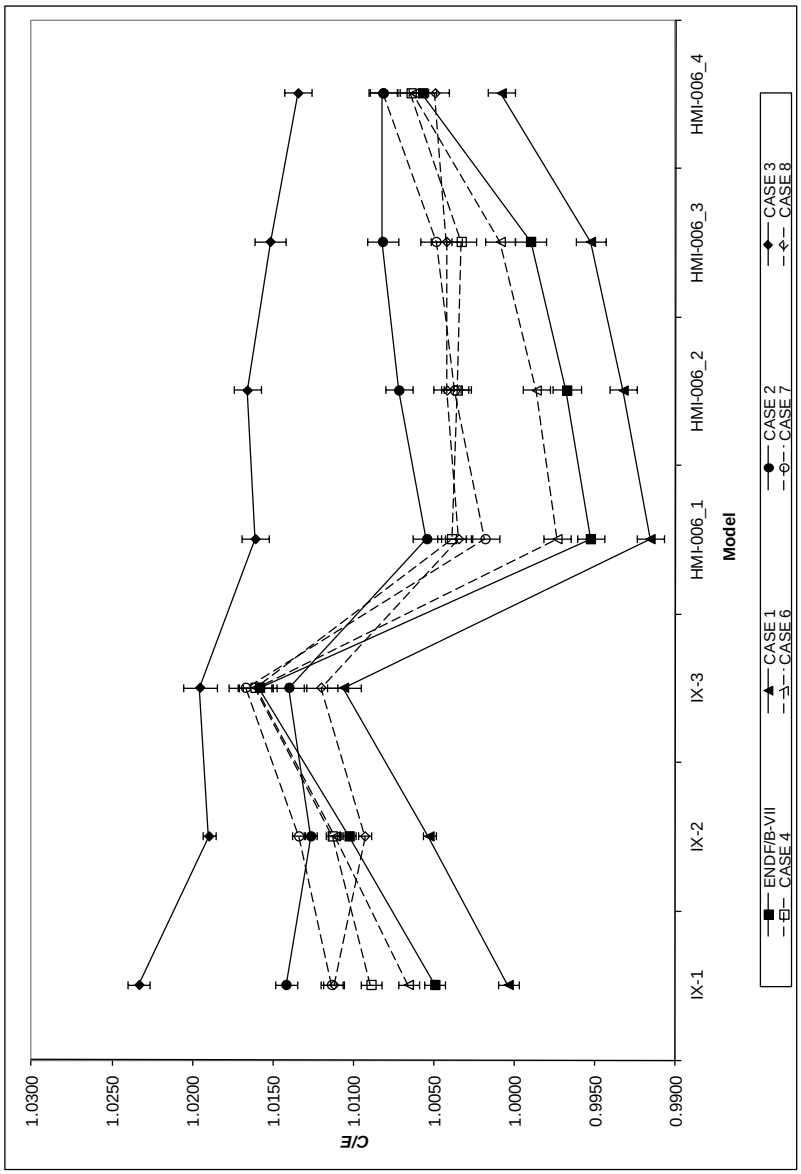

Figure C.1: Calculated values of C/E for each ^{235}U case in the FCA-IX and ZEUS models, including ENDF/B-VII.0 (the "base" case)

Figure C.2: Calculated values of C/E for each ^{235}U case in the FCA-IX models, including ENDF/B-VII.0 (the "base" case)

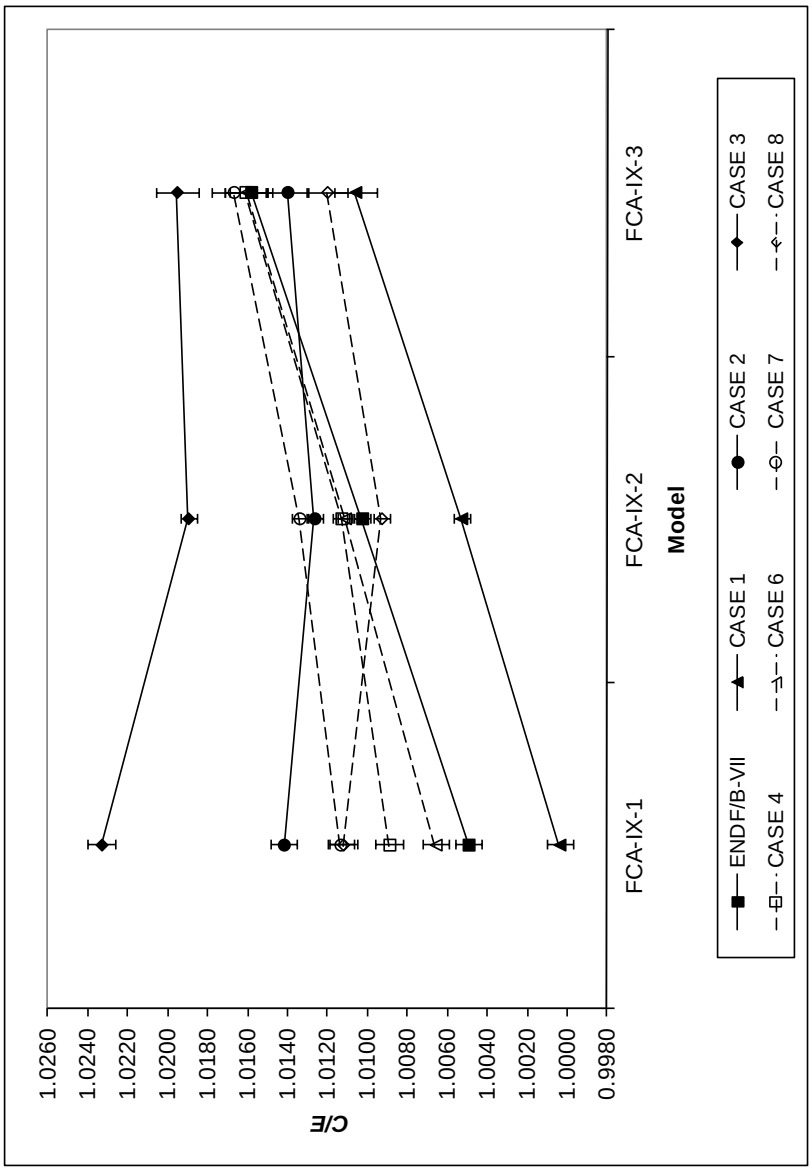

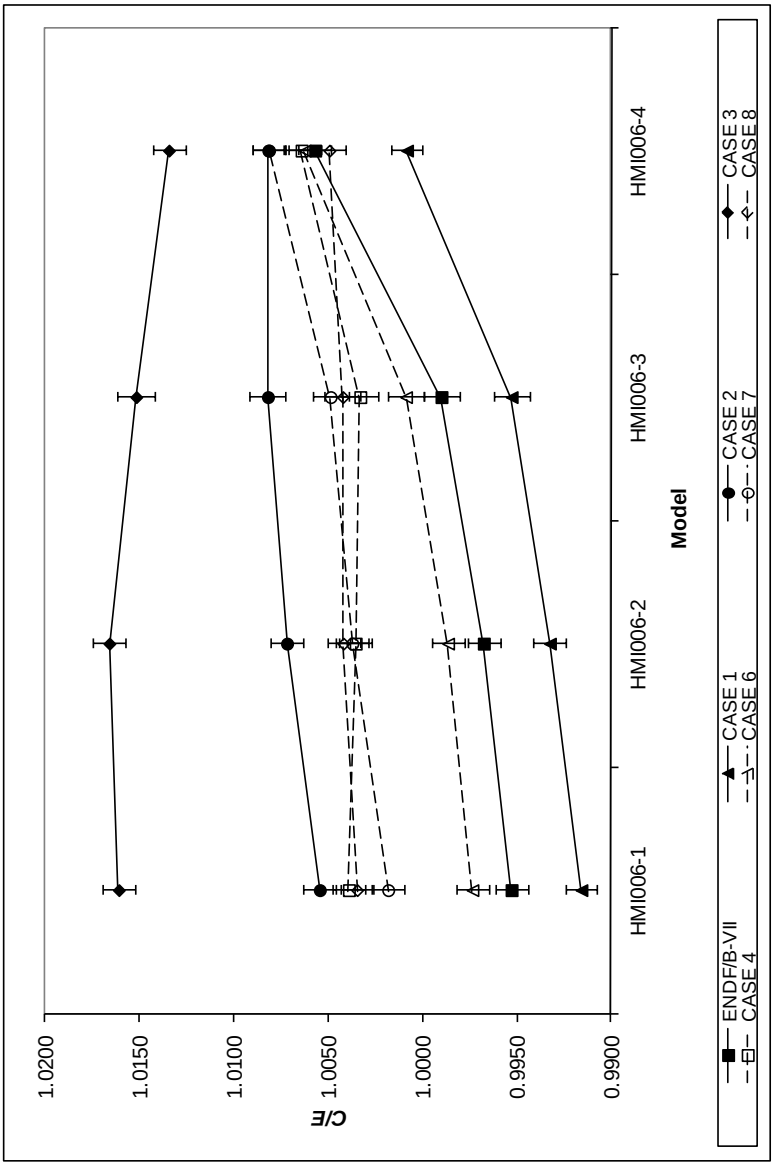

Figure C.3: Calculated values of C/E for each ^{235}U case in the ZEUS (HMI-006) models, including ENDF/B-VII.0 (the "base" case)

Figure C.4: Capture-to-fission ratio (α) plots for each ^{235}U case and each FCA-IX and ZEUS model analysed

The bin labels represent the top of the energy bin; energy bins were selected to isolate effects in the resolved and unresolved ranges of interest

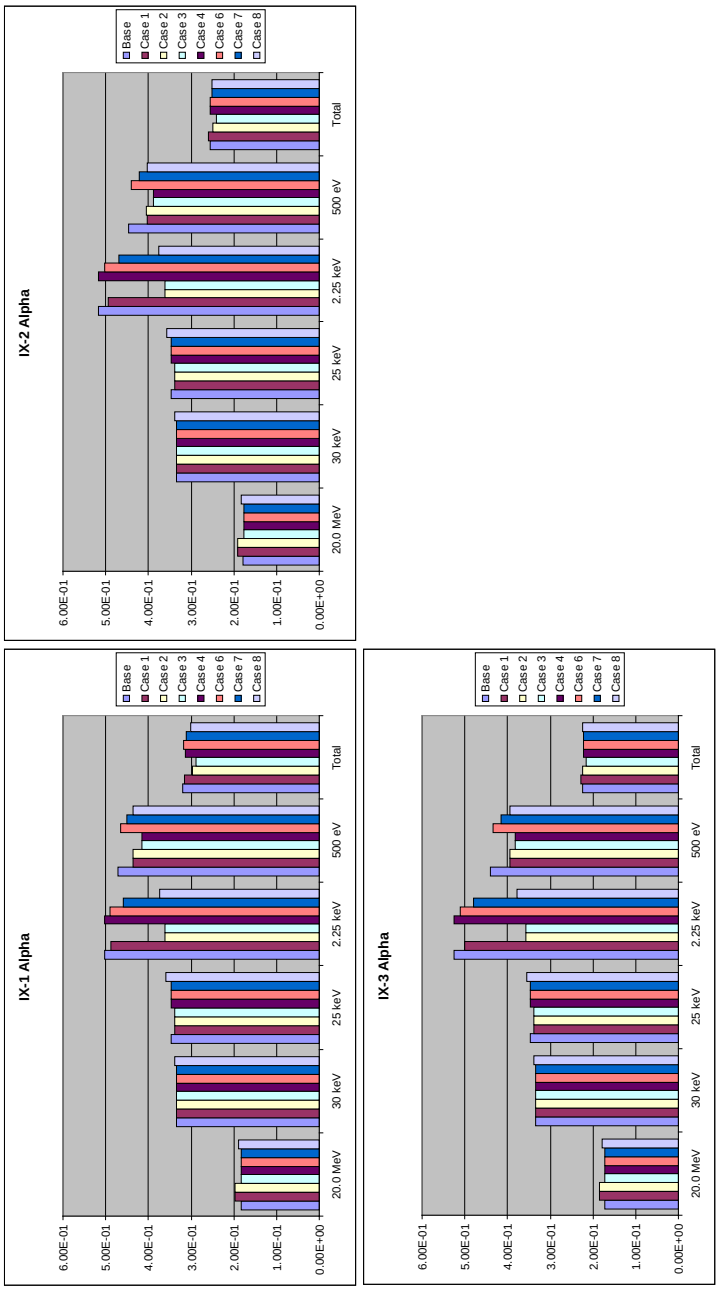

Figure C.4: Capture-to-fission ratio (α) plots for each ^{235}U case and each FCA-IX and ZEUS model analysed (*cont.*)

The bin labels represent the top of the energy bin; energy bins were selected to isolate effects in the resolved and unresolved ranges of interest

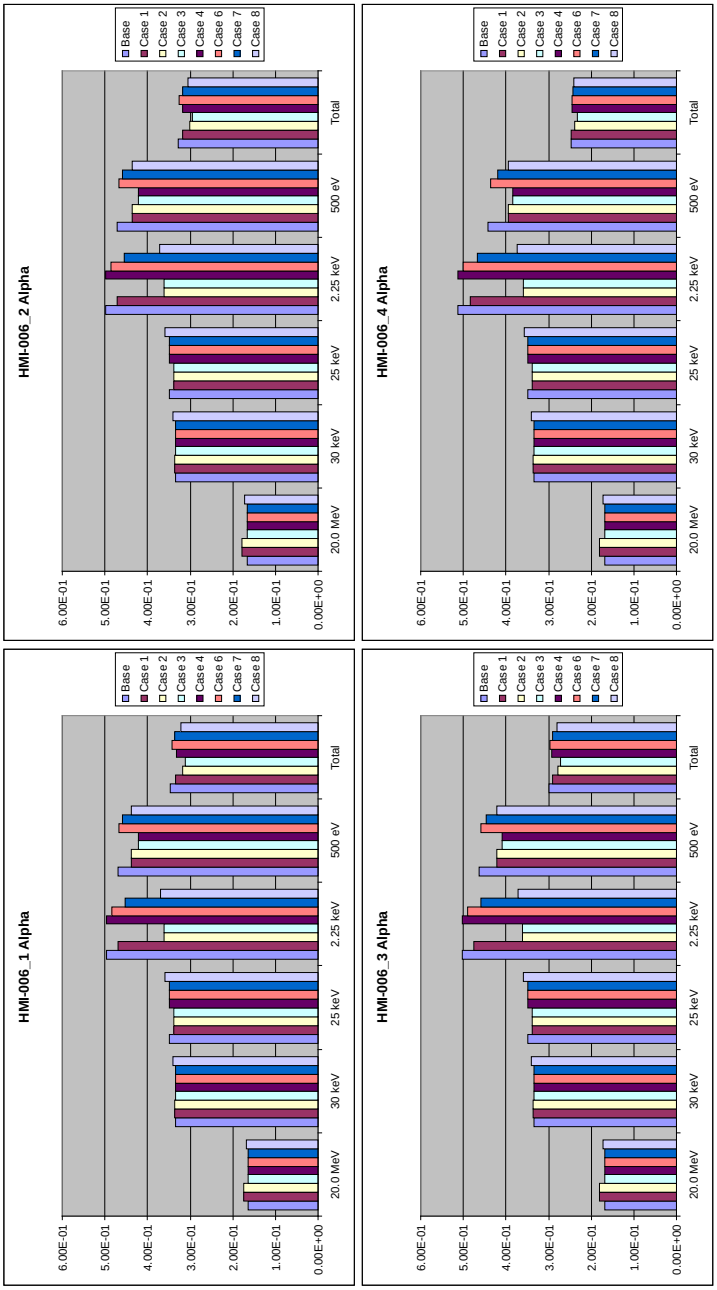

Figure C.5: The C/E trends as a function of the average energy of a neutron causing fission in the FCA and HMI-006 models

All the models show an increasing C/E with increasing average energy of the neutrons causing fission

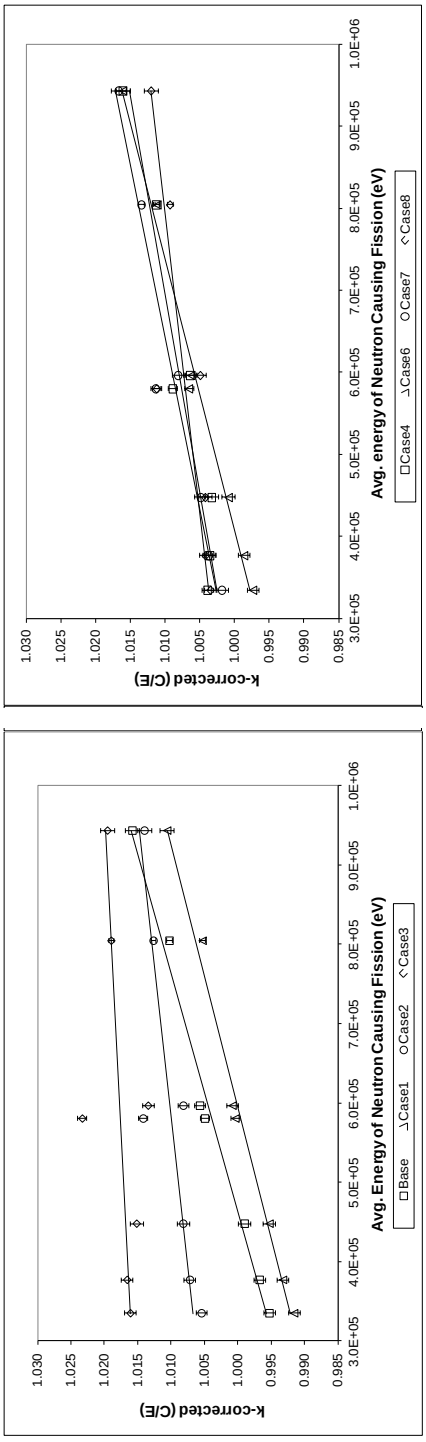

Figure C.6: Ensemble average and standard deviation for C/E of multiplication factor calculated using a suite of 128 ICSBEP benchmarks and ENDF/B-VII.0 cross-sections for ^{235}U

The ENDF/B-VII.0 ^{235}U resolved and unresolved ranges are $E \leq 2\,250$ eV and 2 250 eV < $E \leq 25$ keV, respectively

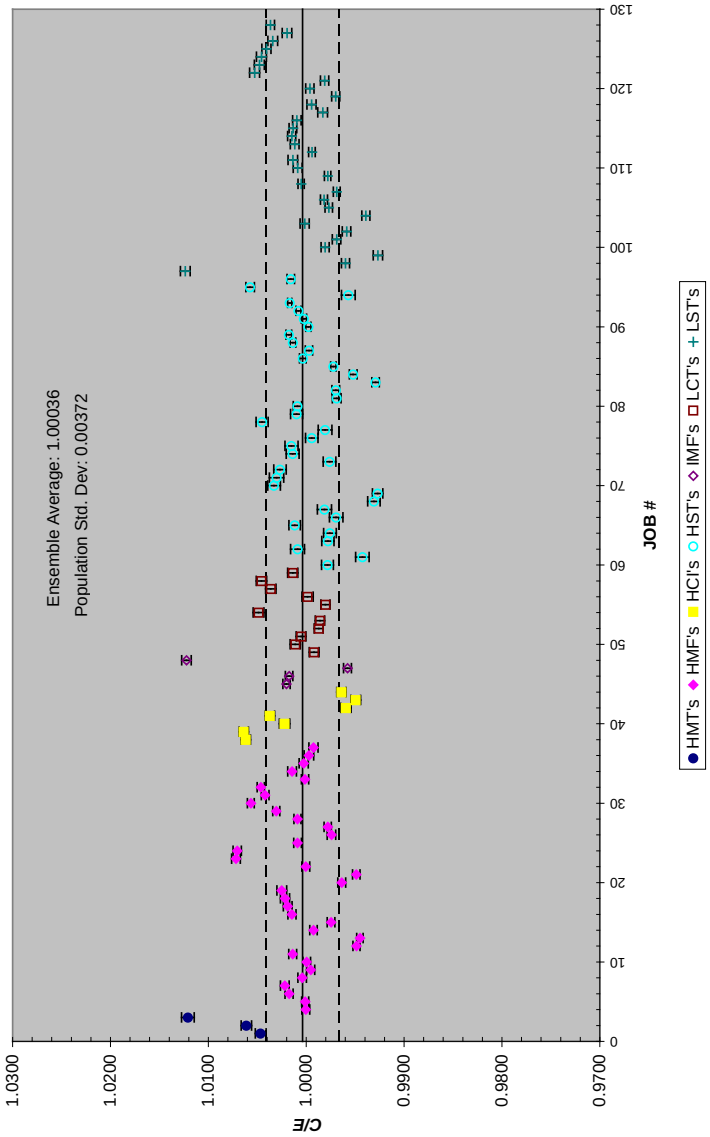

Figure C.7: Ensemble average and standard deviation for C/E of multiplication factor calculated using a suite of 128 ICSBEP benchmarks and JAEA Case 1 ^{235}U

Case 1 ^{235}U resolved and unresolved ranges are $E \leq 2\ 250$ eV and 2 250 eV < $E \leq 30$ keV, respectively; the resolved resonance parameters are from ENDF/B-VII.0 and the unresolved resonance parameters are from JENDL-3.2

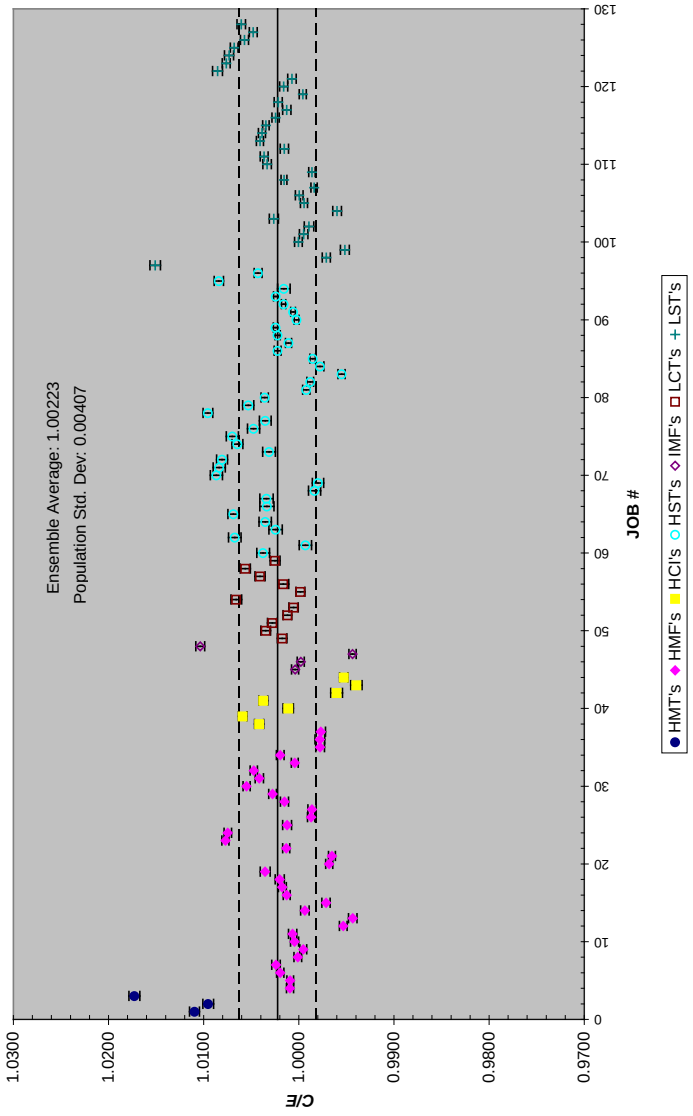

Figure C.8: Ensemble average and standard deviation for C/E of multiplication factor calculated using a suite of 128 ICSBEP benchmarks and JAEA Case 2 ^{235}U

Case 2 ^{235}U resolved and unresolved ranges are $E \leq 500$ eV and 500 eV < $E \leq 30$ keV, respectively; the resolved resonance parameters are from ENDF/B-VII.0 and the unresolved resonance parameters are from JENDL-3.2

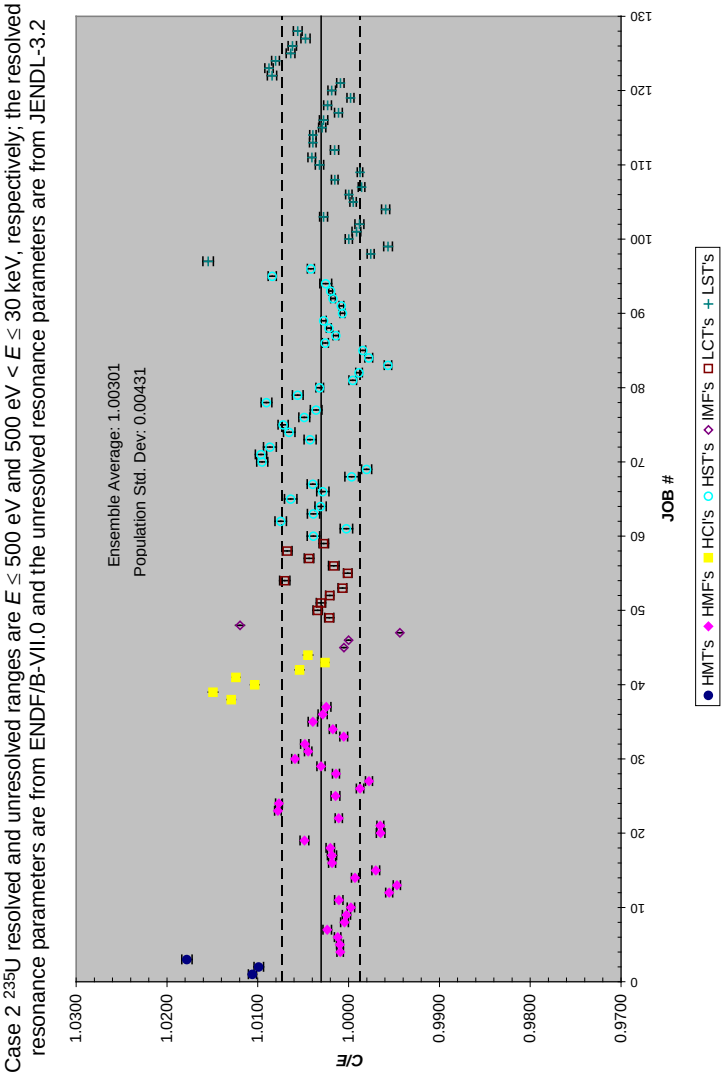

Figure C.9: Ensemble average and standard deviation for C/E of multiplication factor calculated using a suite of 128 ICSBEP benchmarks and JAEA Case 3 ^{235}U

Case 3 ^{235}U resolved and unresolved ranges are $E \leq 2\ 250$ eV and 2 250 eV < $E \leq 25$ keV, respectively; the resolved and unresolved resonance parameters are from JENDL-3.2 and the remaining data are from ENDF/B-VII.0

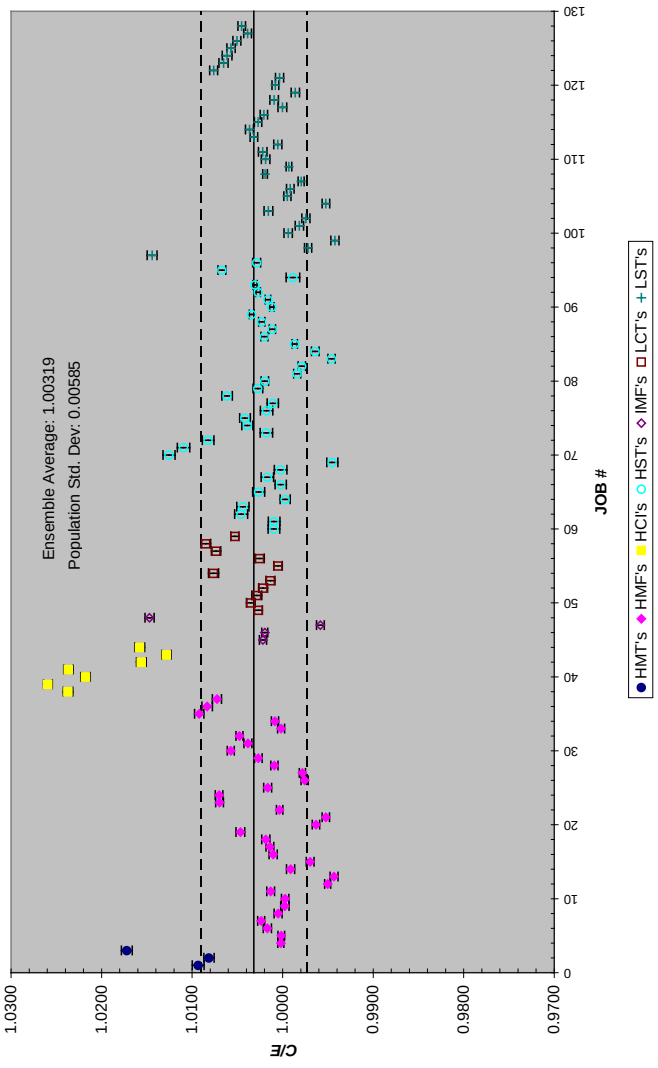

Figure C.10: Ensemble average and standard deviation for C/E of multiplication factor calculated using a suite of 128 ICSBEP benchmarks and JAEA Case 4 ^{235}U

Case 4 ^{235}U resolved and unresolved ranges are $E \leq 2\ 250$ eV and 2 250 eV < $E \leq 25$ keV, respectively; the resolved resonance parameters are from JENDL-3.2 up to 500 eV and the remaining resolved and unresolved parameters are from ENDF/B-VII.0

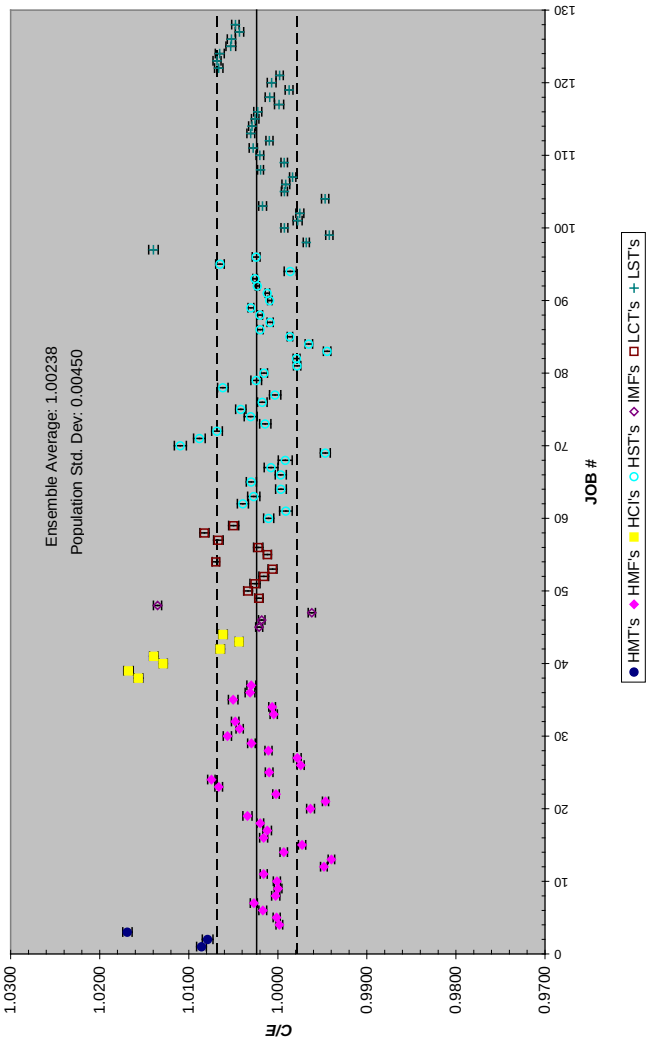

Figure C.11: Ensemble average and standard deviation for C/E of multiplication factor calculated using a suite of 128 ICSBEP benchmarks and JAEA Case 6 ^{235}U

Case 6 ^{235}U resolved and unresolved ranges are $E \leq 2\ 250$ eV and $2\ 250$ eV $< E \leq 25$ keV, respectively; the resolved resonance parameters are from ENDF/B-VII.0 with an approximate reduction in Γ_γ of 3% for resonance energies above ~200 eV and the unresolved parameters are from ENDF/B-VII.0

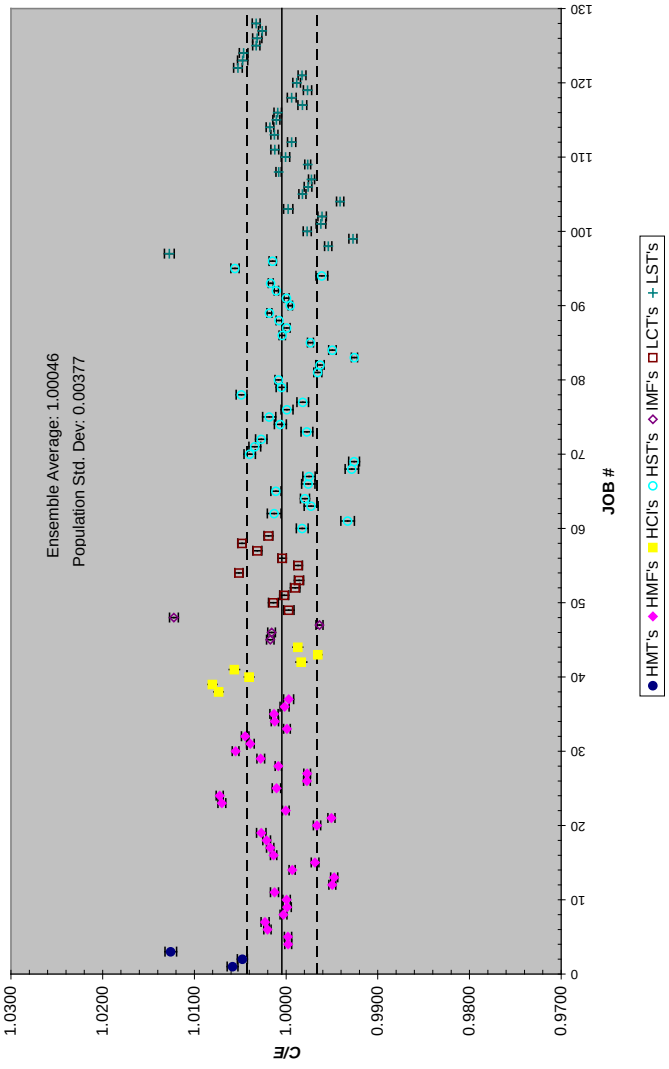

Figure C.12: Ensemble average and standard deviation for C/E of multiplication factor calculated using a suite of 128 ICSBEP benchmarks and JAEA Case 7 ^{235}U

Case 7 ^{235}U resolved and unresolved ranges are $E \leq 2\ 250$ eV and $2\ 250$ eV $< E \leq 25$ keV, respectively; the resolved resonance parameters are from ENDF/B-VII.0 with an approximate reduction in Γ_γ of 10% for resonance energies above ~200 eV and the unresolved parameters are from ENDF/B-VII.0

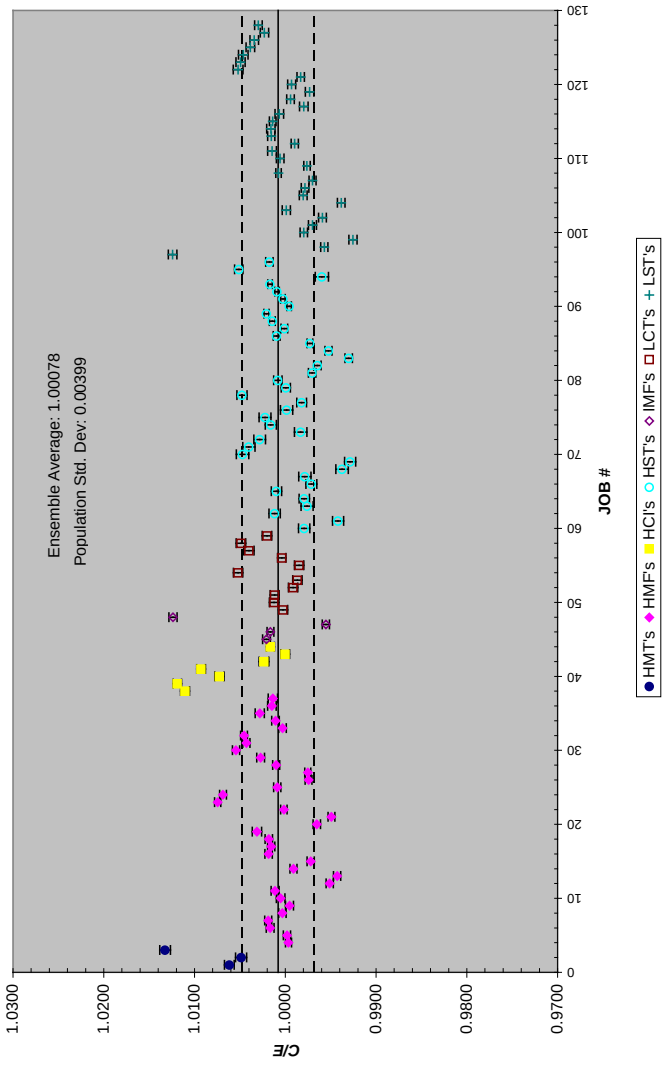

Figure C.13: Ensemble average and standard deviation for C/E of multiplication factor calculated using a suite of 128 ICSBEP benchmarks and JAEA Case 8 ^{235}U

Case 8 ^{235}U resolved and unresolved ranges are $E \leq 500$ eV and 500 eV < $E \leq 30$ keV, respectively; the resolved resonance parameters are from ENDF/B-VII.0 and the unresolved parameters are from a new analysis

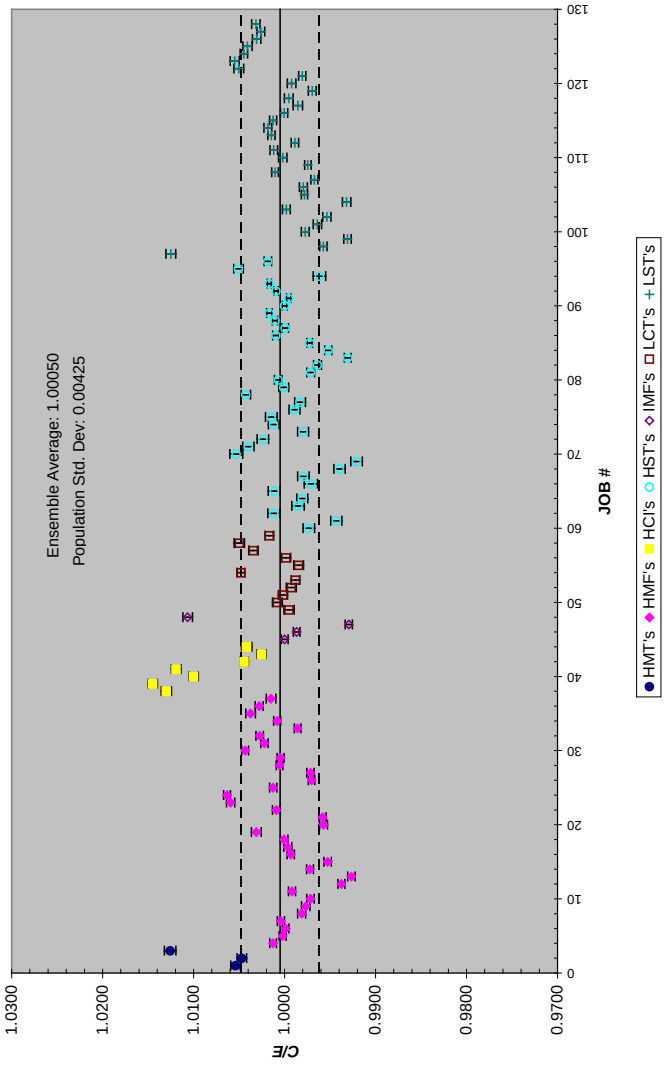

Figure C.14: C/E trends as a function of above thermal leakage fraction (ATLF) for a combined set of HST and LST benchmarks

Cases 1, 2, 3 and 4 have trends of increasing C/E with increasing ATLF

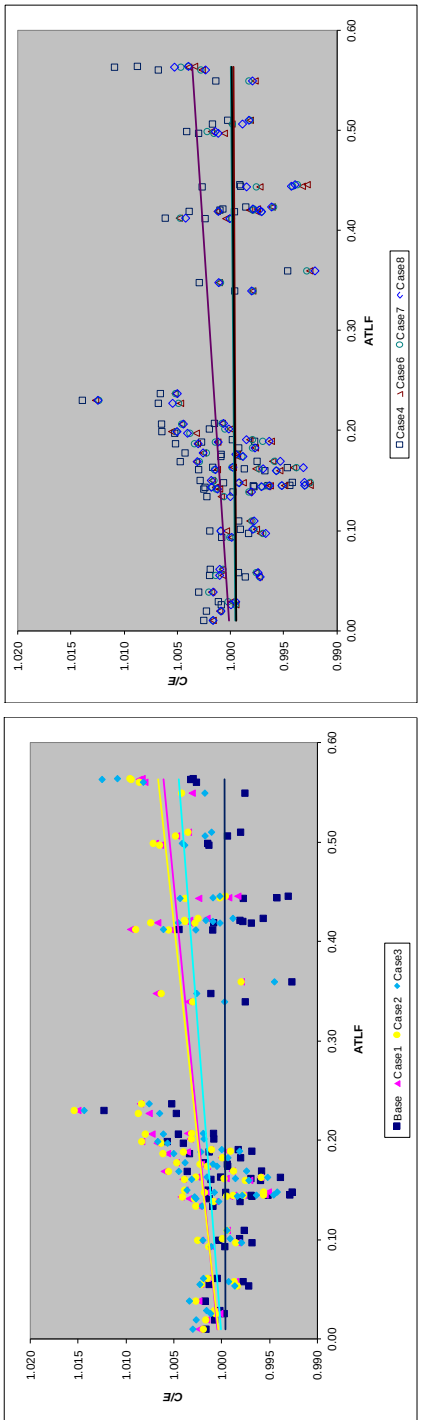

Appendix D: Analysis of BFS-2 sodium-void reactivity experiment with various libraries

M. Ishikawa, G. Chiba, T. Hazama, T. Iwai, K. Numata

Introduction

At the BFS-2 fast critical facility in Russia, an experiment series, BFS-62, was conducted as a collaborative research programme between JNC (the former JAEA) and IPPE in 1999-2003 [1]. The aim of the BFS-62 series was to investigate the nuclear characteristics of plutonium burner cores to support the Russian surplus weapons plutonium disposition project in the BN-600 fast reactor. In BFS-62, measurements were done in five assemblies. The first four (BFS-62-1, 2, 3A and 4) assemblies simulated the transition from the existing uranium-dioxide (UO_2) fuelled BN-600 core to a so-called "hybrid core", where approximately 20% of the UO_2 fuel was replaced by the uranium-plutonium mixed-oxide (MOX) fuel, and all the surrounding UO_2 blanket assemblies by stainless steel (SS) reflectors. The last one (BFS-62-5) studied the full MOX loading characteristics at core centre region. Figure D.1 depicts the layout of a typical case, the BFS-62-3A hybrid core [2].

The sodium-void reactivity (hereafter SVR) of the BFS-62 experiments is considered to be very effective to judge if there is any problem of the ^{235}U capture cross-section in resonance energy, since its sensitivity is very large to the SVR in the enriched-uranium fuel region, but negligible to that in the MOX fuel region. The experimental technique of the SVR measurements is identical in both regions, and the associated errors were reported [2] as similar in the range of ±0.3-0.5 cents (i.e. approximately ±5% except the MEZ region of BFS-62-3A), therefore, the calculation/experiment (C/E) values of both regions obtained with various libraries would give us useful information on the ^{235}U capture cross-sections from the library viewpoint.

Analysis

In the present study, the step-wise SVR of the three assemblies, BFS-62-2, -3A and -5, were analysed applying the heterogeneous cell model for effective cross-sections, and the diffusion-theory-based exact-perturbation

core calculation with transport theory and ultra-fine energy corrections to obtain the best-estimated reactivity. The resulting C/E with various libraries are summarised in Figure D.2. From this figure, we first notice that the C/E of the previous library, JENDL-3.2, are quite excellent for the SVR in both the enriched-uranium and the MOX regions. On the contrary, the three more recent libraries, JENDL-3.3, ENDF/B-VII.0 and JEFF-3.1, show extreme underestimation of the SVR in the enriched-uranium regions[1], but quite good performance in the MOX regions. To find the physical reasons of this large discrepancy, we performed the sensitivity analysis [3] based on the generalised perturbation theory. The sensitivity of a cross-section to an integral core parameter is defined by:

$$S_{m,x,g} = \frac{dR/R}{d\sigma_{m,x,g}/\sigma_{m,x,g}}$$

where R is an integral core parameter (here, SVR), m is a nuclide concerned with R, x is a reaction type (fission, capture, elastic, inelastic, n2n, mu-bar, chi, nu), and g is an energy group number (here, 70 groups in total).

The difference of a C/E value between a certain library ("A" Library) and JENDL-3.2 can be evaluated by multiplying the sensitivity with the cross-section differences and summing up as follows:

$$\frac{R_{"A"Library} - R_{JENDL-3.2}}{R_{JENDL-3.2}} = \sum_m \sum_x \sum_g \left[S_{m,x,g} \times \frac{\sigma_{m.x.g,"A"Library} - \sigma_{m.x.g,JENDL-3.2}}{\sigma_{m.x.g,JENDL-3.2}} \right]$$

where the sensitivity should be calculated with the basic library JENDL-3.2.

To understand the library effect, the two typical cases circled in Figure D.2 are selected: the SVR of the LEZ region in BFS-62-3A and the MOX region in the same core.

1) For the SVR of the LEZ region, the isotope- and reaction-wise contributions of the C/E differences with each library, JENDL-3.3, ENDF/B-VII.0 or JEFF-3.1, relative to JENDL-3.2 are summarised in Figure D.3. Obviously, the C/E changes of the three libraries from JENDL-3.2 are induced from the ^{235}U capture cross-sections. In detail, the JEFF-3.1 library shows the smaller C/E change of 20% compared with JENDL-3.3 or ENDF/B-VII.0 which has a 40% gap, the reason of which originating from the ^{23}Na inelastic contribution of JEFF-3.1 partly cancelling the ^{235}U capture effect.

1. Among the enriched-uranium regions, the C/E values of the HEZ region seem to show different trends than that of the LEZ or MEZ regions. Since the SVR of the HEZ region is found to be dominated by the neutron leakage term, we concentrate here on the SVR of the LEZ regions, the major mechanism of which is the non-leakage, that is, spectral shift term strongly related to the ^{235}U capture cross-section.

2) The isotope- and reaction-wise contributions for the SVR of the MOX region are shown in Figure D.4. All-related cross-section differences contribute little here. Though the ^{23}Na inelastic cross-section of JEFF-3.1 has a rather large contribution similar to the LEZ case, the total C/E change from JENDL-3.2 is quite small because of the cancellation with other nuclide- and reaction-wise contributions.

3) Figure D.5 shows that the sensitivity of ^{235}U capture cross-section to the SVR is very large in the LEZ region around keV energy, but is negligible in the MOX region. On the other hand, the ^{23}Na inelastic cross-section has similar trends of sensitivity in both the LEZ and MOX regions as shown in Figure D.6. This explains the different trends of ^{235}U capture and ^{23}Na inelastic cross-sections in Figures D.3 and D.4.

4) Figure D.7 shows the difference of the ^{235}U capture cross-sections with the three libraries relative to JENDL-3.2. The cross-sections of the resolved resonance energy region below 2.25 keV are identical among the three libraries since they adopt the same resolved resonance parameters supplied from ORNL [4]. Above 2.25 keV, the cross-sections of ENDF/B-VII.0 and JEFF-3.1 are also identical[2], therefore the ^{235}U capture effect of these two libraries on SVR in the LEZ region is the same as shown in Figure D.3. As for the ^{23}Na inelastic cross-sections, JEFF-3.1 is quite different from the other libraries in several MeV energies as can be seen in Figure D.8. This can explain the peculiarity of JEFF-3.1 due to the ^{23}Na inelastic cross-section observed in Figure D.3.

Conclusion

The SVR of the enriched-uranium regions in the BFS-62 experiments was found to be extremely underestimated by the three recent libraries, JENDL-3.3, ENDF/B-VII.0 and JEFF-3.1. From the comparison with JENDL-3.2 and the sensitivity analysis, the large underestimation of SVR could be attributed to the resolved resonance parameters of ^{235}U which were commonly adopted in the three libraries.

2. In Figures D.3 and D.7, very small differences between ENDF/B-VII.0 and JEFF-3.1 are found, because of the unresolved resonance treatment by the Monte Carlo method to generate the 70-group constants.

References – Appendix D

[1] Shono, A., *et al.*, "Reduction of Cross-section-induced Errors of the BN-600 Hybrid Core Nuclear Parameters by Using BFS-62 Critical Experiment Data", *Proc. of PHYSOR 2004 –The Physics of Fuel Cycles and Advanced Nuclear Systems: Global Developments*, 4A, Chicago, Illinois, 25-29 April 2004.

[2] Manturov, G., A. Kochetkov, *et al.*, "BFS-62-3A Experiment: Fast Reactor Core with U and U-Pu Fuel of 17% Enrichment and Partial Stainless Steel Reflector", *International Handbook of Evaluated Reactor Physics Benchmark Experiments (IRPhE)*, BFS2-LMFR-EXP-001, NEA/NSC/DOC(2006)1, OECD/NEA, Paris (2010).

[3] Ishikawa, M., "Recent Application of Nuclear Data to Fast Reactor Core Analysis and Design in Japan", *Proc. Int. Conf. on Nuclear Data for Science and Technology (ND2004)*, Santa Fe, NM, USA, 26 September-1 October 2004.

[4] Leal, L.C., *et al.*, "R-matrix Analysis of ^{235}U Neutron Transmission and Cross-section Measurements in the 0- to 2.25-keV Energy Range", *Nuclear Science and Engineering*, 131, p. 230 (1999).

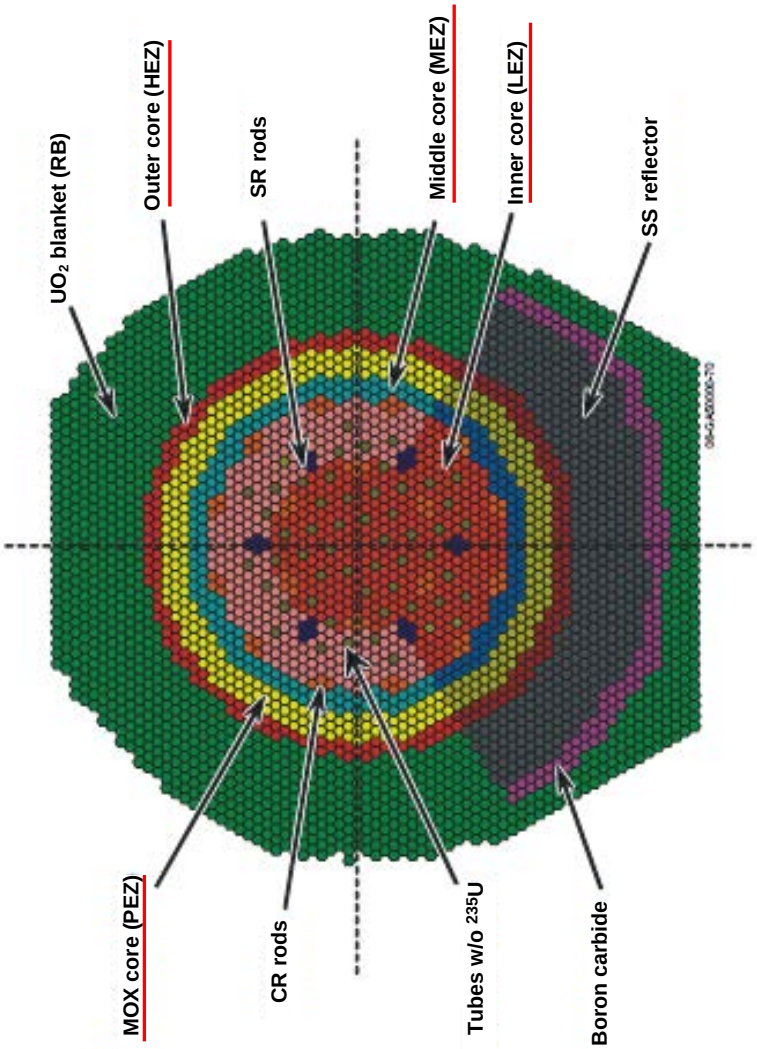

Figure D.1: Layout of BFS-62-3A critical assembly [2]

The LEZ, MEZ and HEZ regions are comprised of enriched-uranium fuel (enrichment: LEZ < MEZ < HEZ); the PEZ (MOX) region consists of plutonium fuel without ^{235}U

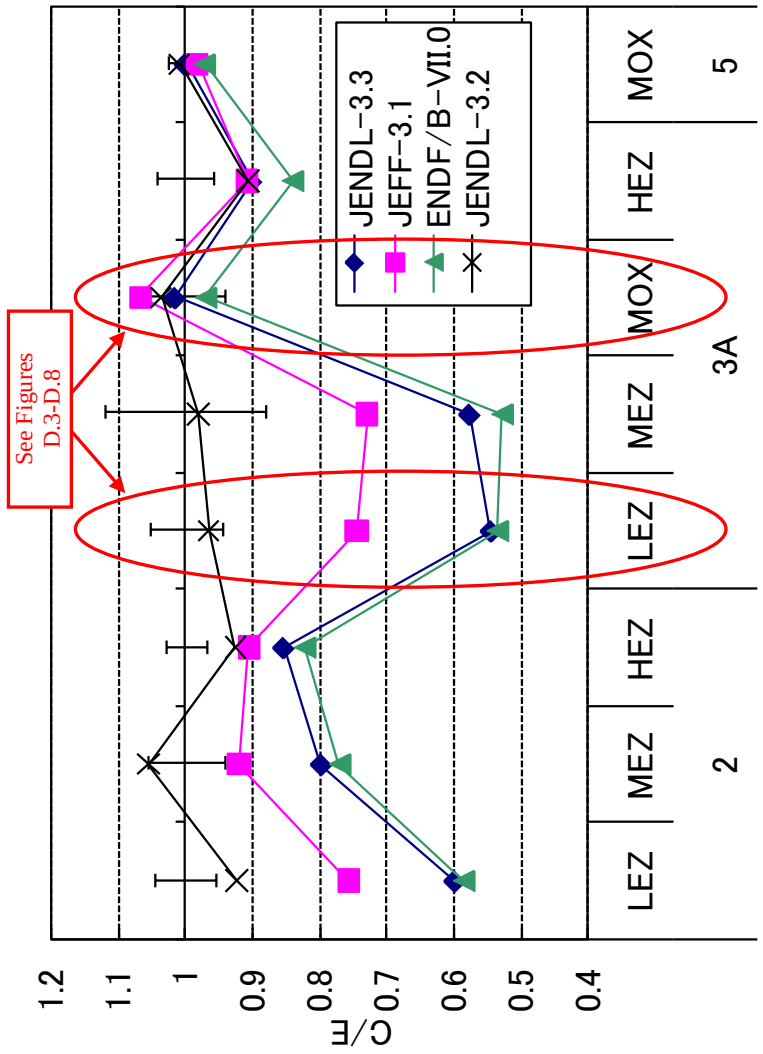

Figure D.2: C/E values of step-wise sodium-void reactivity in BFS-62 experiments

Figure D.3: Isotope- and reaction-wise contribution of the C/E differences with various libraries relative to JENDL-3.2

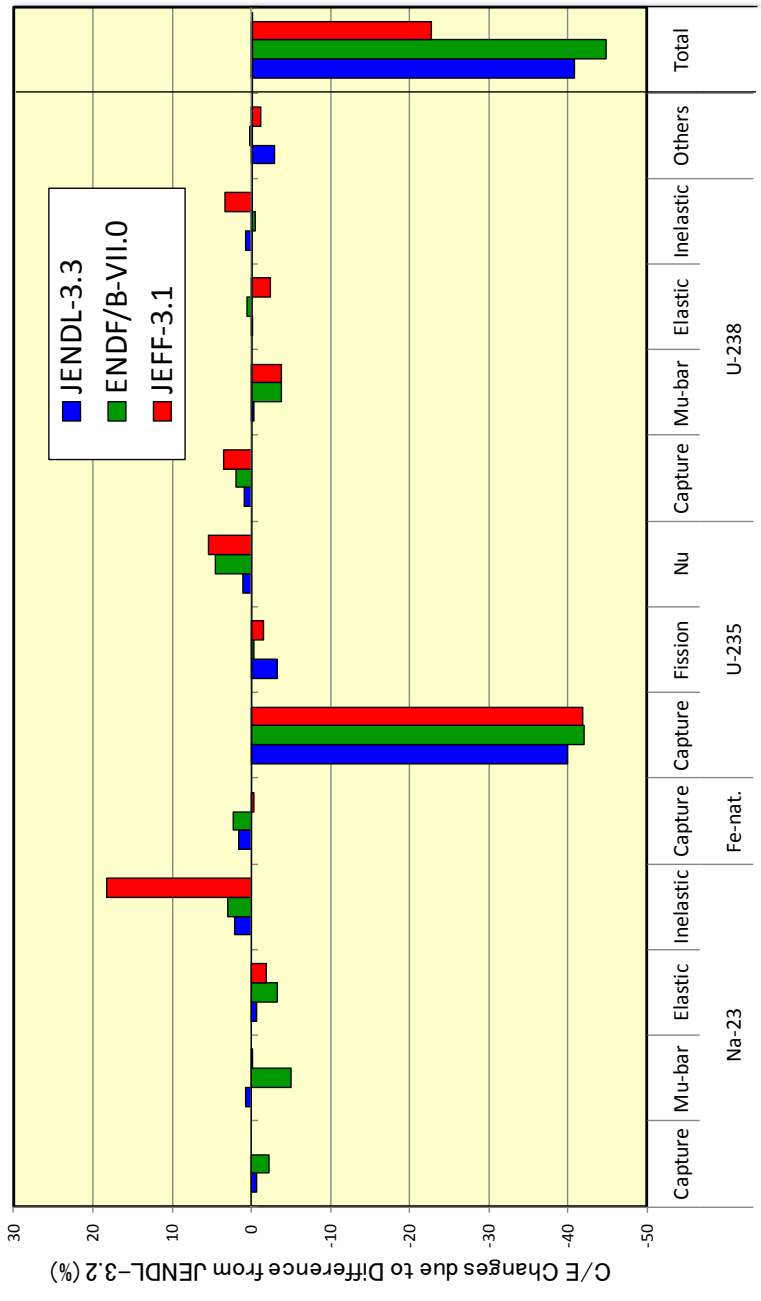

Figure D.4: Isotope- and reaction-wise contribution of the C/E differences with various libraries relative to JENDL-3.2

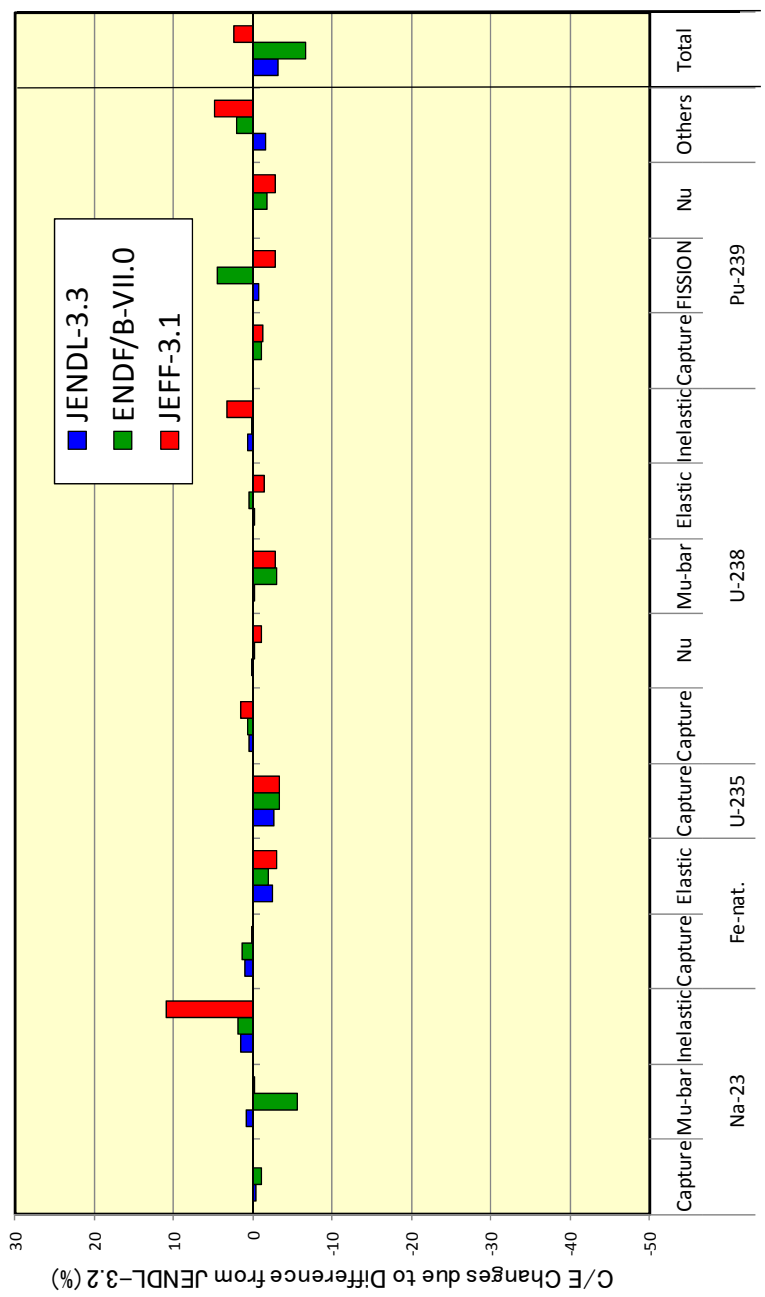

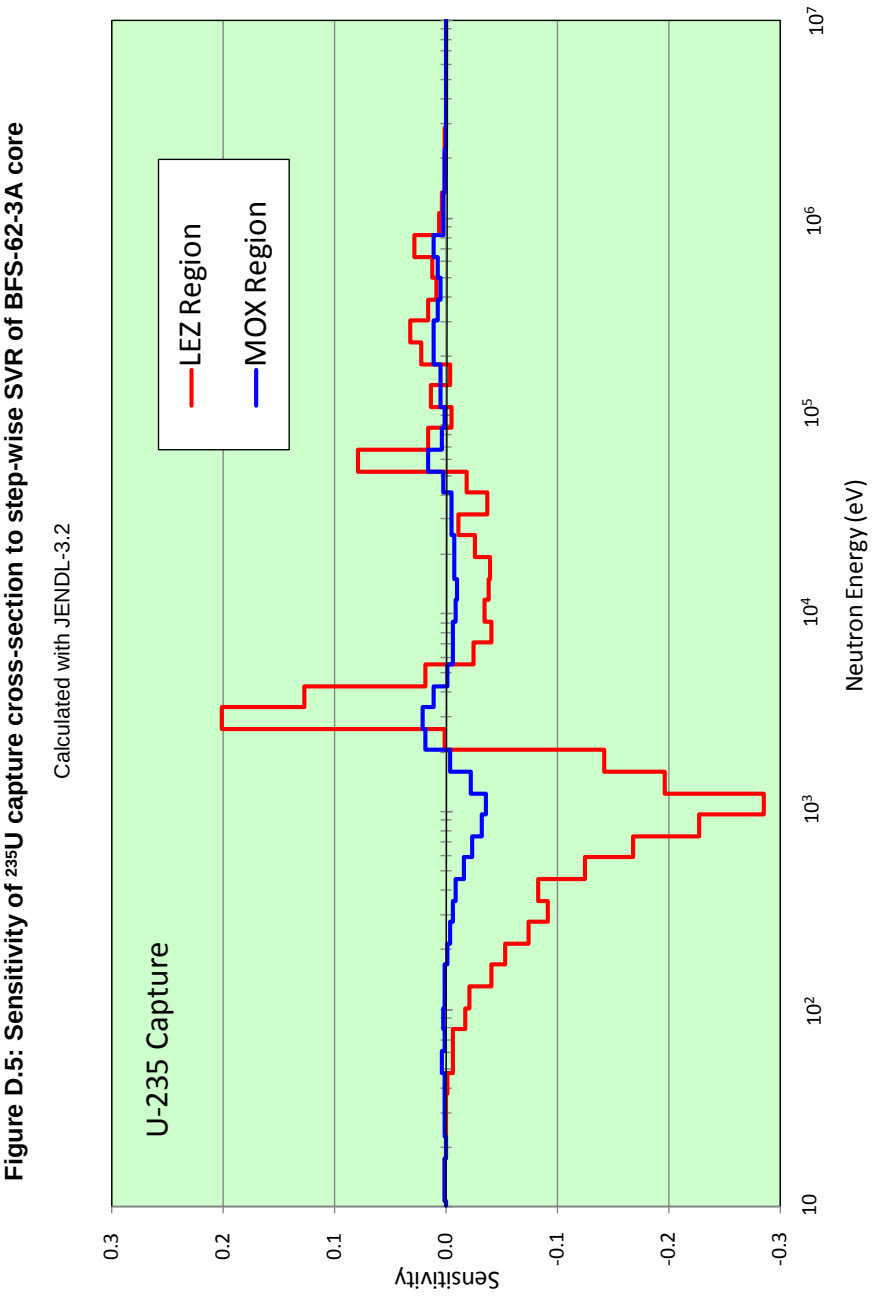

Figure D.5: Sensitivity of ^{235}U capture cross-section to step-wise SVR of BFS-62-3A core

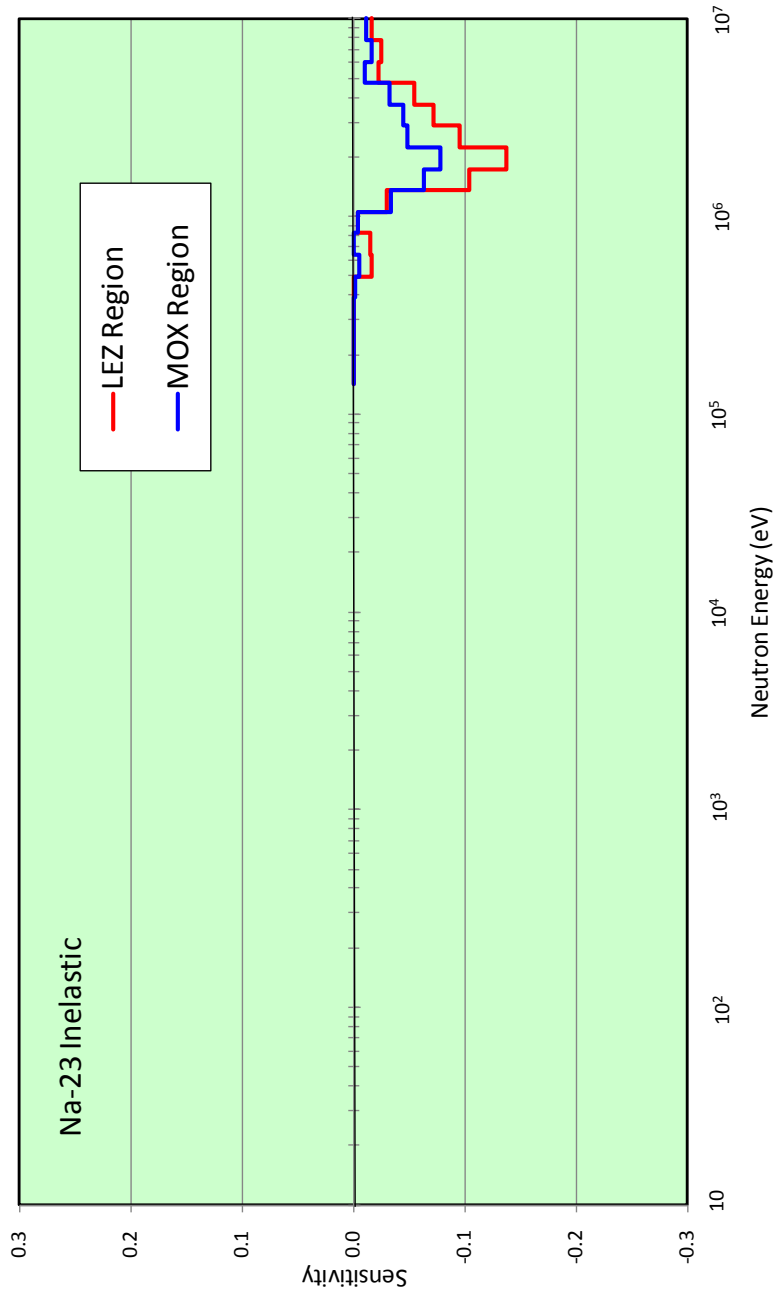

Figure D.6: Sensitivity of ^{23}Na inelastic cross-section to step-wise SVR of BFS-62-3A core

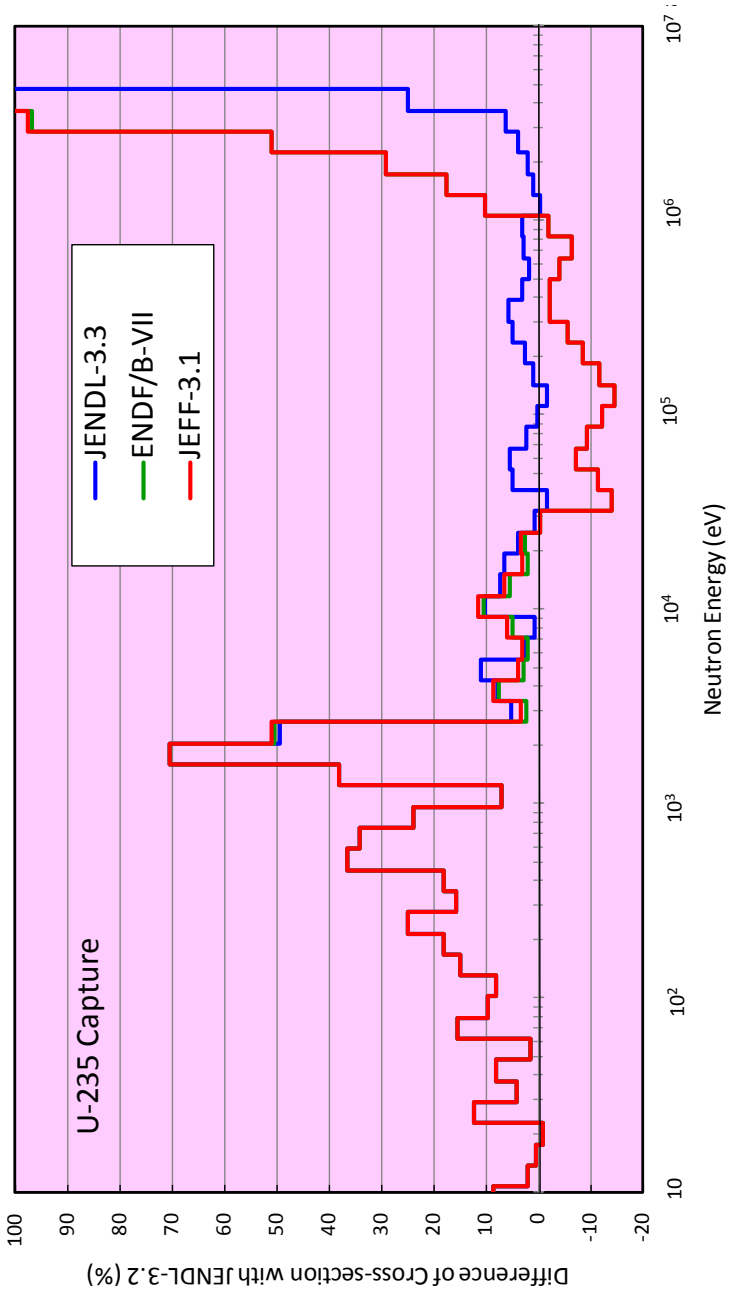

Figure D.7: Difference of ^{235}U capture cross-section with various libraries relative to JENDL-3.2

Below 2.25 keV (upper of resolved resonance energy), the three libraries are identical; above 2.25 keV, ENDF/B-VII.0 and JEFF-3.1 are almost overlapped

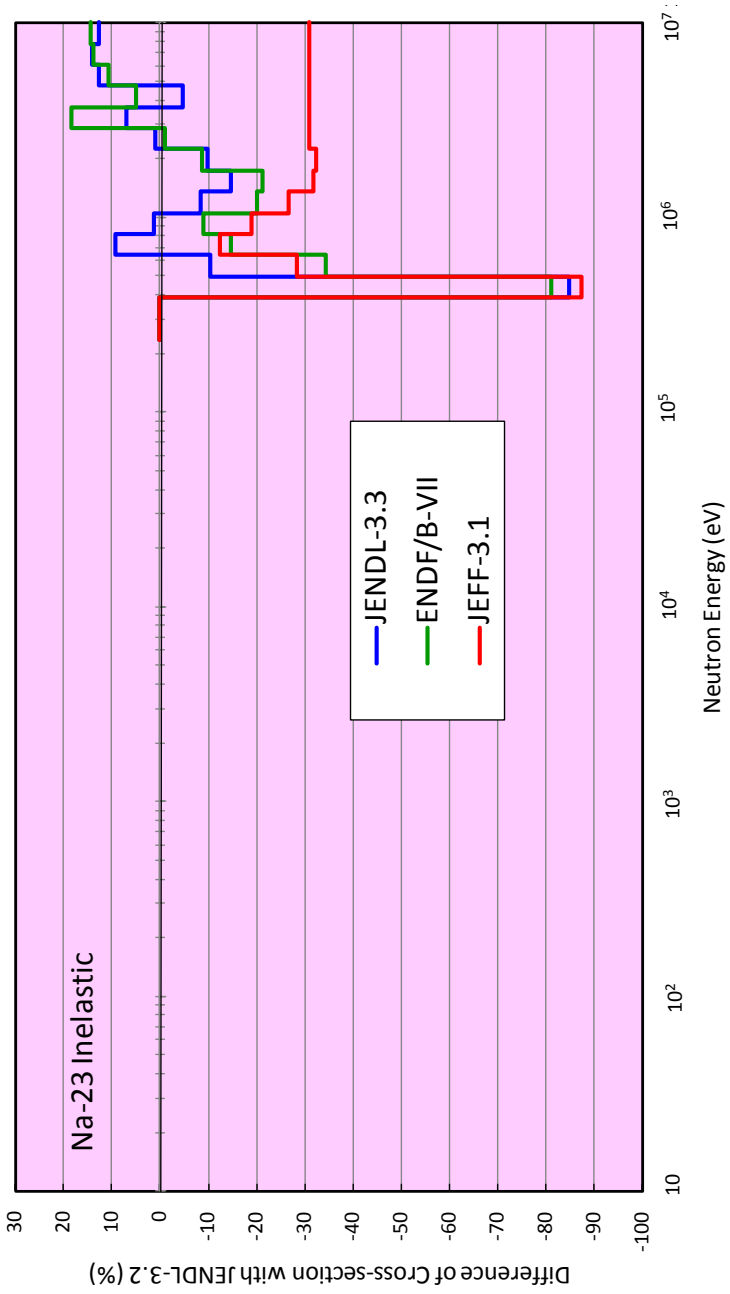

Figure D.8: Difference of ^{23}Na inelastic cross-section with various libraries relative to JENDL-3.2